Surface acoustic wave for microfluidic applications

Luong, Trung Dung

2012

Luong, T. D. (2012). Surface acoustic wave for microfluidic applications. Master’ s thesis, Nanyang Technological University, Singapore.

https://hdl.handle.net/10356/48677

https://doi.org/10.32657/10356/48677

NANYANG TECHNOLOGICAL UNIVERSITY

SURFACE ACOUSTIC WAVE FOR MICROFLUIDIC APPLICATIONS

LUONG TRUNG DUNG

SUPERVISOR: A/P NGUYEN NAM TRUNG

YEAR 2012

Surface Acoustic Wave for Microfluidic Applications

by

Luong Trung Dung

Nomenclature

β_m	Compressibility of medium
β_p	Compressibility of particles
η	Viscosity of medium
κ^2	Electro-mechanical coupling coefficient
λ	Acoustic wavelength
λ_{SAW}	Wavelength of surface acoustic wave
$\mathbf{v}$	Acoustic streaming velocity
$\mathbf{v}_1$	First order acoustic streaming velocity
$\mathbf{v}_2$	Second order acoustic streaming velocity
P	Pressure at a point in liquid
P_0	Zeroth order of pressure at a point in liquid
P_1	First order of pressure at a point in liquid
P_2	Second order of pressure at a point in liquid

R	Relaxation constant
μ	Shear viscosity of liquid
μ’	Bulk viscosity of liquid
ν	Kinematic viscosity of the fluid
ω	Angular frequency of propagating wave
ρ	Density of the liquid
ρ_m	Density of the medium
ρ_p	Density of particles
ρ_0	Zeroth order of density of the liquid
ρ_1	First order of density of the liquid
ρ_2	Second order of density of the liquid
θ	Contact angle
θ_R	Refraction angle of the radiated wave into liquid
D_h	Hydraulic diameter of the channel
F_r	The primary acoustic force on a particle
F_v	The viscous force on a particle
$I_i(t)$	Average intensity of each line *i* along the width of ROI at time *t*
I_{max}	Maximum intensity value

I_{min}	Minimum intensity value
V_p	Particle volume
2d	Transducer pitch
$C_{20}H_{10}Na_2O_5$	Fluorescein disodium salt
GHz	GigaHertz
Pe	Peclet number
Re	Reynold number
Vp – p	Peak to peak voltage
dBm	power referenced to one milliwatt
$\overline{I_\infty}$	Normalized average intensity of line at perfectly mixed state, equals to 0.5
$\overline{I_i(t)}$	Normalized average intensity of each line *i* along the width of ROI at time *t*
c_L	Speed of wave in liquid
c_S	Speed of wave in substrate
f_0	Centre frequency of surface acoustic wave device
k	wave vector
n_e	Refractive index of material for polarizations parallel to the axis of anisotropy

n_o	Refractive index of material for polarizations perpendicular to the axis of anisotropy
p_0	Pressure amplitude
r	Particle radius
v	Relative velocity of particle
v_{max}	Maximum velocity of droplet
D	Diffusion coefficient of the fluorescent dye
U	Mean flow velocity
W	Width of channel
CCD	Charge couple device
DIwater	Deionized water
DNA	Deoxyribonucleic acid
EWOD	Electrowetting on dielectric
FIDT	Focusing interdigitated electrodes
IDT	Intedigitated electrodes
IPA	Isopropyl alcohol
LDV	Laser Doppler vibrometer
$LiNbO_3$	Lithium niobate

$LiTaO_3$	Lithium tantalate
OTS	Octadecyltrichlorosilane
PCR	Polymerase chain reaction
PDF	Probability distribution function
PDMS	Polydimethylsiloxane
PVDF	Polyvinylidene fluoride
PZT	Lead irconate titanate
RF	Radio frequency
ROI	Region of interest
SAW	Surface acoustic wave
SIDT	Slanted interdigitated electrodes
SSAW	Standing surface acoustic wave
dpi	dot per inch
fps	Frames per second
rpm	rotations per minute

Abstract

Surface acoustic wave-based (SAW) microfluidics attracts attention from microfluidic research community due to its simple fabrication, large force and fast, yet efficient operation. The scope of this project is to develope a microfluidic platform based on the advantages offered by surface acoustic wave. Firstly, a literature review is given to present the state of the art of the emerging field of SAW-based microfluidics. SAW-based microfluidics can be categorized into droplet-based applications and continuous-flow applications. Droplet is actuated into unique behaviours depending on the applied SAW power. A wide range of droplet based applications have been employed utilizing these behaviours. In a continuous-flow system, applications are further categorized based on the interference of travelling SAW and standing SAW with the bulk liquid. The fabrication of SAW-microfluidic platform is based on standard microfabrication technology. Electrodes are patterned and lift off on a piezoelectric substrate to form a SAW device. Employing soft lithography, microfluidic channel system is fabricated and bonded to the SAW substrate.

First, the utilization of active surface-acoustic-wave-driven micromixers was investigated. Due to the small channel dimensions, flow characteristics in microfluidic devices was naturally laminar and mixing at microscale is poor. Large disturbance force induced

by transverse SAW could be exploited to enhance mixing quality effectively and with high throughput. Surface wave with a frequency of megahertzs was launched perpendicular to a side-by-side flow of water and fluorescent dye solution. Mixing quality was significantly enhanced compared to diffusive mixing. In this type of SAW mixer, two different designs of electrododes for generating SAW were studied : parallel design and focusing design. Under the same working condition, focusing design showed a superior performance compared to the parallel design.

Second, the experimental characterization of a liquid droplet driven by surface acoustic wave was demonstrated. The kinematics and deformation of the droplet on a silanized piezoelectric substrate was investigated at different driving voltages and droplet volumes. The kinematics of the droplet is characterized by four regimes: initial stationary state, acceleration with strong deformation, deceleration and steady motion with constant velocity. The maximum velocity of the droplet is proportional to the square of the applied voltage and does not change significantly with its volume. Bellow a critical volume, the steady velocity increases with the applied voltage. Above this volume, the steady velocity decreases with the applied voltage. In general, a larger droplet volume results in a higher steady velocity.

Third, the effect of surface acoustic wave (SAW) on the droplet formation process in flow focusing and T-junction configurations was investigated. Observation has shown that droplet is stretched along the propagation direction of the wave. Droplet shape does not have a circular shape as formed under a pure hydrodynamics formation. For the same change in droplet size, the formation process under SAW was compared to the correspond-

ing hydrodynamic counterpart with varying flow rates. The results show that pumping effect induced by surface acoustic wave affects the size of the droplets and their formation frequency.

Fourth, particles sorting based on SSAW was demonstrated. Acoustic radiance force induced in liquid by SSAW attracted particles to pressure nodes (anti-nodes). Employing a pressure node inside a microchannel, it is shown that particles are able to be sorted into a outlet of interest by turning SAW on. The sorting process is fast and effective.

Contents

List of Figures

List of Tables

Acknowledgement

I wish to give my sincere appreciation and gratitude to my research supervisor Dr. Nguyen Nam-Trung for his invaluable guidance and encouragement during my research project at the Thermal and Fluid Research lab. His insight knowledge, research vision and working attitude impress me a lot.

My research would not be complete without the help from Dr. Claus Dieter Ohl from School of Physical and Mathematical Sciences. I would like to thank him and his group for the use of his lab and equipments.

I am very grateful to Phan Vinh-Nguyen, Song Chaolong and Patrick Tan for their helpful advice and constant support when I start to embark into the field of microfluidics.

I would also like to thank my labmates: Xu Bin, Li Haiwang, Zhao Cunlu, He Jinhua, Ge Zhengwei, Liang Jian, Huang Yuli, etc. They are always there when I need their help.

Specials thanks go to Pek Soo Siong, Ho Kar Kiat, Hoong Sin Poh, Nordin Bin Abdul Kassim from Micromachines Lab 1; Yuan Kee Hock from Thermal and Fluid Research lab and Ng Teng Kwee from Communication Lab for their assistance during my work.

Finally, my deepest appreciation would go yo my wife Dawn Duong. Without your kindness, understandings and support, I probably would not have made it this far.

Chapter 1

Introduction

1.1 Surface Acoustic Waves

Surface acoustic wave is an elastic wave which travels along a confined surface of an elastic material with an amplitude that decays exponentially along the depth of the substrate [1]. This wave features a composite vibration mode containing both a longitudinal and a shear vertical vibrations. That means the substrate where a SAW propagates will attend two vibrations. Eventhough SAW was discovered by Lord Rayleigh in 1885, it was not until 1970 when SAW could be excited and detected by a electrode pattern on a piezoelectric crystal surface namely interdigitated electrodes (IDT)[2]. This so-called IDT is designed to have parallel electrodes with identical period from one end to the other end. When a radio frequency (RF) voltage is applied, piezoelectric substrate contracts and expands due to the redistribution of charges. A periodic strain field is generated in the piezoelectric crystal that produces a standing surface acoustic wave. This standing wave leads to the launching of an elastic wave with both longitudinal and transverse vibrations along the propagation

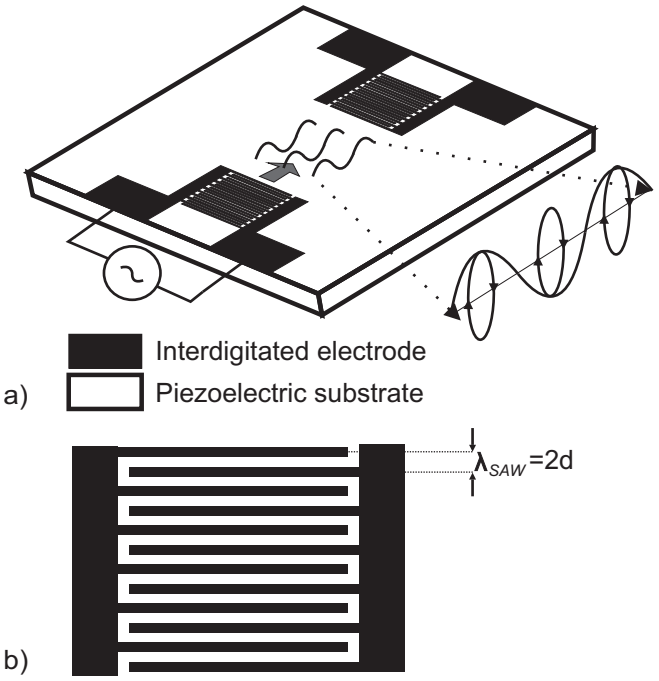

Figure 1.1: SAW device principle: (a) SAW generation and vibrations along a piezoelectric surface; (b) Interdigitated electrode concept.

of the waves where the wave front is parallel to the electrode finger. The combined effect causes point near the surface to move in an ellipse which is in a plane normal to the surface and parallel to the wave propagation as shown in Figure 1.1 (a). The IDT operates most efficiently when SAW wavelength matches the transducer pitch $\lambda_{\mathrm{SAW}} = 2d$, Figure 1.1 (b). The central frequency f_0 of the SAW could be determined by the relation: $f_0 = \frac{c_S}{\lambda_{\mathrm{SAW}}}$,where c_S is the wave propagation speed of SAW in the substrate. When the wave is incident on a receiving IDT in the propagation line of the SAW, the mechanical stress was converted back into an electrical signal and induces a current flow in each electrode arm. The addition of current contributions in the receiving IDT is also optimized when the transducer periodicity matches the acoustic wavelength. The conversion between electrical and acoustic energy is known as electromechanical coupling coefficient of a piezoelectric substrate.

1.2 Surface Acoustic Waves for Traditional Applications

SAW has been successfully employed in many applications over the past few decades. The most common use of SAW can be found in the radio frequency (RF) telecommunication. Normally, the resonance frequency of a SAW device is determined by the piezolectric material and the IDT pitch. Only a RF signal with the working frequency matching this resonance frequency could be used in such device. The dependence of SAW device on the input frequency has led to a wide usage of SAW in RF applications such as transmitter, receiver or bandpass filter. There are, on average, four SAW devices that could be found in current mobile phones [3].

Since most of SAW energy is confined to a thin substrate layer of four to five wavelengths near the surface. SAW propagation line is extremely sensitive to any surface pertubation. Successful utility of this property could be found in chemical and biochemical sensors. Surface of SAW is chemically or biologically treated so that it will bond to target objects passing through the surface. In this type of sensors, when the analytes pass through the propagation line, the target objects bond with the substrate changing the resonance frequency. The shift in the central frequency of the device (known as mass loading effect), before and after the bonding, could be used to examine and quantify the concentration, the mass, etc. of the target [4].

Surface acoustic wave is used in optical switches, modulators and filters as well [5]. The periodic mechanical deformations generate periodic distribution of electric charges across the crystal lattice. These changes generate a refractive index grating in the material which can be used to modulate the light incident onto the material. In the presence of SAW in a medium, a change of the refractive index is caused by pressure fluctuation created by

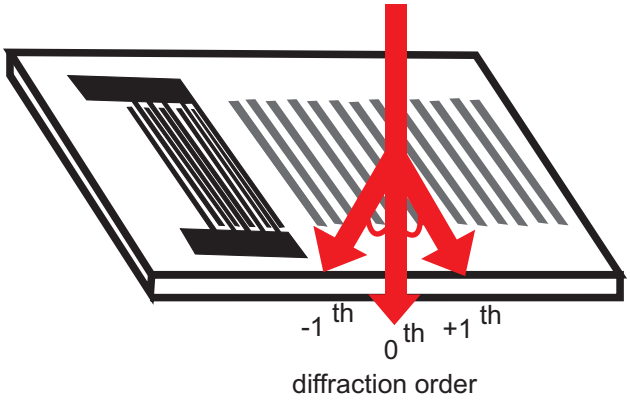

Figure 1.2: An SAW acousto-optic modulator.

sound waves. Such mechanism is known as acousto-optic effect. Acousto-optic modulator devices were relized by switching the surface acoustic wave on and off. When SAW is turned off, the light beam is undiverted and the intensity of light directed at the Bragg diffraction angle is zero (light intensity at $+1^{th}$ and -1^{th} diffraction order are zero). However when SAW is turned on, due to a refractive index grating, the internsity of light at the Bragg diffraction angle increase as shown in Figure 1.2.The device is operated as a modulator by keeping the acoustic wavelength fixed and varying the driving power to vary the amount of light in the deflected beam. In acousto-toptic filters, the desired wavelength of the optical wave can be diffracted acousto-optically by tuning the frequency of the acoustic wave [6].

1.3 Surface Acoustic Wave for Microfluidic Applications

In recent years, SAW has been attracting attentions from microfluidic research communities. SAW microfluidic working mechanism is based on the efficient energy transferred from the megahertz (MHz) wave into the liquid, which is due to the mismatch of sound ve-

locities in the substrate and fluid. When SAW comes into contact with liquid along its path, the leaky SAW, with decaying amplitude, is launched into the bulk liquid. The refraction angle of the radiated wave could be calculated based on Snell's law: $\theta_R = sin^{-1}(c_L/c_S)$, where c_S and c_L are the sound speeds in the substrate and in the liquid, respectively. Due to the refraction of acoustic energy into liquid, acoustic radiance pressure is built up inside the liquid and results in internal streaming following the wave propagation. However, internal flow circulation depends on the nature of the experimental setup. As shown in Figure 1.3, the circulation is in a clockwise direction [7] for droplet and a counter clockwise direction for liquid in a confined channel [8]. This so-called acoustic streaming effect is the foundation for applications of SAW in microfluidics. Compared to other actuation mechanisms in microfluidics such as surface gradient [9], thermal capillarity [10], electrowetting [11], magnetism [12], the apparent advantages of SAW are large force, fast operation and simple electrodes network. Current technologies make the fabrication of SAW devices relatively cost-effective. Moreover, the simple integration of SAW devices into microscale system promises an excellent solution for fluid miniaturization platforms.

The criteria for a piezoelectric substrate in SAW-based microfluidic applications are a relatively high electro-mechanical coupling coefficient (κ^2), transparence to the incident light within 400 nm to 850 nm (in order to use with inverted microscope) and cost effectiveness. In general, quartz, $LiNbO_3$, and $LiTaO_3$ are the most widely used ceramics materials in SAW microfluidic applications. Table 1.3 summarize the properties of some common SAW substrates [13]. Double-sided polished Y-cut 128° $LiNbO_3$ is our substrate of choice based on its relatively large electromechanical coupling coefficient and the ability for two directional SAW generation. Such high coupling coefficiently allows two-port

Table 1.1: Common piezoelectric SAW material and their properties

	ST-X Quartz	128° $LiNbO_3$	Y-cut $LiNbO_3$	ZnO/Quartz
SAW velocity (m/s)	3158	3980	3488	2900
κ^2	0.14	5.5	4.9	1

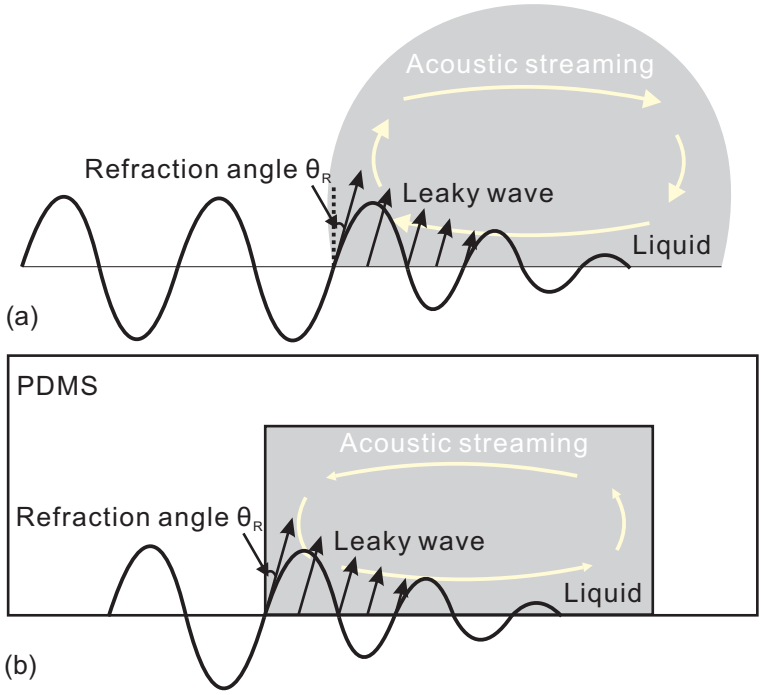

Figure 1.3: Acoustic streaming in (a) droplet and (b) confined channel

acoustic-wave devices to utilize IDTs comprised of nearly an order of magnitude fewer pairs of fingers than quartz. Table 1.3 summerizes common piezoelectric SAW material and their properties [13].

1.4 Objectives and Scopes of the Project

The main objective of this project is to ultilize the advantages of SAW in microfluidics for possible fluid handling applications. The applications covered in the project include

continuous-flow microfluidics and droplet-based microfluidics. The project also aims to develop fabrication techniques for SAW-based microfluidic devices. Microchannel platform fabricated in an elastomeric material is to be bonded to a SAW substrate to realize an active mixer. Droplet-based applications require a planar platform in which hydrophilic tracks are exploited to deliver fast actuation and precise control of droplets. One interesting aspect is the large disturbance force induced by SAW in fluid flow. Exploiting this large disturbance force, an active SAW mixer platform is proposed. Experiments of SAW mixing are carried out at different flow rates under applied voltages. The mixing efficiencies of these mixing experiments are calculated to investigate the mixing qualities of this SAW-driven micromixer. Droplet actuated by SAW on a planar piezoelectric substrate offers ultrafast yet simple operation. Droplet kinematics on a planar surface as a function of droplet size and applied SAW energy are investigated. The relationship between the displacement velocity of the droplet with droplet size and SAW energy are studied. Different operating regimes of the droplet on such platform will be analyzed. The acoustic streaming flow generated by SAW is another approach for active droplet formation. The effect of focusing SAW to water droplet formation in a carrying oil under T-junction and focusing configuration will be investigated. The relationship of droplet radius and droplet formation frequency will be studied. Acoustic radiance force induced by standing SAW is able to manipulate microparticles. A microfluidics sorter based SSAW device is to be proposed. The sorting of a single size of microparticles triggered by SSAW between two outlets will be investigated. It will be useful for future applications of size-selective sorting of microparticles.

1.5 Organization of Report

Chapter 1 introduces the background of this research. The objectives and scope are also discussed and defined in the Chapter.

Chapter 2 presents the literature review for the topic of the thesis. The reviewed works are catergorized under droplet-based SAW-based microfluidics and continuous-flow SAW-based microfluidics. Droplet-based applications are reviewed based on their unique droplet behaviours induced by SAW. In continuous-flow microfluidics, applications are reviewed based on the inteference of a single SAW or multiple SAWs with fluid flows inside microchannels.

Chapter 3 summerizes the existing acoustic streaming theory.

Chapter 4 presents the fabrication of SAW based microfluidic devices of this project. Interdigitated electrodes patterning were patterned by a lift-off process. Microchannels were fabricated by a standard soft-lithography. The channel was then integrated onto the SAW substrate through a oxygen plasma bonding process to form a SAW-based active mixer. Tracks are patterned on a SAW substrate. A hydrophobic layer was coated on the substrate subsequently. Hydrophilic tracks are formed by lifting-off this material in aceton. Characterization of the SAW device is reported in this chapter to determine the working frequency.

In chapter 5, the concept of SAW induced mixing of continuous flow was applied to a micromixer in which high flow rate of samples are used. Side-by-side samples of water and fluorescent dye solution were introduced into the inlets. Transversal acoustic streaming wee induced by an IDT placed perpendicularly to the channel to quickly mix the fluids. Mixing

qualities of different electrode designs were investigated.

Chapter 6 presents the experimental characterization of a liquid droplet driven by surface acoustic wave on a planar Y-cut 128° rotated lithium niobate substrate. The kinematics and deformation of the droplet were investigated at different driving voltages and droplet volumes. The results from the investigation reported here can be used for optimizing the driving scheme of SAW-driven droplet-based microfluidics.

Chapter 7 presents an investigation of surface acoustic wave in droplet formation using flow focusing and T-junction configurations. Observation has shown that droplet was stretched along the confinement microchannel. Droplet shape did not have a circular shape as formed under a pure hydrodynamics formation. Pumping effect induced by surface acoustic wave also affect the generated droplet volumes and forming rate.

Chaptor 8 demonstrates the sorting of microparticles by exploiting standing surface acoustic wave. Particles were hydrodynamically focused into an outlet. When SSAW was formed, micro-particles would experience an acoustic radiance force. They were pushed by this radiance to a pressure node. By aligning the pressure node to another outlet, particles followed the node and were sorted into that particular outlet.

Chapter 9 concludes the future works proposed for this research.

Chapter 2

Literature Review

A number of works have been reported recently in the literature on SAW-based microfluidics. Reviews on these works were published recently by Yeo and Friend [14], Fu et al. [15] and Wixforth et al. [16]. In these literature reviews, SAW microfluidic applications are categorized into droplet-based applications and continuous-flow applications. In droplet-based applications, droplets are actuated into unique behaviours depending on the applied SAW power. A wide range of droplet based applications have been employed based on these behaviours. In a continuous-flow system, applications are further categorized based on the interference of the travelling SAW and the standing SAW with the bulk liquid.

2.1 SAW and Droplet Based Applications

Under different power loads, droplet behaviours such as droplet oscillation, droplet actuation, droplet jetting and droplet atomization were observed. In this section, publications

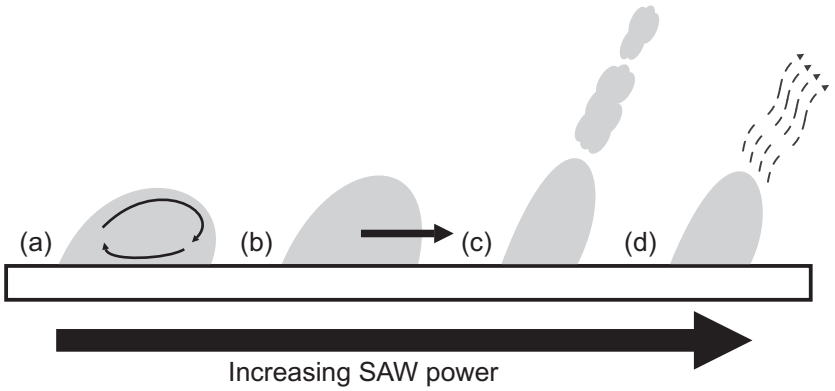

Figure 2.1: Different modes of SAAW induced droplet manipulation: (a) Droplet oscillation; (b) Droplet actuation; (c) Droplet jetting; (d) Droplet atomization.

on SAW based droplet manipulation are summarized according to the different droplet behaviours. As shown in Figure 2.1, when the RF power is applied, acoustic streaming is induced due to the leaky wave radiated into the droplet. At a low power, droplet oscillates at its position, Figure 2.1(a). Wide range of applications utilizing this effect includes droplet mixing, droplet heating, particle patterning and particles concentration. Increasing the power, acoustic streaming is strong enough to result in a significant inertial force and to drive droplet in the wave propagation direction , Figure 2.1(b). Droplet actuation has been used for pumping, sample collecting and sample dispensing. Several methods of droplet positioning are proposed for a well controlled SAW droplet platform. Further increasing the power, acoustic streaming is so violent that the liquid is jetted into the air as shown in Figure 2.1(c). Droplet jetting is suitable for ink-jet printing applications. If the applied power is too high, strong capillary waves at the droplet surface overcome the capillary stress and result in atomization, Figure 2.1(d).

2.1.1 Droplet Oscillation and Its Applications

Active Droplet Micromixer

When a radio frequency (RF) input power is lower than a critical value, pressure gradient is generated inside the droplet. This gradient is not strong enough to actuate a droplet but still induces acoustic streaming in the liquid. Flow patterns and recirculations are formed as shown in Figure 2.2(a). When SAW is launched into the liquid from the right side, circulation follows the clockwise direction as seen from the side view. From the top view, the left portion of the droplet has a counter clockwise circulation as opposed to a clockwise circulation formed in the right portion of the droplet and the direction of the flow is in the same direction with the wave propagation. Mixing of reactant inside a droplet is important in many biological applications. However, the mixing is difficult and slow due to the relatively low Reynolds number in microscale. Droplet mixers based on electrowetting on dielectric (EWOD) has been reported in the literature [17]. This method involves splitting and merging a droplet to generate flow advection and thus can enhance mixing. Alternative method is to employ the internal streaming generated by SAW. Rapid mixing inside droplet caused by this internal flow has been achieved and reported in the work of Frommelt et al. [18] and Wixforth et al. [19]. The mixing efficiency was found to be effective for a droplet with diameters larger than the SAW wavelength. This is due to the fact that acoustic power would couple more effectively into such droplets to induce a stronger flow. Active droplet-based SAW mixers generally offer a very fast and effective solution. The mixing rate could be controlled simply by adjusting the input power from a single IDT in contrast to a more complicated electrode network in EWOD based mixer.

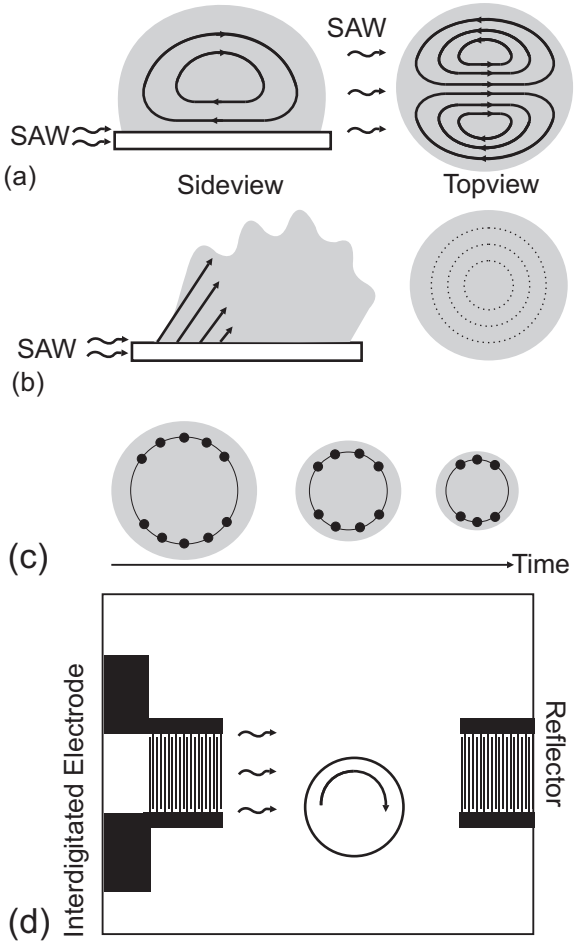

Figure 2.2: Acousitic streaming in a droplet: (a) Flow pattern of induces acoustic streaming under effect of SAW; (b) Surface vibration and ring-like pattern formed inside droplet; (c) Point wise patterned formed inside droplet with increasing time; (d) Symmetry breaking of SAW leads to unidirectional flow circulation.

Droplet Particle Patterning

If the droplet contains colloid of nanoparticles, unique particle assembly is observed inside the droplet. These unique patterns depend on the power input of the SAW and the droplet diameter as reported by Li et al.[20]. In this experiment, the frequency of the applied input was 20 MHz. Under a low applied power, the pattern was ring-shape structure with a distance between the rings to be half of the SAW wavelength, Figure 2.2(b). A laser Doppler vibrometer (LDV) was used to confirm the vibration of the free liquid surface at a very small amplitude. This surface vibration was believed to form a standing wave on the droplet surface and drove the particles to the pressure nodes which created the ring like structure in the experiment. Upon increasing the input power, low frequency capillary-viscous vibrations of 1 kHZ strongly interfered with surface standing wave to form point wise colloid islands in the circular nodal lines. The number of colloidal islands formed at intersection points between the 20 MHz nodal lines and the 1 kHz circular nodal ring decreased with time as shown in Figure 2.2(c). The reason was the evaporation of droplet with time which leads to the change in the number and the positions of colloid islands. If the input power was further increased, significant flow circulation was presented and colloid islands structure was disturbed. A transient metastable state was established in which continuous cycle consists of colloid erasure and colloid islands formation took place subsequently. At even higher power, the internal streaming became dominant, permanent particle dispersion in a bulk droplet was observed.

Droplet Particle Concentration

Particle concentration at small scale is not an easy task since large radial force is needed to overcome the surface tension and focus the particles in the droplet. Such radial force could be generated using SAW through symmetry breaking of the acoustic wave propagation across the substrate. By placing the droplet asymmetrically in the propagation line of SAW, Figure 2.2(d). Li et al. [21] demonstrated asymmetric pressure fluctuations inside a droplet which gave rise to a unidirectional flow circulation, and hence, the suspended particles. Once the particle concentration was sufficiently high within a particular streamline of the acoustic streaming convective flow, the shear-induced migration gave rise to an inward radial force that concentrated the particles at the centre of the droplet. Other methods to create such asymmetric pressure were to introduce a diagonal cut of the substrate or to absorb half of the acoustic wave. Shilton et al. [22] intensified the circulation by introducing focusing interdigitated transducer electrode (FIDT) to generate a higher amplitude surface wave. Exploiting four FIDTs, concentration of fluorescent polystyrene particles of 0.5 μm in diameter was achieved rapidly after a few seconds.

Droplet Heater

The interaction of SAW and liquid could be used as a microscale heating process. Mechanisms of heating droplet by SAW are understood due to the piezoelectric substrate heating by the wave propagation and by radiated SAW energy into the liquid. Beyssen et al. [23] demonstrated a droplet heating system based on such mechanisms, Figure 2.3. In this work, a 10 μL water droplet was heated from an initial temperature of 18°C to 30°C under an applied SAW power of 1.5 W. At a low input power, the effect of substrate heating

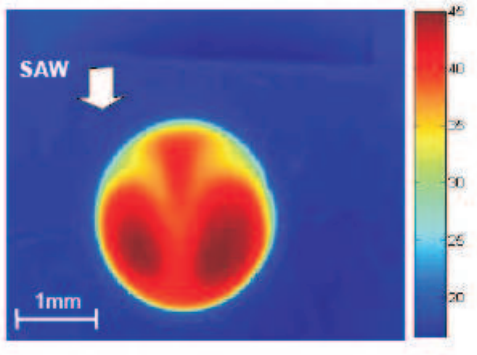

Figure 2.3: Infrared image of a droplet under 1.6 W SAW irradiation.

is inferior to that of radiated energy. The viscosity of the liquid is also a parameter that influences the droplet heating. A glycerol droplet of 10 μL was successfully undergone three heating cycles of 55°C peak with an input power of 1.6 W. It could be a potential heating scheme for polymerase chain reaction (PCR) applications where no droplet movement is required. The heater allows to duplicate sequences DNA at the three temperature cycles (55°C $\rightarrow$ 73°C $\rightarrow$ 98°C).

2.1.2 Droplet Motion and Its Applications

Increasing SAW input power beyond a critical value causes the pressure gradient inside the droplet to be larger than the surface force, and thus results in the droplet motion along the wave propagation direction. Due to the fact that piezoelectric ceramics substrate is naturally hydrophilic, and wetting area of a droplet is large, the device requires a higher input power to drive a droplet as compared to a hydrophobic surface. To improve the performance of droplet actuation, surface treatment process in which a hydrophobic thin layer is deposited on the substrate is needed. Different materials have been reported in the literature [24, 25]. Polyvinylidene fluoride (PVDF) offers the lowest surface friction of

85 μN. Teflon is also a good hydrophobic surface with the contact angle larger than 100°. A thin CF_x hydrophobic layer could be achieved by using an expensive plasma deposition process. However, self assemblied mono-layer (SAM) of octadecyltrichlorosilane (OTS) was found to be the better solution in SAW droplet based microfluidics due to its simple and cost-effective coating process [26, 27]. A sufficiently thin hydrophobic layer (thickness in the range of tens to hundreds of nm) couples the SAW into the droplet more efficiently compared to generally thicker films coated by other methods.

Droplet Pumping

In many biological applications, droplet pumping is an important task. One popular method is a EWOD driven droplet. Drawbacks of this method are the low driving force and the slow processing time. Acoustic streaming induced by SAW can move a droplet with large force and at a high speed. Micropump driven by SAW has been proposed in the literature [28, 29]. The speed of droplet motion achieved was in the range of centimeters per second. For improved control of droplet path, hydrophilic tracks on a hydrophobic treated piezoelectric surface were exploited in order to guide the droplet more accurately, Figure 2.4(a).

The track is the surface of piezoelectric substrate and the rest of the surface is coated with a thin layer of OTS. This process could be easily fabricated by a lift-off process or by an etching process where Renaudin et al. [30] used a simple hydrophilic track on a silanized $LiNbO_3$ substrate to precisely pump a 1.5 μL droplet to a point of interest, Figure 2.4(b,c). Thalhammer et al. reported a SAW platform for two dimensional pumping and actuating of droplet [31]. Droplet pumping and merging has been successfully operated

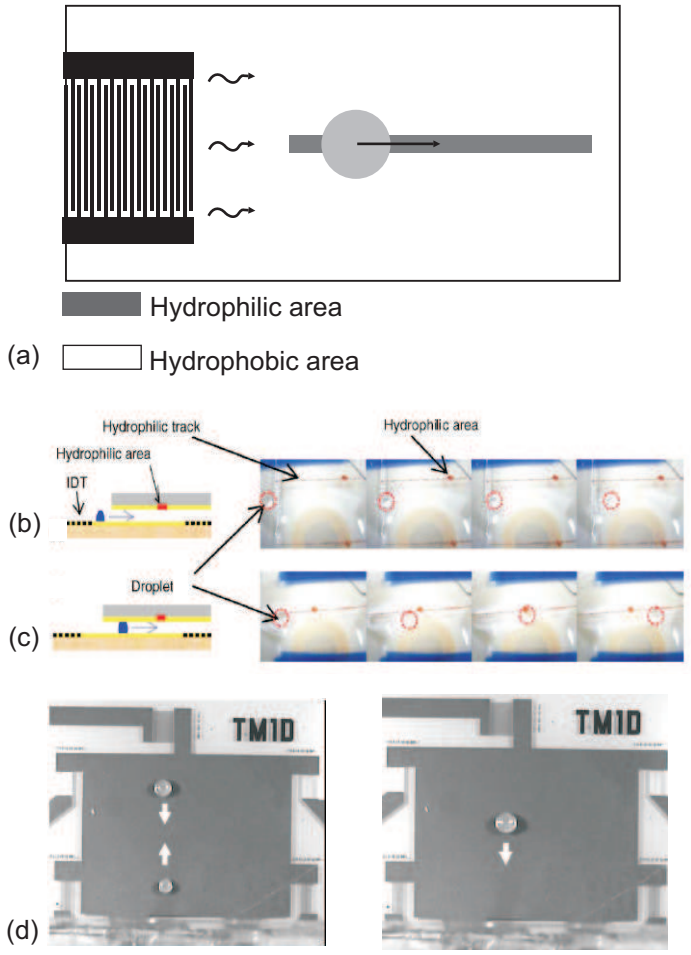

Figure 2.4: Droplet pumping by SAW: (a) A schematic of SAW droplet pumping on a hydrophilic track;(b) Droplet insertion between two planes; (c) Linear trajectory of a squeezed droplet and crossing of a hydrophilic area designed on the cover and (d) time series of two droplets (300 nl and 500 nl volume) being moved towards each other and merged.

in some applications such as PCR, hybridization [32]. In this work, two droplets (300 nl and 500 nl volume) were moved towards each other and merged. The merged droplet was subsequently pump to another location as shown in Figure 2.4(d). A potential microfluidic SAW processor could be attractive for various applications.

A new concept in SAW-based microfluidics pumping and merging exploits a slanted finger IDT [33]. In other methods, the droplet need to be positioned along a hydrophilic track in order to be actuated to the point of interest. The system comprises a slanted IDT coupled to a glass superstrate. The hydrophilic glass superstrate was patterned with a hydrophobic silane patch using standard lithography to produce an area of hydrophilic dots with a radius of r = 80 μm. Fluid manipulations of a 2 μL drop of hydroxylamine hydrochloride (1.67 mM) and sodium hydroxide (3.33 mM) and a 2 μL drop of silver nitrate solution (10 mM) being moved, merged, mixed and the reduced silver being concentrated, by centrifugation was reported. Three different frequencies were used to navigate between each manipulation: $f_3 = 11\ MHz$ moves the left hand droplet to the centre, $f_4 = 9.2\ MHz$ moves the right hand droplet to merge it and $f_5 = 9.6\ MHz$ mixes and concentrates the reduced silver in the centre of the droplet, Figure 2.5. In this technique, only by changing the SAW excitation frequency, droplet could be pumped and merged in a more programmable fashion. The usage of SIDT offers a high degree of functional integration.

Droplet-based Particle Collection

In various biological applications such as environmental monitoring, fungi, bacteria, etc need to be collected by a carrier at an expected concentration. Tan et al. [34] exploited droplet movement and the internal streaming for particle collecting. In this experiment,

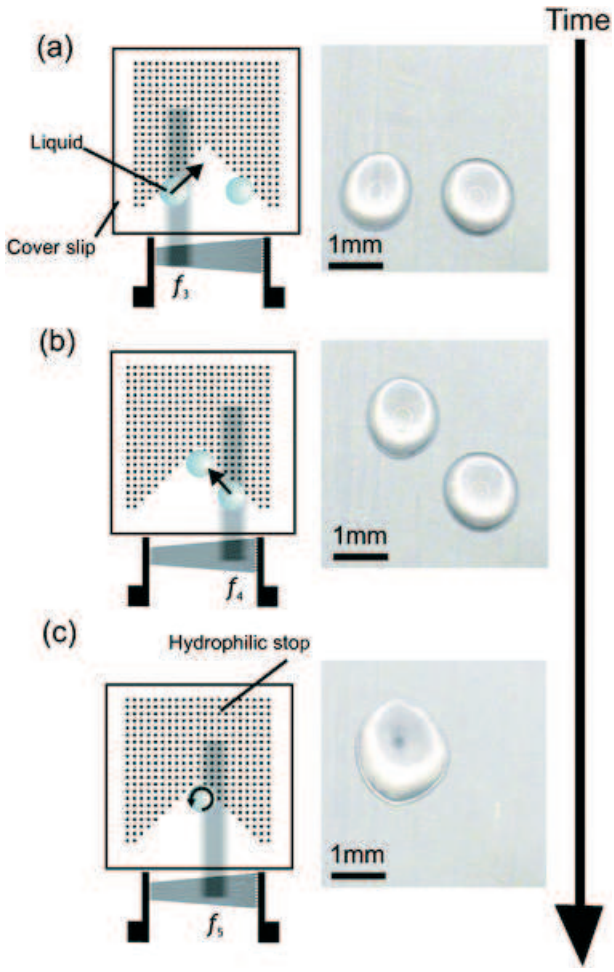

Figure 2.5: Schematic representations of the device showing stills from a movie at the different stages during a series of fluid manipulations by operating SIDT at three different frequencies.

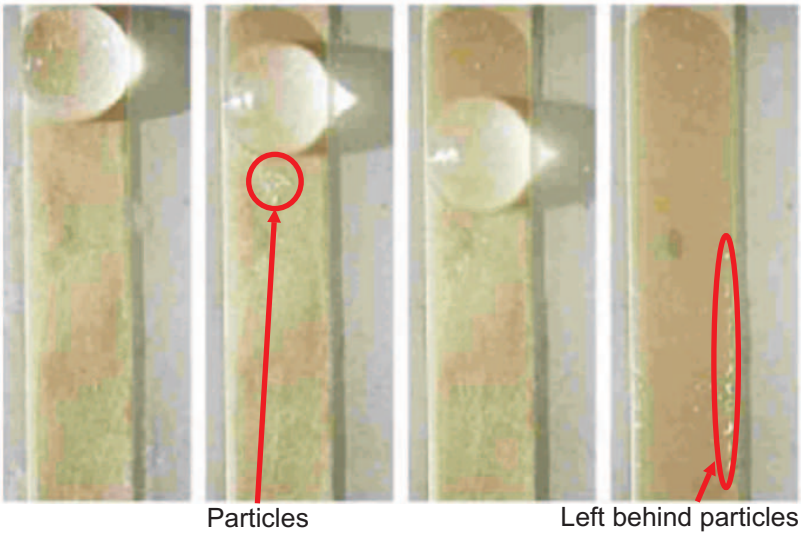

Figure 2.6: Rapid and efficient collection and concentration of 10 μm melamine microparticles on a substrate by sweeping carrier drops across the surface using the SAW. A portion of particles was left behind.

10 μm dry particles were collected by an actuated water droplet along a hydrophilic track. The leaky force makes its more effective to sweep up the particle from the surface into the bulk liquid. The collection process only took a few second per run, much faster than collection method based on electrowetting. However, some of the particles are left behind during the operation, Figure 2.6. Pollen has been reported to have a collection efficiency of 45-68%, while the efficiency is 61-69.8% for bacteria was achieved in this work.

Droplet Sample Dispensing

Strobl et al. [35] has demonstrated a cost-effective method to dispense droplet at nano and pico liter range using SAW. An array and a single passive sample SAW driven dispenser was introduced. This method is achieved elegantly by utilizing hydrophilic area on the silanized $LiNbO_3$. A hydrophilic checker box consisting of 65 μm size square patterns was formed on the substrate, Figure 2.7(a). When the water droplet was driven to pass the area, it left behind a small amount of water in the hydrophilic squares. An array of

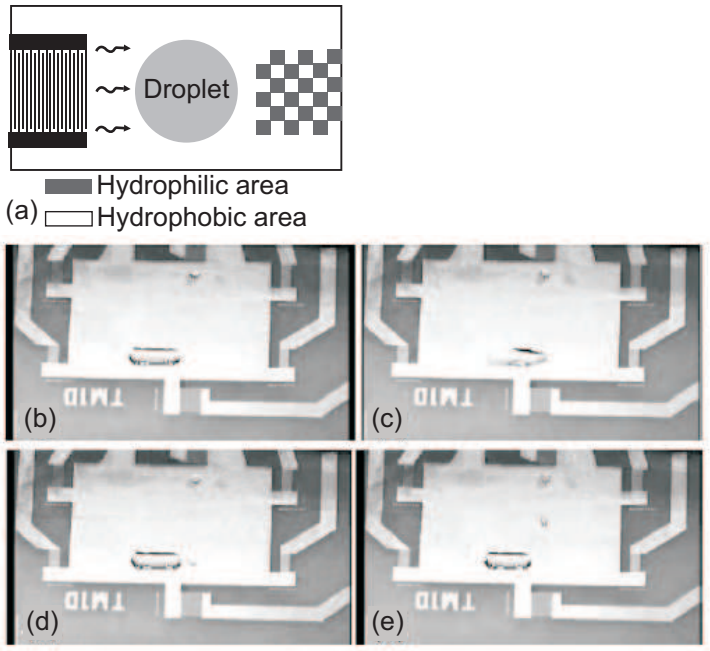

Figure 2.7: Droplet dispenser: (a) Layout of a checker box dispenser; (b) The IDT on the left is activated to push the reservoir droplet towards the hydrophilic anchor; (c) The hydrophilic anchor is wetted by the reservoir; (d) Switching off the SAW retracts the reservoir droplet leaving a small droplet at the anchor site. (e) A second SAW is used to push the dispensed droplet toward a container anchor (Strobl et al.,2004).

droplet was formed with estimated droplet volume at around 50 pL. A fluid reservoir was formed by a large hydrophilic spot, and the amount of fluid dispensed is based on a small hydrophilic spot anchored next to the reservoir. One IDT actuated the fluid to cover the anchor. Upon turning off the signal, the fluid retracted back and left the anchor area wet. The dispensed droplet was subsequently moved to other location by another transducer. The spot in the experiment had the diameter of 300 μm and the droplet volume was about 2 nL. The process is shown in Figure 2.7(b-d). The array and the passive dispenser worked fast, reliably without expensive external control system.

Droplet Detection

Droplet positioning on a planar platform is important in many applications. Besides traditional methods, SAW has been reported to detect droplets as well. The working principle of detecting droplet using SAW is based on the strong attenuation in intensity of the transmitted wave. Bennes et al. [36] demonstrated the improvement in detection by exploiting the step-by-step displacement of the droplet with a pair of uniform IDT. Instead of a continuous RF signal, a pulse modulated RF signal was applied to the input of the transmission IDT to drive a droplet in a step-by-step motion. With the modulation frequency of 5 Hz, pulse duration of 30 ms, a 0.4 μL droplet could be actuated and detected with the resolution of 100 μm. Wu et al. [37] has employed the slanted inter-digitated transducers for droplet detection ,Figure 2.8(a). In this configuration, two SFIT were used for unidirectional detection with one as the transmitter and the other as the receiver. With the SFIT design, the centre frequencies varied within a passband according to the maximum and minimum of the finger pitch. When the droplet moved in the direction perpendicular to the IDT from location 1 and 2, its position could be tracked by monitoring the transmitted signal in the working passband of the device. The corresponding frequencies, where high transmission loss was observed, would indicate the positions of the droplet in the line. By varying the number of fingers and the size of the aperture, the passband and the amplitude of the wave could be adjusted. This design has the advantages over the uniform IDT in detecting droplets with a size smaller than the aperture of the transducer. Nevertheless, the whole passband (in a range of a few MHz) of the device required continuous scanning in order to keep track of the droplet position. Renaudin et al. [38] proposed another method to detect droplet in line with a single IDT using echo wave. A pulsed excitation RF sig-

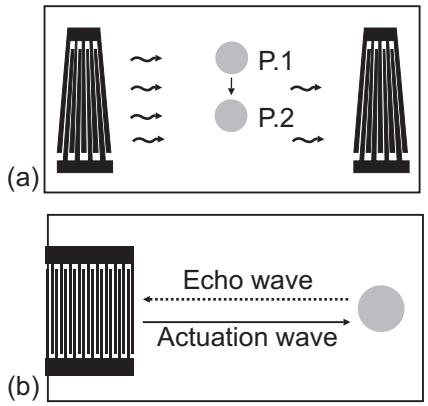

Figure 2.8: Droplet detection: (a) Droplet detection employing slanted IDT; (b) Droplet detection with a single IDT through the echo wave.

nal was applied to actuate the droplet. A second pulse signal was sent afterwards and its corresponding reflected signal was recorded, Figure 2.8 (b). Based on the time difference between the excitation signal and the reflected signal, the position of a droplet was calculated. The work reported to be able to receive the echo signal of the droplet as small as 0.2 nL. Furthermore, with the orthogonal detection being limited by the aperture size of the transducer pair, this method definitely provides a much wider detection range compared to the above methods.

2.1.3 Droplet Jetting and Its Applications

Current inkjet technology employs thermal and piezoelectric actuators, where the ink is ejected perpendicularly to the nozzle surface. With the application of SAW, a nozzle-free ink ejector could be made [39]. When the applying power was larger than 1W, the radiant force was strong enough to eject droplet from the bulk liquid in contact with the SAW substrate. The droplet was ejected at an angle θ_R equivalent to 22.6° in the reported work (this angle could be calculated based on Snell's Law with a speed of wave in the substrate of 3900 m/s and the speed of wave inside water as 1500 m/s, and agrees well with

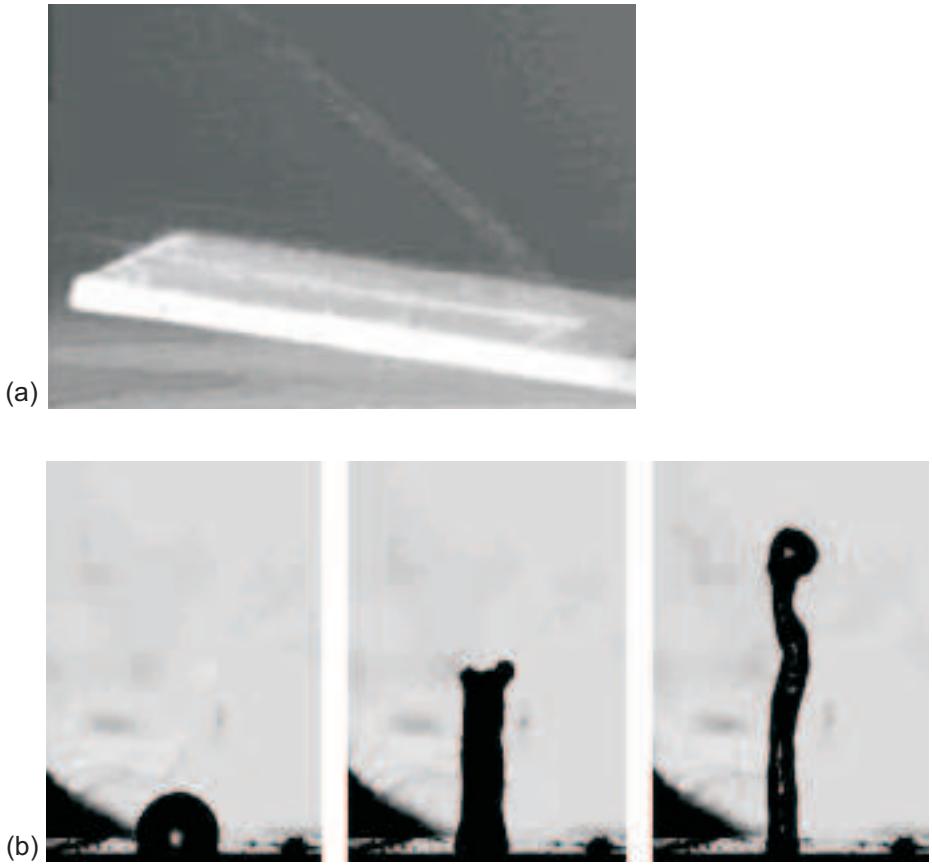

Figure 2.9: (a) Droplet jetting induced by a single SAW; (b) Snapshots of a droplet jetting induced by a pair of SAWs.

experimental result, Figure 2.9(a).

Tan et al. [40] demonstrated another method utilizing two opposite FIDT at the ends of the substrate to drive the convergence of two SAWs at a point above which a liquid drop is placed as shown in Figure 2.9(b). The radiation from two sides of the droplet resulted in an elongated liquid column with an angle of about 90°. These SAW ejectors are free of nozzle head and offer a more cost effective solution as compared to the current ink ejector.

2.1.4 Droplet Atomization and Its Applications

As the leaky SAW propagates in the fluid, capillary waves are generated at the liquid-air interface. If the applied power is sufficiently large, the acoustic stress dominates the

capillary stress and destabilises the interface. Liquid atomization is induced, and continuous mist of droplets is evaporated in-flight. This technique has been used for biodegradable polymeric nanoparticles generation [41]. A polymeric excipient was dissolved into a solvent drop. A solvent droplet was then atomized by SAW and left behind solidified polymeric particles which are relatively monodispersed. With this technique, 150-200 nm spherical clusters were formed and comprised sub-50 nm particulates as observed from TEM, Figure 2.10(a). Spatial ordering of periodic polymer has been patterned on a substrate by SAW atomization as well. A droplet of a polymer solution was dispensed to a SAW track through a needle placing above the substrate. When this solution was in contact with the SAW, acoustic streaming displaced the droplet and left behind a trailing thin film layer of typically 10 μm thickness. Due to the thin thickness, the film was quickly evaporated. The break-up of the film in both transverse and longitudinal direction produced evenly spaced solidified polymer droplets. It was observed that the longitudinal spacing was approximately half of the SAW wavelength while the transverse spacing was about half of this value as shown in Figure 2.10(b). The dependence of the pattern periodicity as well as the polymer spot size on a lone parameter, namely the SAW frequency or wavelength as reported in the work of Alvarez et al.[42]. This relationship therefore endows the process with the ability for controllability and fine tuning, which is a key advantage over other conventional patterning methods.

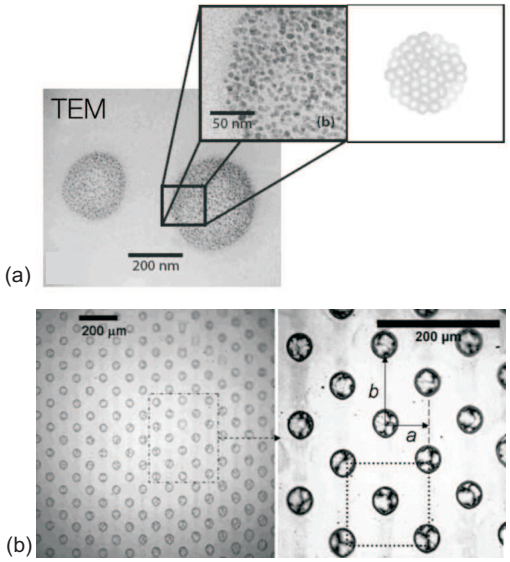

Figure 2.10: Nanoparticles synthesis: (a) 150−200 nm polymer nanoparticles synthesized using the SAW atomization technique formed by sub-50 nm particulates aggreration; (b) Two-dimensional array of polymer spots produced by the SAW translation and atomization process is extremely regular and organized with the longitudinal pitch spacing as half of the transverse pitch spacing *b*.

2.2 SAW Continuous Flow Applications

Early applications of SAW in microfluidics mainly focused on droplet based microfluidics. The integration of SAW on a channel microfluidic system has been researched more intensively recently. Applications in continuous flow such as pumping, mixing, sorting and patterning have been reported. The fabrication usually requires an additional step to fabricate the channel and to combine it with a piezoelectric substrate. On the one hand, open channel can be fabricated by direct pattern transfer to a SU-8 coated on the substrate. On the other hand, closed channel, usually made of PDMS, can be treated by oxygen plasma and bonded to the substrate. The applications are categorized according to interference of a single SAW or multiple SAWs which create standing surface acoustic wave (SSAW).

2.2.1 SAW Propagation and Its Applications

SAW Micropump

Not only SAW was used as a pump in droplet-based microfludics, but also in continuous-flow microfluidics. Compared to other methods, SAW-driven micropump is not in contact with the liquid, which can offer the diverse use of chemicals without affecting the electrode.

SAW pumping of liquid through open channel system has been reported. Saiki et al.[43] pumped the fluid between two reservoirs through a channel of 1 mm width and 220 μm depth with a flow rate of 4 μL/s. The fluid velocity was proportional to the applied voltage. However there was a limited working range for the input signal. If the signal voltage exceeds 65 V_{p-p} the fluid in the channel started to vaporize. Fukuoka et al.[44] used a similar setup to pump the liquid in a closed square loop channel (Figure 2.11a). A mixture of dye and aluminium powder was used for visualization in the experiment. Relationship between the number of the fingers and comb pitch was characterized for optimal performance. A maximum flow velocity of 108 mm/s was achieved by using a 200 μm comb pitch. Flow could be directed by positioning the IDTs. Lindner et al. [45] proposed a micropump with which the piezoelectric transducer was attached to the bottom of the substrate on which the channel was formed. SAW was generated by the transducer, and the wave was radiated into the liquid through the substrate under the refraction angle. This method is not limited to the size of the channel and offers more choices for the substrate of the system. A similar approach has been demonstrated with an open channel ablated by laser into the substrate in Figure 2.11b [46]. As with the SAW-driven transport, the micropumping velocities achieved are extremely high, on the order 1 cm/s, which is one to two decades larger than

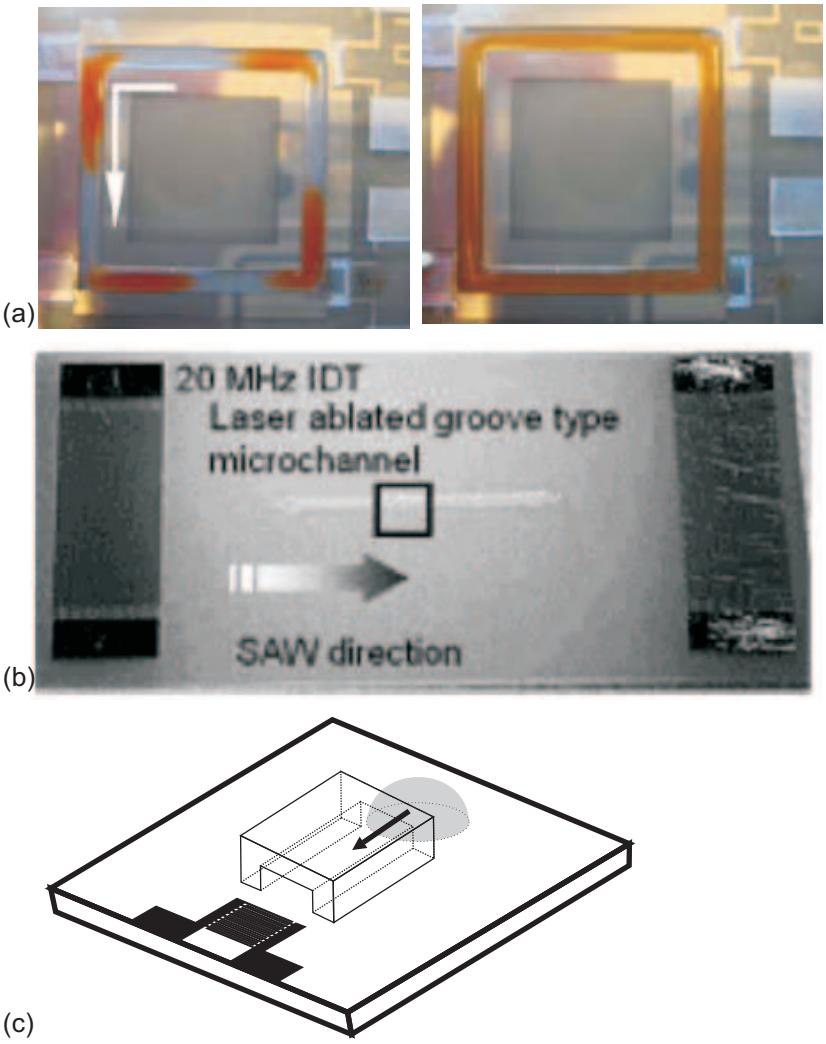

Figure 2.11: SAW micropump: (a) Counterclockwise flow in open channel driven by a IDT pitch of 200 μm; (b) A microchannel is laser ablated into the SAW substrate; (c) Fluid retraction through a closed PDMS channel.

that possible with electrokinetic micropumps.

Fluid could also be pumped through a closed microchannel [47]. A PDMS closed channel was mounted on the $LiNbO_3$ substrate. The channel was aligned along the wave propagation direction. A drop of water was placed at one end of channel further away from the IDT as shown in Figure 2.11(c). The overall force balance at the liquid-solid interface system did not allow the channel to be filled. Upon switching on the transducer, the fluid is extracted to the other end through the microchannel by liquid atomization and condensa-

tion. The process continued until the fluid retracted to the opposite end. The velocity was observed to be up to 2.6 mm/s for water. This method provides an effective mechanism for withdrawing liquid for lab-on-chip applications. However, high input power (30 dBm) is required to achieve an efficient pump rate. Based on the above method, Masini et al. [48] employed multiple SAWs in counter flow micropumps for on-chip liquid motion control in two-dimensional (2D) microchannel arrays. By selectively exciting single or multiple SAWs, fluids could be drawn from their reservoirs and moved towards selected positions of a microchannel grid. Splitting of the main liquid flow was also demonstrated by exploiting multiple SAW beams. The results showed that these SAW counterflow micropumps were good candidates for truly integrated on-chip fluidic networks allowing liquid control in arbitrarily shaped 2D microchannel arrays.

SAW Micromixer

Mixing in microchannel is a challenging task due to the natural laminar characteristics of flows. Rapid mixing of liquids inside a sealed microchannel could be achieved with the usage of SAW. Srithiran et al. [49] demonstrated a SAW mixer in a Y-shaped channel, Figure 2.12(a). The SAW device was placed directly under the junction of the inlets for an effective mixing effect. The wave propagation was designed to be perpendicular to the flow direction. The channel reported was 75 μm in depth and 100 μm in width. Water was filled in one inlet while fluorescent beads (1 μm diameter) diluted in water was introduced to the other inlet, Figure 2.12(b). Different voltages were used to verify the mixing efficiency at a fixed flow rate of 250 μm/s. Complete mixing state was achieved at a distance of 2 mm downstream, when SAW power was turned on [Figure 2.12(d)], compared to a mixing

fraction of 50 % (purely due to molecular diffusion) at the distance of 50 mm downstream, Figure 2.12(c). Another micromixer utilizing SAW on a Y-cut 128° $LiNbO_3$ was reported by Tseng et al. [50]. In this work, a Y-shaped PDMS channels were bonded directly onto the SAW substrate through an O_2 plasma surface treatment process. The parallel type (where the wave propagation is parallel to the flow direction) and the transverse type (the wave propagation is perpendicular to the flow direction) were investigated. Rhodamine B dyes and buffer solutions (sodium borate) were electrokinetically driven (100 V/cm) by a high-voltage power supply from two inlets of the channels. Mixing efficiency of more than 80 % was reported at 2 mm downstream from the mixing junction, Figure 2.12(f). The parallel type mixer was reported to have a better mixing efficiency than the transverse type.

SAW Sorter

Droplet motion could be directed in a microchannel by SAW [51]. SAW sorting is independent of the properties of the objects to be sorted such as dielectric constant or charge because it actuates a bulk fluid flow. The microchannel was 50 μm in depth and 100 μm in width. Mono dispersed water droplet entered the channel from the bottom and flowed toward the left outlet based on the PDMS channel design, Figure 2.13(a). The IDT was placed perpendicular to the left of the channel. When the SAW power was turned on, acoustic streaming would drive the droplets to the right outlet. Individual droplets were actively directed along separate microchannel paths at a high volumetric flow rates. This phenomena is useful for droplet sorting. Franke et al. [52] further improved this method to actively direct cell in a microchannel. Utlizing flow focusing, cells were aligned at the middle at the channel by two shealth flows. A SIDT with tapered shape with a

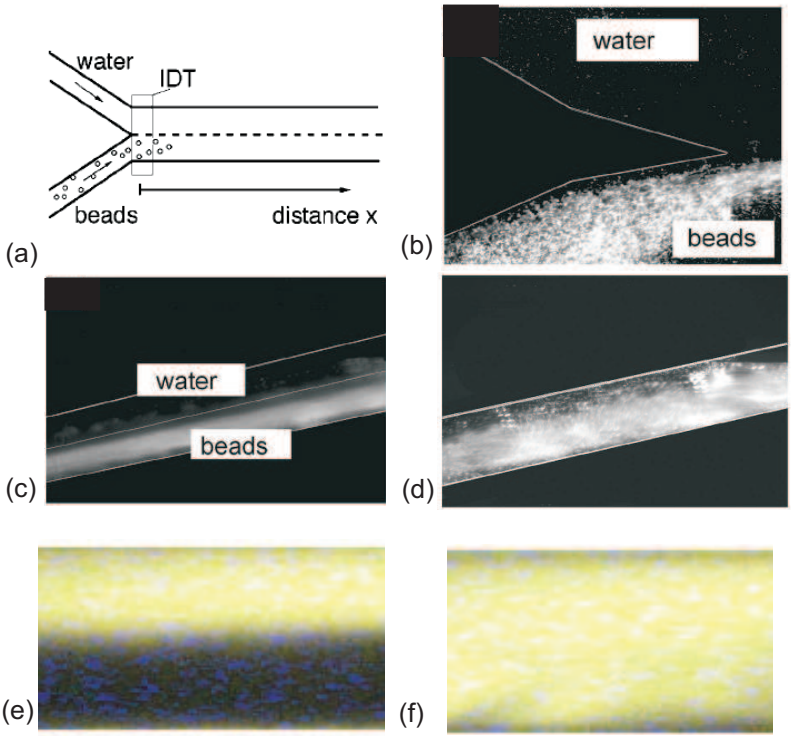

Figure 2.12: SAW induced laminar flow mixing inside a microchannel: (a) Schematic drawing of the setup; (b) Laminar flow (beads flow and water flow) at the channel entrance without mixing; (c) Laminar flow inside the microchannel without mixing, and (d) mixing of the bead flow with water flow upon applying SAW (e-f) images of fluorescence dyes (Rhodamine B) in the microchannel of the parallel-type active mixer when SAW is turned on for 2 s.

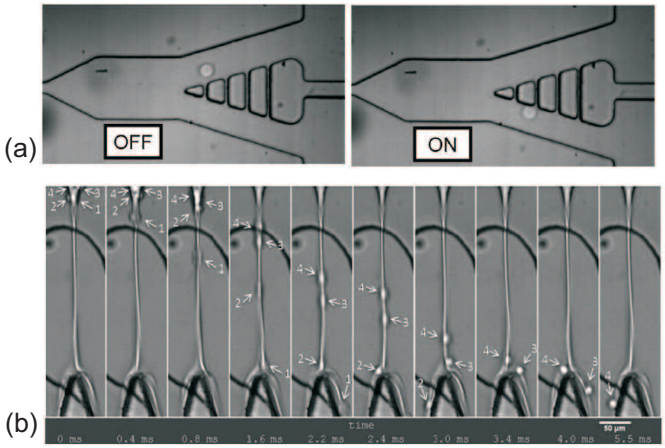

Figure 2.13: Droplet switching(a) Droplet was direct from the top channel to the bottom channel when SAW is turned ON (Franke et al., 2009); (b) A time sequence of MV3 cells sorted at a high rate of 1 kHz in collect and waste outlets upon application of a periodically oscillating SAW amplitude (Franke et al., 2010).

decreasing finger repeat distance varying from 23 to 28 mm was placed perpendicularly to the flow. The purpose of using SIDT is to maintain a narrow wave path width for the sound wave propagating on the substrate because the finger spacing only obeys the resonance condition at one position. By switching the SAW on and off, a small portion of the focus flow would be deflected by the SAW. Cells, hence, could be sorted into the collecting and waste channels respectively. MV3 cells were sorted at a high rate of 1 kHz in this work, Figure 2.13(b). SAW sorter offers an alternative solution compare to other methods with advantages such as fast response time, high throughtput and simple integration.

Another sorting method reported by Franke et al. [53] utilizing SAW generated microvortices in microfluidic channels for the accumulation of microparticles. Liquids were confined to virtual tracks simply by chemical modification of parts of the chip surface. A OTS layer was deposited on top of a Y-cut 128° $LiNbO_3$. A closed loop design was then patterned and subbsequently formed by etching the OTS in oxygen plasma. The hydrophilic track was exposed and liquids were confined to desired geometries by surface

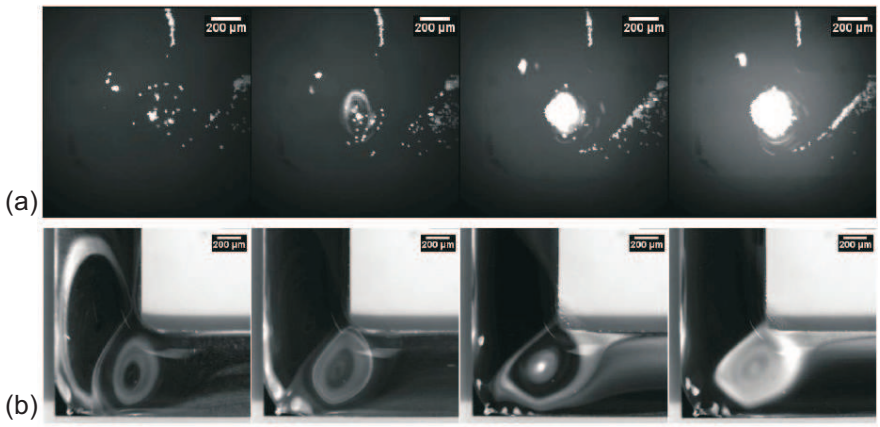

Figure 2.14: Microparticles accumulation due to a SAW induced vortice at a corner of an open fluid channel (a) Particles of 4.8 μm diameter accumulate with time (upper row); (b) smaller particles of 0.55 μm diameter were successfully trapped by increasing the power of the SAW (lower row).

tension. The corner of a rectangular microchannel is irradiated by a wide SAW beam. When SAW was launched into the liquid corner, flow patterns were created typically in the form of two vortices. Particles injected into the flow were accumulated and dynamically trapped in one of these vortices. The collected particles stayed in the position of the vortex when SAW is turned off. Generally, larger particles can be collected at more moderate SAW power levels compared to smaller particles, Figure 2.14(a). By adjusting the SAW power level, smaller particles (0.55 μm diameter) could also be trapped in the vortice, Figure 2.14(b). Particles size could be sorted by tuning the applied SAW power.

2.2.2 Standing SAW and Its Applications

Standing SAW microfluidic devices exploit multiple IDTs on a piezoelectric substrate. The interference of waves generated by these IDTS created a standing wave with periodic distribution of pressure nodes and anti-nodes in the liquid medium contacting the substrate. Particles in the suspension liquid would be driven towards either the nodes or anti-nodes

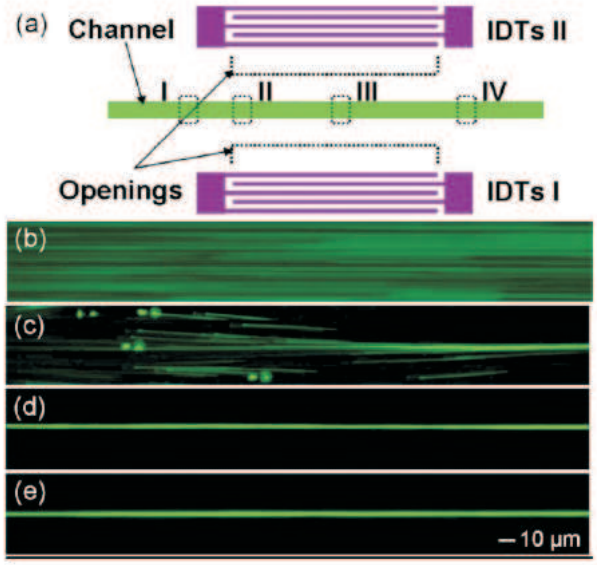

Figure 2.15: PArticle focusing: (a) Schematic of a SSAW particle focusing device; (b-e) Captured images of fluourescent particles at positions I-IV.

depending on the density and the compressibility of the fluid medium. Various applications have been demonstrated utilizing this particles redistribution.

Particle Focusing

Particle focusing could be achieved by a few methods: 3D-hydrodynamics, dielectrophoresis and others. A new method was proposed by Shi et al. [54] employing standing surface acoustic wave to focus particle. The device consists of a pair of interdigitated transducer deposited on $LiNbO_3$ and a PDMS channel bonded between the transducers, Figure 2.15(a). A RF signal was applied to transducers launching SAW from opposite direction into the microchannel and formed a SSAW. If the channel is designed to have the width of half the pitch, only one node (or antinode) appeared inside the channel. Particles were pushed to this single node (antinode) due to the acoustic force, Figure 2.15(b). A dilute solution (1.176×10^7 beads/mL) of 1.9 μm diameter fluorescent polystyrene particles in water was used in the experiment. Stable focusing was achieved with a line width of 5 μm. This

method is frequency dependent, and the focusing width is inversely proportional to the frequency. Devices with with working wavelengths of 100 μm and 200 μm respectively were tested under the same applied power (25 dBm). The measured focusing width for device II (200 μm) is approximately 10 μm about twice of width measured in device I (5 μm). This observation can be explained by the balance of the acoustic radiation forces and the interparticle forces which are originated from the acoustic oscillation between particles within the focusing band, where the particles are close to each other. When particles are driven close to each other toward the pressure node by the acoustic radiation forces, the total effect of the interparticle forces will become repulsive to balance the minimum acoustic radiation force as explained by Shi et al [54]. SSAW based-focusing device provide a simple, fast method compared to other current focusing techniques.

Particle Patterning

Particle manipulation and patterning have many potential applications in biological micro array, tissue engineering or bio sensor array. An active method utilizing SSAW for particles patterning has been proposed. When SSAW is generated in a fluid medium, pressure nodes and antinodes are induced due to acoustic pressure. Dispensed particles, when in contact with such environment, would be attracted toward pressure nodes or anti-nodes formed in a fluid channel/chamber. Particles alignment into line was achieved inside a fluid chamber with a pair of IDTs positioned opposite each other [55]. 1 μL aqueous suspensions of latex particles, at a concentration of 4.5×10^5 μL^{-1}, were pipetted onto the lithium niobate surface in the SAW beam path, defined by the acoustic aperture between the transducer pairs. The distance between lines could be adjusted by changing the work-

ing resonance frequencies. For powers above 0 dBm applied to each transducer, the latex particles within the fluidic channel arranged themselves perpendicular to the SAW propagation direction with a separation equal to half of the SAW wavelength, Figure 2.16(a). The stability and speed of line formation was observed to improve as a function of applied power, so the following measurements were therefore performed at the maximum available power of 17 dBm per IDT. SSAW two-dimensional particles patterning could be formed by rearranging the position of multiple IDTs. Wood et al. [56] used two pairs of SAWs with the chamber positioned at the centre, Figure 2.16(b). The standing wave would drive particles into an array with spacing equal to half of the SAW wavelength (or half of the pitch). Inside a chamber of a diameter of 1.2 mm, 456 nodes were reported to form an array of particles. Shi et al. [57] retrieved similar results with only 2 transducers arranged in the orthogonal direction. The device layout reported in this work is shown in Figure 2.16(c). Due to this configuration, the period of the 2D pattern would be $\sqrt{2}/2$ times the SAW working wavelength. The size of the bead aggregations at the pressure nodes can be tuned by altering the applied power. The higher is the applied SAW power, the higher is the acoustic radiation force resulting in closer bead aggregations. By reducing the concentration of the beads, single-particle patterning can be achieved. The spacing of the array could be adjusted by manipulating the SAW frequencies. The so-called ”SAW tweezers” offers advantages such as high speed, low power consumption and easy integration into a system.

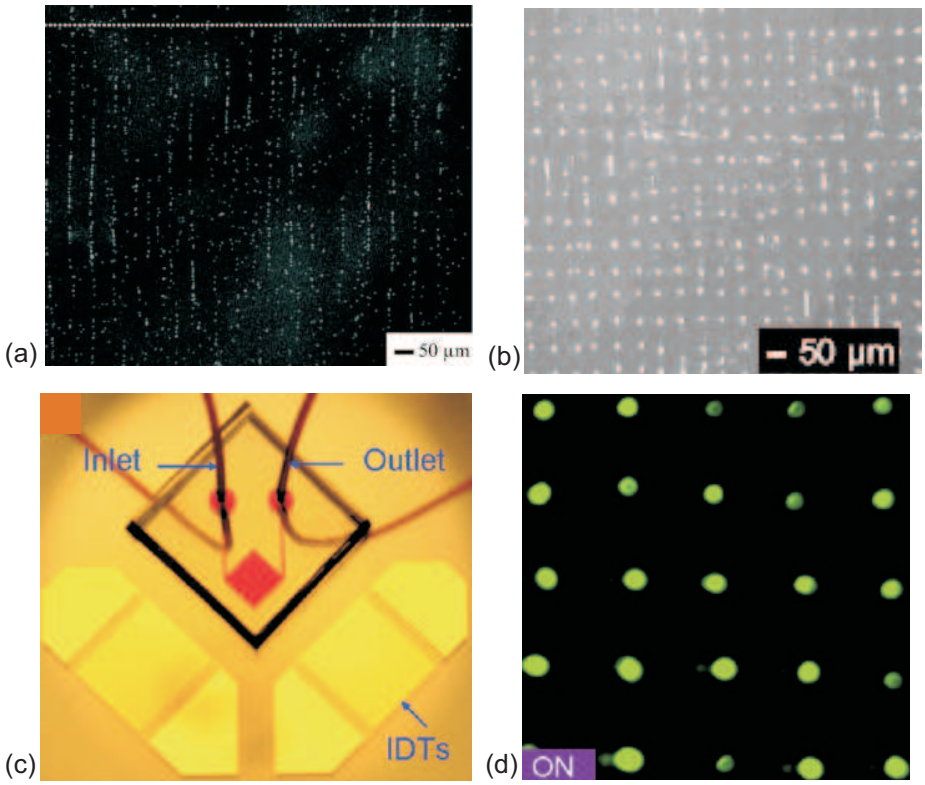

Figure 2.16: (a) Particles alignment with one pair of IDTS; (b) 2D particles patternings due to SSAW generated by 2 pairs of IDTS; (c-d) ”SAW twezzer” device and distribution of the microbeadswith by 2 IDTs in orthogonal configuration.

Particles Sorter

An effective particle sorting system is crucial for applications in medical diagnosis and biological field. The sorting mechanism is based on either the size or the particle physical properties of the particle. Besides its applications in focusing, patterning, SSAW also provides an active, fast, simple and high throughput mechanism in sorting particles [58]. The device consisted of a pair of IDT with a PDMS channel bonded between them. The mixture of particles with different sizes was squeezed between the two outer inlets and the sheath flow was injected through the middle inlet to form three laminar flows inside the channel. Upon activating the two transducers, the SSAW was formed on the piezoelectric surface. Based on the channel design, only one pressure node (antinode) was formed inside the channel. The particles could be attracted to this pressure point (node or anti-node) only if the acoustic force is larger than the shear flow force.The primary acoustic force F_r and the viscous force F_v on a particle can be expressed as:

$$F_r = -\left(\frac{\pi {p_0}^2 V_p \beta_m}{2\lambda}\right)\phi(\beta,0)\,sin(2kx), \tag{2.1}$$

$$\phi = \frac{5\rho_p - 2\rho_m}{2\rho_p + \rho_m} - \frac{\beta_p}{\beta_m}, \tag{2.2}$$

$$F_v = -6\pi\eta r v, \tag{2.3}$$

where p_0 is pressure amplitude, V_p is particle volume, λ is ultrasonic wavelength, k is wave vector, k is the distance from a pressure node, ρ_m is the density of the medium, ρ_p is the density of particles, β_m is the compressibility of medium, β_p is the compressibility of

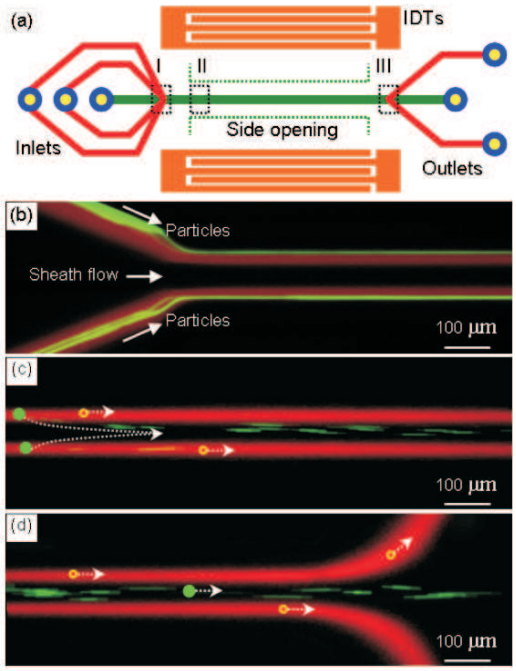

Figure 2.17: The SSAW sorter: (a) Schematic overview of the SSAW sorter; (b-d) Captured images of fluourescent particles at positions I-III.

particles, η is the medium viscosity, r is particle radius and v is relative velocity, respectively. When ϕ exceeds 0, the particles are forced toward the pressure node, and when ϕ is less than 0, the particles are forced toward the pressure anti-node. And when ϕ is larger than 0 and the pressure nodes are located at the walls of the microchannel, the particles experience an acoustical force that drives them toward the channel walls.

Sorting area was the intersection of the microchannel and the SAW aperture. Fluorescence particles of two diameters 4.17 μm (green) and 0.85 μm (red) were used. For green particles of a larger diameter, the acoustic force is large enough to push them into the middle flow, while the red particles remained in the outer stealth, Fig. (11). With the flow speed of 2.5 mm/s, the separation time of the green fluorescence only took 360 ms. The paper reported an efficiency of 80% of large particles migrating to the central stream, which is comparable or higher than other techniques.

Chapter 3

Acoustic streaming

Acoustic streaming is the fluid flow induced by the nonlinear interaction between a sound wave and a fluid medium. Acoustic streaming theory has been firstly studied and discussed in Rayleigh work on theory of sound. Further important works on acoustic streaming have been developed by Eckart [59], Markham [60] and Nyborg [61]. Despite the mature history of the field, it is demonstrated mainly for academic purpose, for example inKkundt's tube. It is only recently that acoustic streaming has found various potential usage in microfluidic applications. In such applications, the induced stream could be exploited as an external mean to enhance mixing and to pattern microparticles and cells.

The streaming phenomena are usually very complicated. The governing equations are nonlinear and anaytical solutions are difficult to get without any assumptions. In the scope of this master project, only fundamental acoustic streaming theory will be provided from the fluid mechanics point of view. Starting with the continuity and Navier-Stokes equations, attempts would be made to derive to the first order and second order fluid equations. The streaming velocity is the solution of the above second order equations. The general solution

method used in this chapter is the successive approximation technique, a common method reported in classical work on acoustic streaming. Employing this method, the governing equations are linearized and could be solved.

The derivation in this chapter follows the work of Moroney in his Phd thesis [62] which is based on Nyborg's key review paper in acoustic streaming theory [61].

3.1 Governing equations

3.1.1 Navier-Stokes equations

The starting point of fluid mechanics are the continuity and the Navier-Stokes equation. A continuity equation in physics is an equation that describes the transport of a conserved quantity:

$$\frac{\partial \rho}{\partial t} + \nabla.(\rho \mathbf{v}) = 0, \tag{3.1}$$

where ρ is the fluid density, $\mathbf{v}$ is the fluid velocity. The above equation could be rearranged by rewriting the time-derivative of the velocity to simplify later derivation. The time-derivative of the velocity is:

$$\frac{\partial(\rho \mathbf{v})}{\partial t} = \rho \frac{\partial \mathbf{v}}{\partial t} + \mathbf{v} \frac{\partial \rho}{\partial t} \tag{3.2}$$

Subtituing the above expression into equation 3.1, the continuity equation is given as follow:

$$\rho \frac{\partial \mathbf{v}}{\partial t} = \frac{\partial(\rho \mathbf{v})}{\partial t} + \mathbf{v} \nabla.(\rho \mathbf{v}) \tag{3.3}$$

The Navier-Stokes is an expression of Newton's law to fluid motion, along the fluid stress is the sum of a diffusing viscous term (proportional to the gradient of velocity), plus

a pressure term.

$$\rho\left[\frac{\partial \mathbf{v}}{\partial t}+(\mathbf{v}.\nabla)\mathbf{v}\right]=-\nabla P+\left[\mu'+\frac{4}{3}\mu\right]\nabla\nabla.\mathbf{v}-\mu\nabla\times\nabla\times\mathbf{v}, \tag{3.4}$$

where μ and μ'are the shear viscosity and bulk viscosity of the fluid respectively. And P is the pressure in the fluid.

Combining equation 3.3 and equation 3.4, the Navier-Stokes equation could be described as:

$$\rho\frac{\partial \mathbf{v}}{\partial t}+\mathbf{F}=-\nabla P+\left[\mu'+\frac{4}{3}\mu\right]\nabla\nabla.\mathbf{v}-\mu\nabla\times\nabla\times\mathbf{v} \tag{3.5}$$

$$\mathbf{F}=-\rho\,(\mathbf{v}.\nabla)\,\mathbf{v}-\mathbf{v}\,(\nabla.\rho\mathbf{v}) \tag{3.6}$$

The term **F** in equation 3.5 is known as a nonlinear body force which results in acoustic streaming. The sign of **F** is arbitrary.

3.1.2 Equation of state

If the liquid is incompressible, the effect of acoustic streaming is difficult to understood. The liquid is therefore needed to be treated as compressible liquid. An equation of state to relate the fluid density to its corresponding pressure must be included in the study. Nyborg used the following equation:

$$P={v_F}^2\rho+R\frac{\partial \rho}{\partial t}, \tag{3.7}$$

where R is a relaxation constant to represent the relaxation effects in the liquid. This relationship is reported to be valid only in the first order approximation. Additional term

will be presented in second order term. For simplicity, Moroney assumed the extra term is negligible.

The equation of state along with continuity equation and Navier-Stokes are a complete set of equation for describing fluid motion in acoustic streaming theory.

3.2 Successive approximation method

As mentioned above, the equations are nonlinear and generally difficult to solve. Successive approximation method is used here. The advantage of the sucessive approximation method is the generation of linear equations for each order of solution.

$$\mathbf{v} = \mathbf{v}_0 + \mathbf{v}_1 + \mathbf{v}_2 + \cdots \tag{3.8}$$

Assuming the steady-state sound field, the static velocity $\mathbf{v}_0$ is 0. Equation 3.8 is rewritten as:

$$\mathbf{v} = \mathbf{v}_1 + \mathbf{v}_2 + \cdots \tag{3.9}$$

Equations for pressure and fluid density at any point in the liquid are as followed:

$$P = P_0 + P_1 + P_2 + \cdots \tag{3.10}$$

$$\rho = \rho_0 + \rho_1 + \rho_2 + \cdots \tag{3.11}$$

Here $\mathbf{v}_1$, P_1 and ρ_1 are first order approximations solutions of the problem. $\mathbf{v}_2$, P_2 and ρ_2 are second order approximations solutions respectively. In this succssive approximation

method, a first order approximation need to be solved and hence is used to get a second-order approximation.

3.3 Boundary conditions

For SAW induced streaming, the fluid flow boundary conditions will be the non-slip condition at the substrate surface. The fluid velocites at the substrate are determined from the surface velocity due to travelling wave. Other boundary conditions depend on the experiment configuration (either droplet or channel configuration).

3.4 Second-order equations and averaging streaming velocity

By deriving equation 3.5, the second-order Navier-Stokes equation is:

$$\rho_0 \frac{\partial}{\partial t}\left(\mathbf{v_2}+\rho_1\mathbf{v_1}\right)-\mathbf{F}_2=-\nabla P_2+\left[\mu'+\frac{4}{3}\mu\right]\nabla\nabla.\mathbf{v}_2-\mu\nabla\times\nabla\times\mathbf{v}_2 \tag{3.12}$$

$$\mathbf{F}_2=-\rho_0\left[\left(\mathbf{v_1}.\nabla\right)\mathbf{v_1}+\mathbf{v_1}\left(\nabla.\mathbf{v_1}\right)\right] \tag{3.13}$$

The second-order continuity equation is:

$$\frac{\partial\rho_2}{\partial t}+\rho_0\nabla.\left(\mathbf{v_2}+\rho_1\mathbf{v_1}\right)=0 \tag{3.14}$$

First order approximation is assumed to be sinusoidal with an angular frequency ω, where ω is the angular frequency of the propagating wave. Second order approximations

to the solutions would yield correction terms to be added to $\mathbf{v}_1$,P_1 and ρ_1 (Nyborg). Where $\mathbf{v}_2$ is the streaming velocity we are seeking. It includes time-independent quantitie and term with frequency 2ω. In other words, the second-order velocity has a static term and a frequency doubled term. By time avaraging the above term by integrating over time (one period) then devide by the peroid of the first-order, only the period static term is left. This is the average velocity of the acoustic streaming which is important in SAW-based microfluidic applications.

Acoustic streaming theory is a complicated topic. In this chapter, only fundamental knowledege of acoustic streaming is presented from the point of view of fluid mechanics. By the method of successive approximation, the first-order approximation quantities are determined and then used to find a second-order approximation. Second-order equations are solved and the velocity solution is the induced streaming velocity.

Chapter 4

Fabrication Technique and Characterization Method

4.1 Fabrication

4.1.1 Piezoelectric Substrate

As mentioned in Chapter 1, Lithium Niobate ($LiNbO_3$) is the substrate of choice in this project due to its high electromechanical coupling coefficient and the ability to generate SAW in two direction. However, $LiNbO_3$ is thermally quite fragile due to a very large temperature coefficient (approximately 80 ppm/°C for a SAW device with propagation in the Z direction on Y-cut $LiNbO_3$) [63]. In order to avoid substrate cracking, a conductive epoxy (CW2400, Chemtronics) was used instead of soldering for the wire connection. Operating voltage should not exceed a certain threshold value. Substrate cracking occurs during experiments when the operating voltage exceeds a value of 100 V peak-to-peak. External

Table 4.1: Properties of $LiNbO_3$ substrate

Optical Anisotropy	Refractive indices	Melting point (C°)	Crystal density (kg/m^3)
Uniaxial, c-axis	n_e=2.203; n_o=2.286	1260	4647

cooling is needed in experiments where high acoustic SAW energy is required. Table 4.1.1 summerizes properties of $LiNbO_3$ substrate [13].

From the above table, $LiNbO_3$ is a biefringence (or double refraction) crystal with two refractive indices, n_e and n_o are the refractive indices for polarizations parallel (extraordinary) and perpendicular (ordinary) to the axis of anisotropy . Hence, light pass through the substrate will shows double refraction. In other word, the $LiNbO_3$ device observed by microscope will display two images. A linear polarizer (Hoya PL) will be needed to filter one of the refraction image.

4.1.2 Mask Design

For the device pattern, features are drawn using the software Clewin (WieWeb software, The Netherlands) - a mask drawing programm. The features are then printed on a high resolution plastic mask with a resolution of 9600 dpi (dot per inch) from Infinite graphics Pte Ltd, Singapore. The minimum critical dimension of the plastic mask is 20 μm. The tone of the mask needs to be set accoding to the nature of the photoresist used in the lithography process. Figure 4.1 shows a layout of a microchannel pattern in a process involving a negative photoresist.

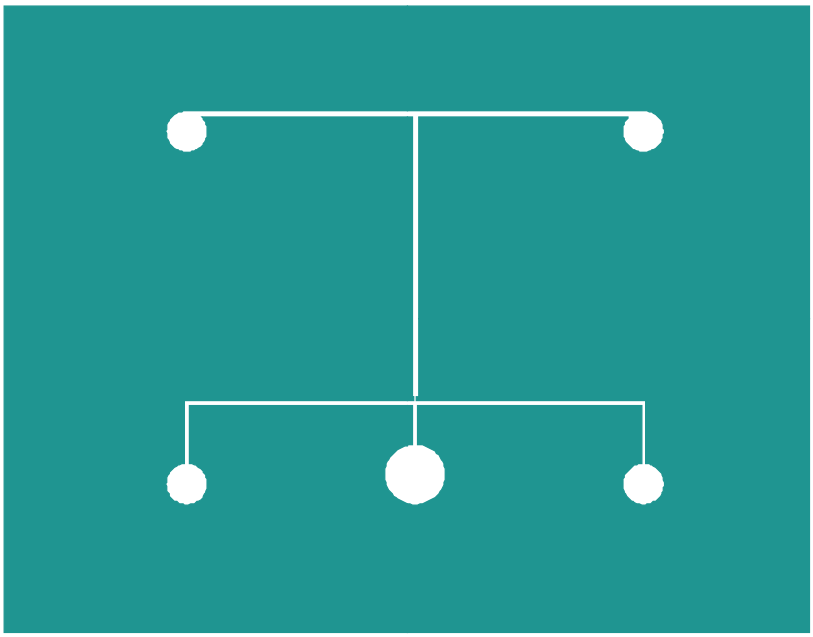

Figure 4.1: Dark tone mask for the fabrication of microchannel.

4.1.3 Interdigitated Electrode Patterning

SAW devices require an IDT to launch acoustic wave on a piezoelectric substrate. The comb-like electrode structure could be fabricated using a lift off process. The metal film used to make the IDT must be thick enough to offer low electrical resistance and thin enough so that it does not present an excessive mechanical load to the SAW. Normally, materials of choices for electrode are aluminum (Al) or gold (Au). Since the operation of SAW device was performed in normal air condition, gold is prefered due to the easy oxidazation of Al. The gold metalization thickness was about 300 nm and a thin layer of chromium (Cr) or titanium (Ti) is used to enhance the adhesion of the gold to the substrate. The detailed process of IDT patterning was shown in Figure 4.2. A double-sided polished Y-cut 128^{o} $LiNbO_3$ was first ultrasonicly rinsed in Acetone for 5 minutes, then in Isopropyl alcohol (IPA) for 5 minutes and finally in DI water for 2 minutes. This rinsing process is an

important step to remove all organics subtances sticking on the substrate surface which may be detrimental to the adhesion of the resist. The wafer is blown dry by a nitrogen (N_2) gun and baked at 120^oC for 15 minutes. This dehydration bake was done to remove any water on the surface that would reduce the adhesion. AZ 9260 photoresist (AZ Electronic Materials) was spin coated on the wafer by a spin coater (Delta80BM). The spin speed of the coating process was 3000 rpm (round per minute) for 30 seconds which results in a resist thickness of $7-8$ μm. Since the metal thickness is less than 500 nm, such photoresist thickness is sufficient for a good lift off result. The coated substrate was then post baked at 95 °C for 1 minute to evaporate the excess solvent and stabilised the film. After the soft baking, the substrate was removed from the hot plate and cooled down at room temperature for around 2 minutes before exposure. An exposure dosage of 270 mJ/cm^2 was found to be an optimal dosage for the process, Figure 4.2. Since AZ9260 is a positive photoresist, the cross-link of chemical is broken and the exposed area will be soluable in a diluted solution of AZ100 developer (AZ100:DI water = 1:2.5 in volume), Figure 4.2(c). Eventhough the majority of exposed photoresist was dissolved, a thin residue resist layer would remained on the surface of the substrate. To achieve better adhesion, a mild oxygen plasma process (descum) was performed to etched away this residue layer (Teknix RIE). Layers of Ti (20 nm) and Au (300 nm) was subsequently sputtered on the processed substrate by a sputter magnetron (Coaxial), Figure 4.2(d). Excessive metal was lifted off in acetone and IDT was formed on the substrate, Figure 4.2(e).

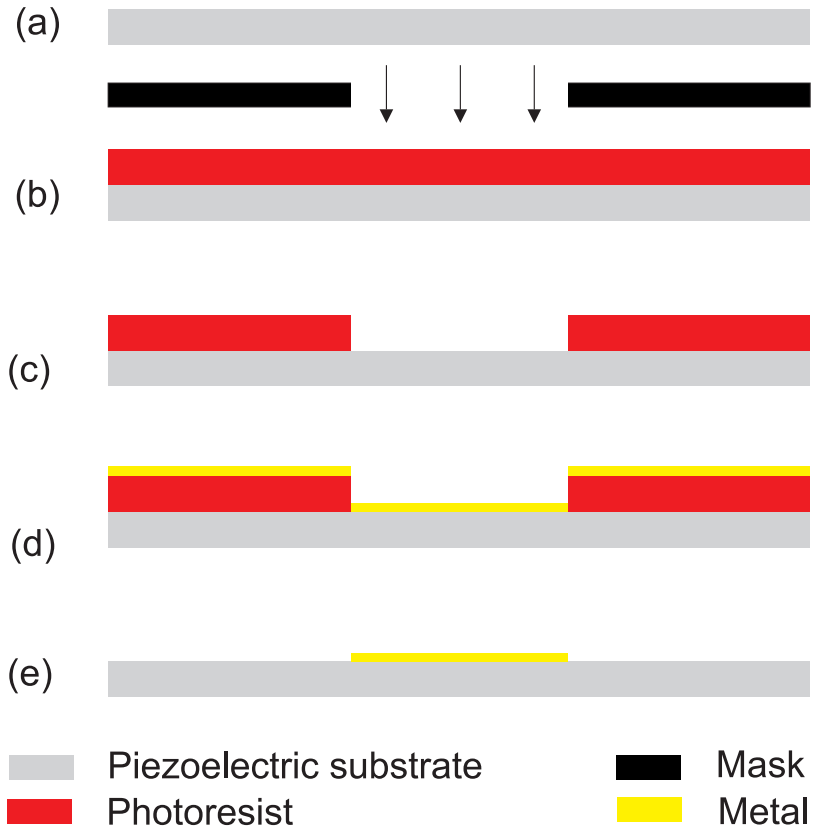

Figure 4.2: Lift off process for IDT electrode patterning.

4.1.4 Fabrication of Microchannel

As mention in the literature review, closed microchannel were fabricated by using PDMS material. The fabrication of PDMS microfluidics device using a standard soft-lithography technique was reported [64]. The mold for the microchannel was fabricated using the SU-8 epoxy (Micro Chem) which is the most common molding media used for the fabrication of PDMS-based microfluidic devices. SU-8 is a low cost negative photoresist which offer structures of a uniform height. Different grade of SU-8 is commercially available based on the viscosity of products. Depending on the height of the fabricated PDMS channel, a SU-8 product was chosen accordingly. In the experiment of this project, channel height ranges from 50 μm to 100 μm. Hence, spinning SU-8 2050 at 1700 rpm to 3000 rpm can obtain the target thickness. Similar results could also be achieved by using a less viscous SU-8 2035 at a lower spinning speed. The thickness versus spin speed characteristics of different SU-8 products (2000 series) are shown in Figure 4.3.

The detailed process of fabricating a SU-8 mold is shown in Figure 4.4. A single-sided Si wafer is cleaned in a piranha solution (a mixture of H_2SO_4 and H_2O_2) at 95°C for 30 minutes and rinsed in DI water for 5 minutes. The process is carried on to make sure that the wafer surface is free of organic residue and to promote better adhesion of SU-8 to silicon. The wafer was dried by a spin dryer (Calitech) and baked at 120°C for 15 minutes. This dehydration bake was done to remove any water on the surface that would reduce the adhesion. SU-8 2050 was dispensed to the wafer and few minutes were needed to let the SU-8 cover the whole Si surface. This step is neccessary for an improved uniformity of coating surface due to the high viscosity of SU-8. The wafer was then spin coated on a spin coater (Delta 80BM) at 3000 rpm for 30 seconds to achieve a thickness of 50 μm.

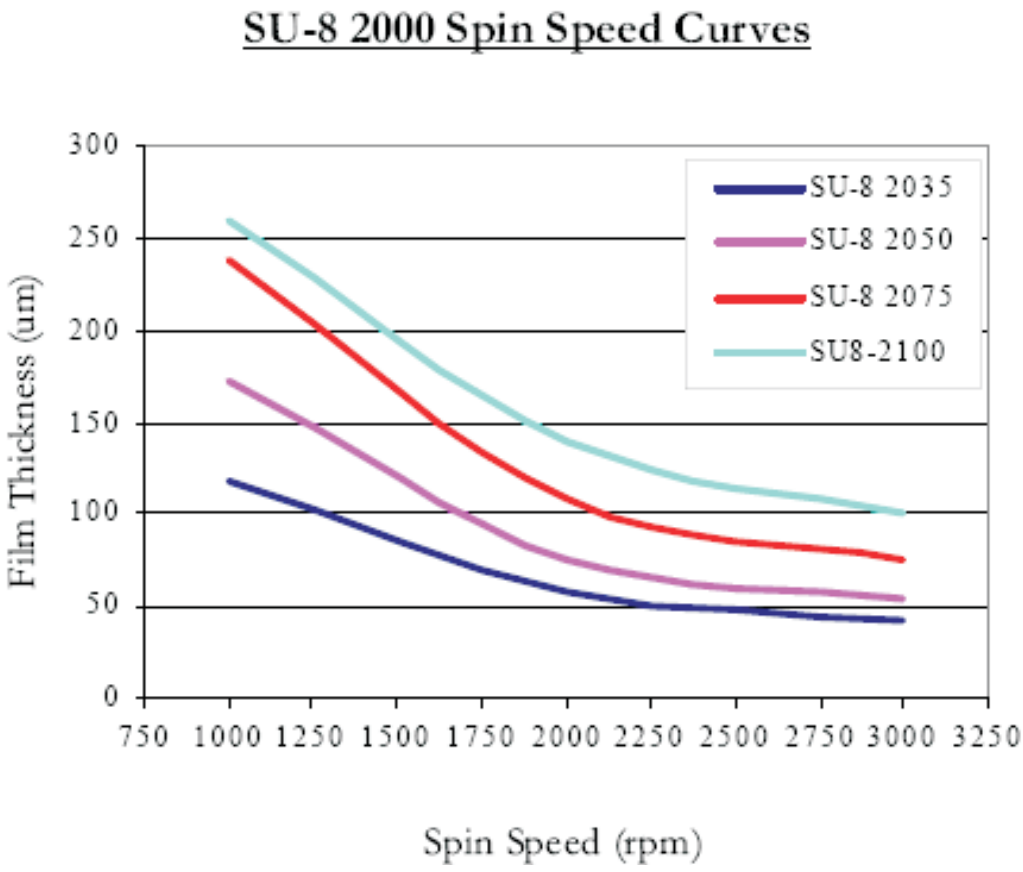

Figure 4.3: Thickness vs spinspeed of SU-8 2000 series

The prebake process was carried out afterwards on a hotplate with baking steps 65 °C for 5 minutes and 95 °C for 20 minutes. To avoid craks of such thick SU-8 layer, the temperature was slowly ramp between the above steps. After baking, the substrate was removed from the hot plate and cooled down at room temperature for 30 minutes. The patterns were transfered from a plastic mask with a resolution of 9600 dpi (Infinite graphicsPte Ltd) to the wafer by exposing to near ultravoplet (350-400 nm) radiation. An exposure dosage of 320 mJ/cm^2 was found to be optimal for the process after a few trial tests, Figure 4.4(b). The crosslinked resist is further enhanced by a post bake process of the wafer in a hot plate. A similar two step baking at 65 °C for 5 minutes and 95 ^{o}C for 10 minutes was used. The structures were then developed by immersing the substrate into the SU-8 developer (Micro Chem) for about 10 minutes. Since the resist was quite thick, IPA was frequenlty used to clean the waste SU-8 from sticking to the surface and slowing down the developing process. After developing, the wafer was blown dry with a nitrogen gun. SU-8 mold was then ready for PDMS casting, Figure 4.4(c).

The casting process started by mixing the silicone elastomer base with the curing agent (Dow and Corning's Sylgard 184) in a 10:1 weight/weight ratio. The silicone mixture is full of small air bubbles and needed to be degassed in a vacuum flask for about one hour until the mixture is clear and transparent. The SU-8 mold was placed in an Aluminum foil shaped in the form of an petri disk. The degassed PDMS was then poured onto the SU-8 mold wafer. Air bubbles generated during the pouring process were removed by blowing gently onto the surface. The casted wafer was then put into an oven at 80 °C for 2 hours for the mixture to cure and to solidify. After curing, PDMS was cut and peeled off from the SU-8 mold Figure 4.4(d). Fluid access holes are formed by punching the PDMS with

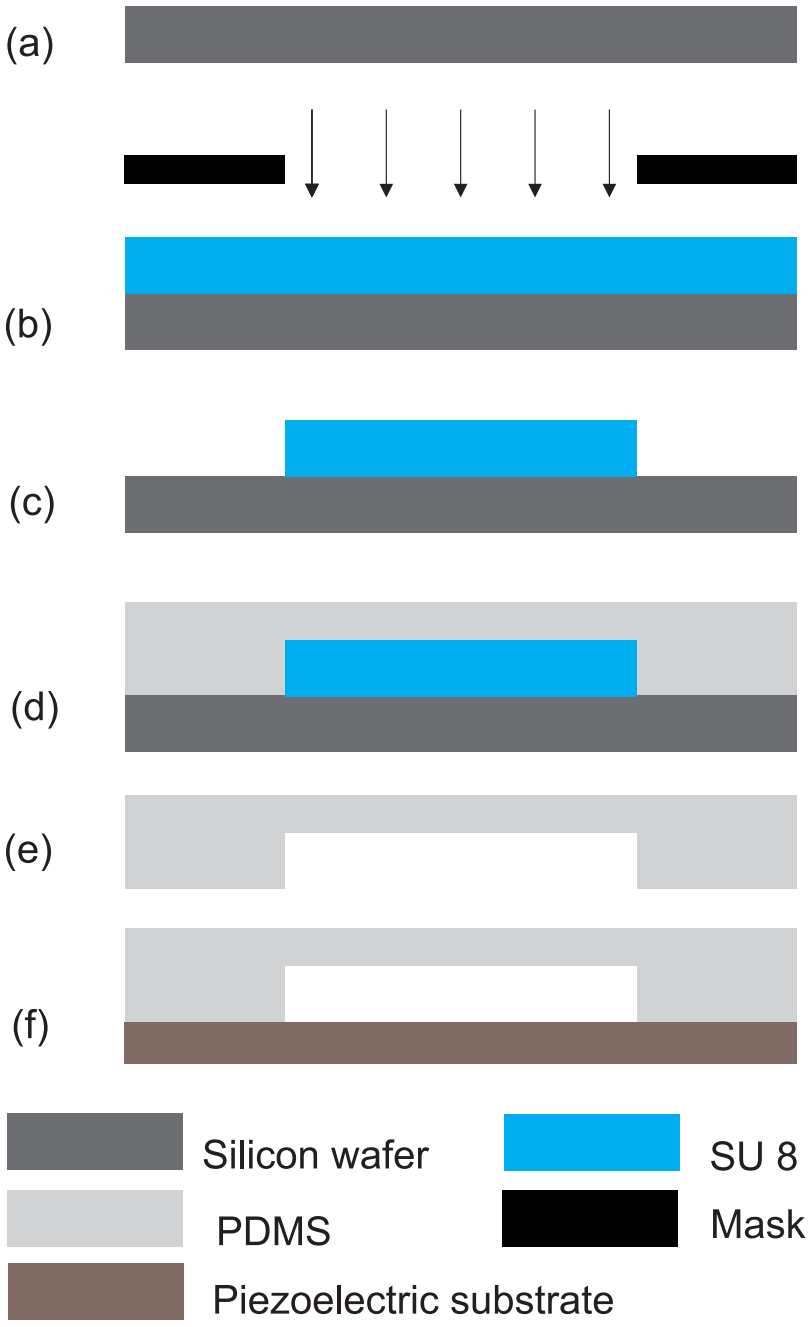

Figure 4.4: Fabrication process of the SU-8 mold and the PDMS device.

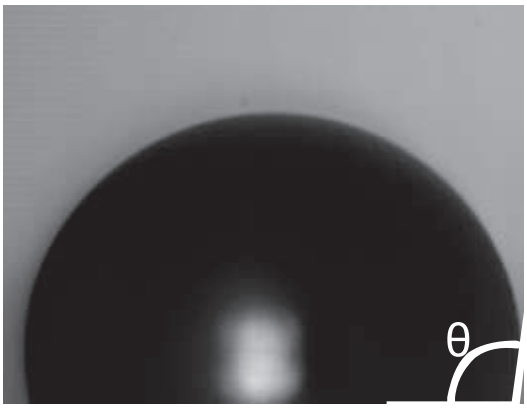

Figure 4.5: Droplet shape on a silanized piezoelectric substrate with a contact angle of $\theta \approx 105^{\circ}$.

a Harris uni-core puncher (Jed Pella, Inc). The PDMS channel was then soaked in IPA for 15 minutes followed by rinsing in distilled DI water. The PDMS part was then blown dry using the nitrogen (N_2) gas at high pressure. This is to prevent dirt and dust from accumulating on the PDMS cast. A dehydrate bake is then performed in an oven at 100 °C. PDMS channel and piezoelectric substrate is treated in an oxygen plasma cleaner (Technix) for 30 seconds, align and bonded together, Figure 4.4(d). For a better bonding integrity, a post bake process of the bonded sample at 80 °C was recommended.

4.1.5 Hydrophilic Track Patterning

In droplet-based microfluidic applications, droplets are actuated on the surface of a piezoelectric substrate. Due to the hydrophilic surface property of the piezoelectric material, water droplet has a small contact angle of $\theta = 15^{\circ}$ (on a clean and polished $LiNbO_3$ substrate) which could impede the droplet motion due to the large friction. A silanization process is, therefore, required to increase the contact angle and, hence results in better droplet actuation. For the silanization of $LiNbO_3$ substrate, octadecyltrichlorosilane (OTS, (CH_3)-$(CH_2)_{17}$-$SiCl_3$, Sigma Aldrich) was used to form a self assemblied mono-molecular

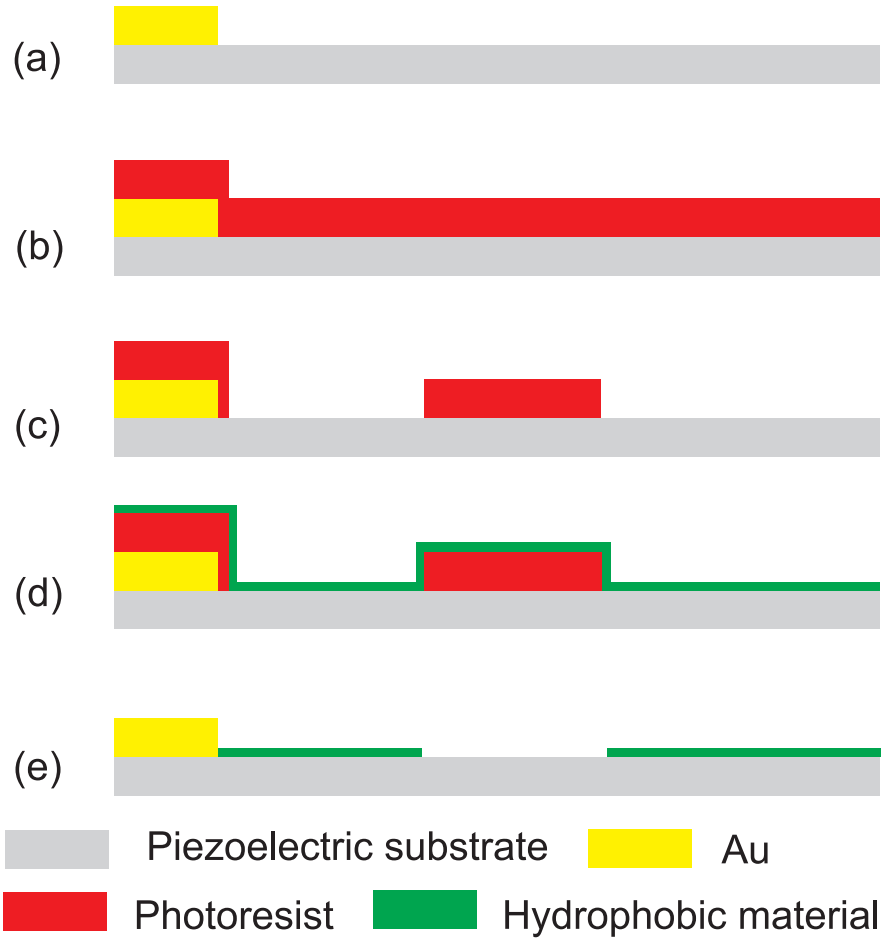

Figure 4.6: Fabrication process of a hydrophilic track on a $LiNbO_3$ substrate.

layer on the substrate. A solution of OTS (0.05% in volume) in Haptane (Sigma Aldrich) was first mixed. The piezoelectric substrate was then cleaned by O_2 plasma for 10 minutes and immersed in the above solution for 15 hours. Subsequently, the substrate was rinsed in IPA, dried and tempered at 120°C for 30 minutes. Such treatment could significantly increase the contact angle while preserving the device performance. Figure 4.5 shows the droplet shape on a silanized surface with a contact angle $\theta \approx 105°$.

In some applications, a hydrophilic track is required to guide or transport droplet more accurately. The forming process of such track could be done by a lift-off process. The fabricated $LiNbO_3$ substrate with gold electrode was subsequently cleaned by acetone, IPA

and water to remove residue organic substance. The substrate was then dyhadrated and spin coated with AZ9260 using a spin coater (Delta 80BM) at 3000 rpm to form a thin layer of resist of a thickness of 78 μm. A post bake process at 95 °C for 1 minute was performed to remove the excess solvent, Figure 4.6(b). A UV exposure dosage of 270 mJ/cm^2 with a track pattern was done on the coated substrate. The sample was then developed in an AZ developer solution (AZ400:DI water = 1:2.5 in volume) for 30 seconds, Figure 4.6(c). The sample was subsequently blown dry by N_2, silanized (as discuss above) [Figure 4.6(d)] and lift-off of photoresist in acetone. The sample with hydrophilic tracks was then ready for testing, Figure 4.6(e).

The fabrication process of microfluidic device based on SAW is carried on in Micromachines Lab 1, School of Mechanical and Aerospace Engineering, Nanyang Technological University, Figure 4.7.

4.2 Device Characterization

A network analyzer with a working bandwidth raging from 300 kHz to 1.5 GHz (Agilent E5061A ENA-L RF Network Analyzer) was used to characterize the resonance frequency of the fabricated device. The device could be measured using one-port (S_{11}) or two-port measurements (S_{12}/S_{21}). One-port measurement requires only one IDT as the emitter and receiver. In this method, an AC signal with fixed input power but varying frequencies was applied to the IDT. The reflected signal, which travels back from the device along the same signal cable, was used to transmit the input signal was captured. The resonant frequency was determined when the output has a minimum value. Two port-measurement

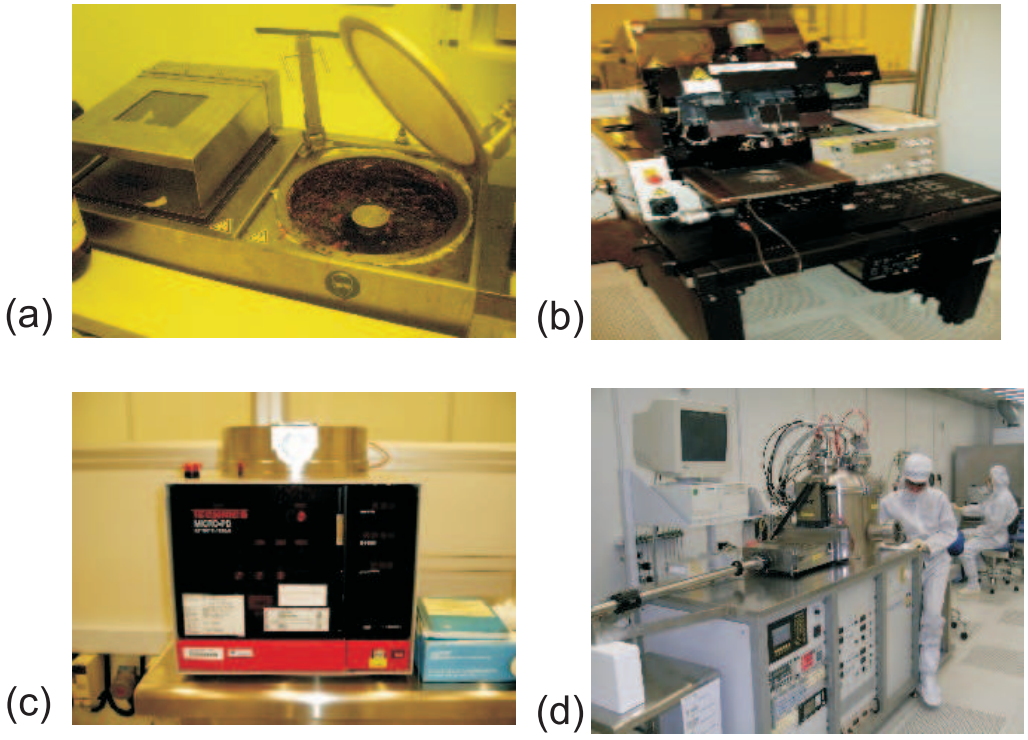

Figure 4.7: Microfabrication equipment: (a) Spin coater; (b) Mask aligner; (c) Reactive ion etching (RIE); (d) Sputter magnetron.

utilizes a pair of IDTs with one working as emitter and the other as receiver. When an AC signal with fixed input power but varying frequency was applied to the emitter, the signal is measured at the receiver. When a peak is deteted at output, the applied frequency was determined as the working frequency.

Figure 4.8 shows the measured signal S_{11} and S_{12} using ine-port and two-port measurements, respectively. The SAW appears to have multiple resonance frequencies, only the frequency that matches with the electrode design was used for optimal result. For SAW device with the electrode pitch of 125 μm, the working frequency appears to be around 13 MHz, Figure 4.8.

Table 4.2 summerizes working frequencies of SAW devices with 125 μm electrode pitch. The working frequencies appear to have a value of 13$\pm$0.5 MHz. These variations

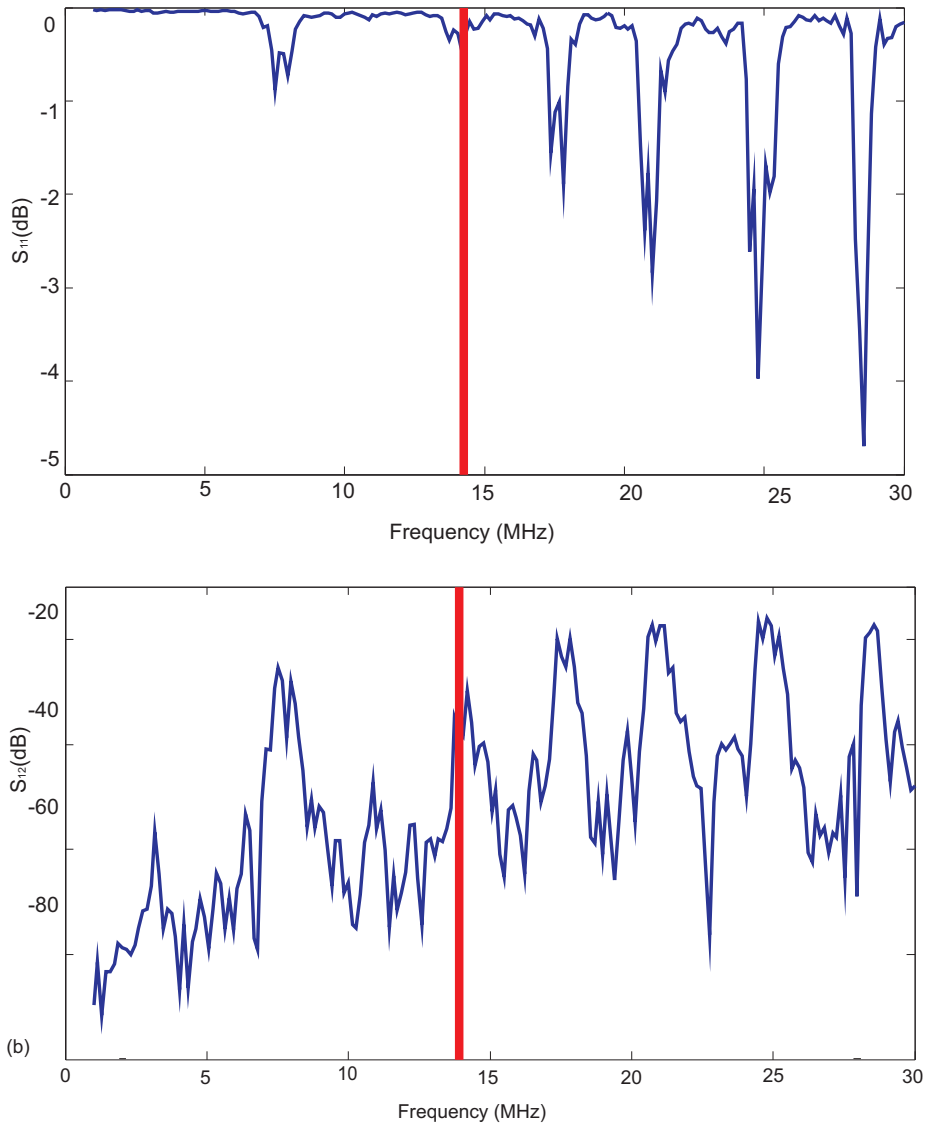

Figure 4.8: SAW device characterization: (a) In one-port measurement, resonance are depicted at frequencies where losses in S_{11} appear; (b) In two-port measurement, resonance are depicted at frequencies where spikes in S_{12} appear.

Table 4.2: Working frequencies of SAW devices with electrode pitch design of 125 μm

	Device 1	Device 2	Device 3	Device 4
Working frequency (MHz)	13.04	13.2	13.5	12.8

are due to substrate orientation and errors in lithography process.

Chapter 5

High-throughput Micromixers Based on Acoustic Streaming Induced by Surface Acoustic Wave

5.1 Motivation

Micromixer is one of the functional blocks in a microfluidic platform besides micropumps and microvalves. Many biological processes such as DNA hybridization, cell activation, protein folding involve reactions and require rapid mixing of reactants. Due to the miniaturization of the flow channels,hydrodynamic flow is governed by low Reynold numbers. The flow in microchannels is laminar and mixing of continuous flow relies purely on molecular diffusion. As a result, mixing in microchannel is a challenging task and attracts great attentions from the research community. There has been an exponential increase in the numbers of publications about micromixer recently [65]. In general, micromixers can

be catogerized as passive mixers and active mixers [66, 67]. Passive mixers utilize diffusion and chaotic advection mechanism and do not require and external force. Active mixers utilize external force to disturb the flows and enhance mixing. For passive mixers, improving mixing based on diffusion means increasing the contact interface and reducing the diffusion length. Koch et al. [68] and Hinsman et al. [69] realize these concepts by splitting the inlets into parallel lamination streams. Another approach is to introduce a three dimensional interdigitated inlet streams [70]. Splitting and recombining the streams in serial sequences could further reduce the mixing time [71, 72]. Chaotic advection could be generated in a microchannel by exploiting geometrical channel designs. A simple concept was reported by Yi et al.[73] with a bend-induced mixer. Modified Tesla structure [74], twisted channels [75] or serpentine channels [76] induce chaotic advection and significantly improve mixing. Passive micromixers often offer simple designs and easy integration into many microfluidic platforms.

In general, mixing in high throughput applications require active mixer in which external disturbances are employed. Different types of external disturbances have been reviewed such as pressure [77], electrohydrodynamics [78], dielectrophoresis [79], magnetohydrodynamics [80], and heat [81]. Acoustic energy is another candidate for realizing active mixers. Yang et al. [82] generated an acoustic field using a piezoelectric lead zirconate titanate (PZT) membrane to enhance mixing. Bubble-based acoustic mixers [83, 84] have shown significant improvement in mixing performance.

Exploiting SAW to induce acoustic streaming is another method to enhance mixing. Applying an alternate-current (AC) voltage on the electrodes at a right frequency will launch an elastic wave along the substrate surface. When this elastic wave is in contact

with the liquid with induce acoustic streaming or acoustic disturbance to the flow. Generally, advantages of SAW based micromixer lie in its simple fabrication, large disturbance force and especially fast operation compared to the other methods. In chapter 2, SAW-based micromixer have been categorized as SAW-based mixer in droplet microfluidics and in continuous flow microfluidics. The working principle of SAW droplet based micromixer is based on strong internal flow induced by the propagated wave inside droplet. Mixing quality is reported to be effective for droplet with diameters larger than the SAW wavelength due to the better coupling effect of acoustic power into the droplet. By tuning the SAW input power, mixing rate and mixing efficiency could be adjusted accordingly. SAW has been widely demonstrated for rapid mixing in droplet microfluidics [18, 7, 28]. Few studies on SAW-based micomixer in continuous flow have been reported in the literature by Sritharan et al. [49] and Tseng et al[50]. In the work of Sritharan et al., complete mixing was achieved at a distance of 2 mm downstream of a Y-channel with the influence of SAW. In the work of Tseng et al., a mixing efficiency of more than 80% at 2 mm downstream from the inlet junction with Peclet number on the order of $\mathrm{Pe} = 7 \times 10^3$.

The concept of SAW induced mixing in continuous flow is applied to a micromixer in which high flow rate of samples are used. Flow rates of water and fluorescent dye solution in a side-by-side configurations are 2 ml/h, 5 ml/h and 10 ml/h. Interdigitated electrodes are placed from a distance perpendicular to the mixing channel. The Peclet number could be as high as $\mathrm{Pe} = 74.4 \times 10^3$ in the experiment. This value is much higher compared to the above mentioned two SAW-based micromixers works. Good mixing was achieved at a0 distance of 10 mm downstream from the inlet junction even at such high Peclet number. For the first time, focusing interdigitated electrodes (FIDT) is employed

to concentrate the acoustic energy and therefore significantly improved the mixing quality compared to the traditional IDTs. Our SAW micromixer is fabricated based on standard fabrication technology (refer to chapter 3.1): lift-off process to form IDT Au electrodes on a 128° rotated Y-cut $LiNbO_3$ substrate of 500 μm thickness, soft-lithography to form PDMS microchannel, oxygen plasma treatment for bonding of microchannel on to the substrate.

5.2 Device Concept

The SAW-driven micromixer consists of a microchannel bonded to a piezoelectric substrate. The microchannel has two inlets and two outlets. The detailed dimensions of the mixing channels are depicted in Figure 5.1(a). The liquids to be mixed are introduced in a side-by-side configuration. The electrodes of the conventional parallel design and the focusing design are shown in Figure 5.1(b). When a radio frequency signal is applied to the electrode, SAW is generated and propagates transversal to the mixing channel. Acoustic streaming occurs when the wave interfere with the liquids. Mixing is induced due to the disturbance caused by the transversal acoustic streaming. By varying the applied voltage and the flow rate, mixing effects can be studied. The electrodes of the focusing design are concentric arcs with an opening angle of 90°, Figure 5.1(c). By adapting the arc shaped interdigitated electrode design, the acoustic energy becomes focus [37] and can be described by Gaussian beam theory elsewhere [85]. This focus wave energy gives rise to the higher amplitude and larger disturbance force generated accordingly as compared to the conventional parallel design. The channel is positioned at the focal point of focusing design to achieve optimal mixing.

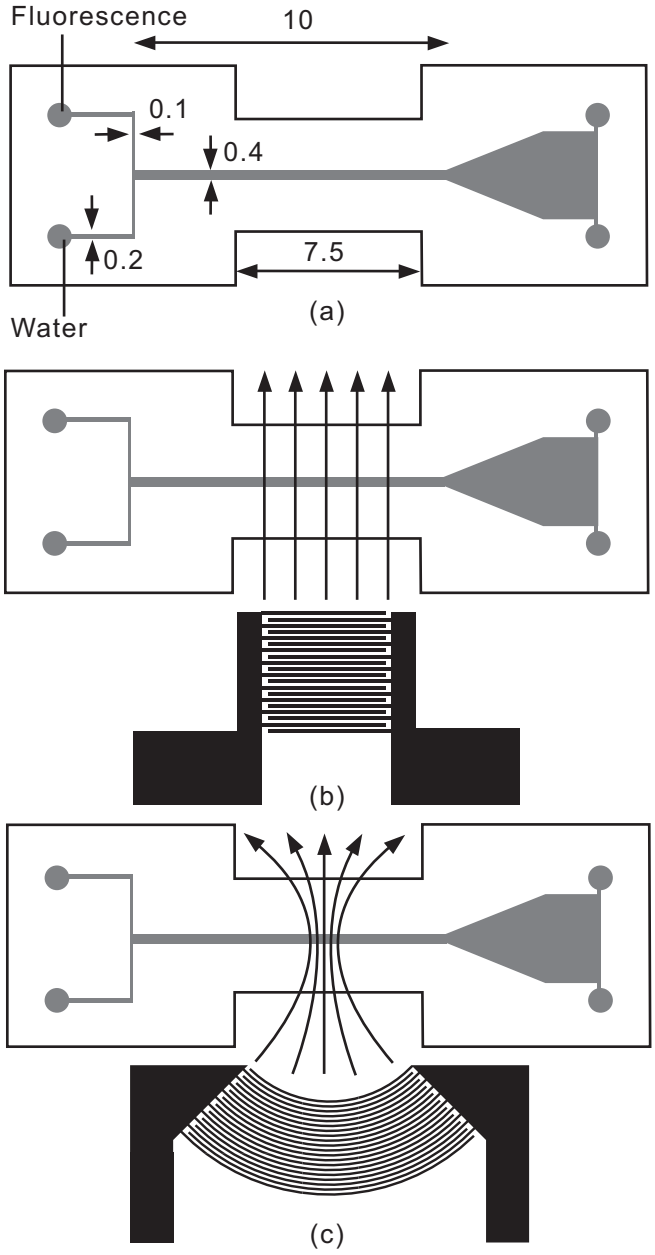

Figure 5.1: Schematic of the SAW micromixer: (a) Geometry and dimension of the mixing channel (length unit is millimeter); (b) Parallel interdigitated electrodes design; (c) Focusing interdigitated electrode design.

5.3 Experimental Setup

The interdigitated electrodes have ten fingers pair with and electrode width and a spacing of 125 μm each. The device was characterized using a RF network analyzer (Agilent E5061A) using the single electrode pair as both the emitter and the receiver. The first resonance frequency of the generated SAW was measured at 13 MHz. A continuous AC signal was generated by a signal generator (Tektronix AFG3022) and amplified by a RF power amplifier (EN440LA, 35 W). The signal was subsequently fed directly to the interdigitated electrodes to generate the SAW.

The liquids are delivered from two 2.5 ml glass syringes via plastic tubing (Cole-Palmer). Both syringes were driven by a syringe pump (Cole-Parmer, 749000-05). The first liquid used in our experiment was DI water from MiliQ system (Milipore). The second liquid was a solution of a green fluorescent dye (fluorescein disodium salt $C_{20}H_{10}Na_2O_5$, Acid Yellow 73) and DI water. The fluorescent dye has an excitation wavelength of 540 nm and an emission wavelength of 610 nm. The mixing process was observed with the help of an inverted microscope (Nikon Eclipse TE2000-S) using an excitation filter for 540 nm, a dichroic mirror for 565 nm and an emission filter for 605 nm. The images were captured by a high-speed monochrome charge couple device (CCD) camera (Photron Fastcam APX RS). The recording speed used in the experiment was 50 frames per second. The mixing quality was evaluated based on the intensity value of images captured which are proportional to the actual concentration of the fluorescent dye. The images were taken at the end of the channel which is 10 mm downstream from the inlet of the mixing channel.

The fluorescent images of the mixing channel were recorded before and after launching the SAW. To quantitatively characterize the mixing effectiveness of our mixer, a region of

interest (ROI) was defined in the captured images and processed by a customized MATLAB program. Intensity values of each pixel were first captured. The average intensity of each line i along the width of ROI at time t was subsequently extracted as $I_i(t)$. This value is then normalized based on the maximum value $I_{\max}$ and the minimum value $I_{\min}$ of the unmixed states:

$$\overline{I_i}(t) = \frac{I_i(t) - I_{\min}}{I_{\max} - I_{\min}} \tag{5.1}$$

where $\overline{I_i}(t)$ is the normalized average intensity of line i at time t. The mixing efficiency at time t is calculated as:

$$\eta(t) = 1 - \frac{\sqrt{\frac{1}{N}\sum_{i=1}^{N}\left(\overline{I_i}(t) - \overline{I_\infty}\right)^2}}{\sqrt{\frac{1}{N}\sum_{i=1}^{N}\left(\overline{I_i}(0) - \overline{I_\infty}\right)^2}} \tag{5.2}$$

where N is the number of lines along the width of ROI, $\overline{I_i}(0)$ and $\overline{I_i}(t)$ are the normalized average intensity value of line i before turning on the SAW ($t \leq 0$) and time t. The normalized intensity value of each line in the perfectly mixed state is denoted as $\overline{I_\infty}$. Due to the same flow rates of the liquids at the inlets, this value is $\overline{I_\infty} = 0.5$ in our case. The key parameters governing the flow characteristics and the mass transport are the Reynolds number Re and the Peclet number Pe. The Reynolds number is the ratio between the advective transport and momentum transport:

$$\mathrm{Re} = \frac{U D_{\mathrm{h}}}{\nu} \tag{5.3}$$

where U is the mean flow velocity, D_{h} is the hydraulic diameter of the channel and ν is the kinematic viscosity of the fluid (ν=$0.8 \times 10^{-6}\mathrm{m}^2/\mathrm{s}$). The Peclet number Pe is the ratio

Table 5.1: Flow rates, Reynolds numbers and Peclet numbers used in the experiment.

Flow rate (ml/h)	Reynolds number	Peclet number
2	3.1	14.8×10^3
5	7.7	37.2×10^3
10	15.4	74.4×10^3

between the advective transport and the diffusive transport:

$$\mathrm{Pe} = \frac{UW}{D} \tag{5.4}$$

where W is the width of the channel, and D is the diffusion coefficient of the fluorescent dye. The diffusion coefficient of the fluorescent dye used in our experiments is $D = 1.5 \times 10^{-9}\mathrm{m}^2/\mathrm{s}$.

In this study, mixing experiments at three different flow rates of 2 ml/h, 5 ml/h and 10 ml/h were carried out. Table 5.1 summarizes the corresponding Reynolds numbers and Peclet numbers used in the experiments.

5.4 Results and Discussion

The mixing effect due to acoustic disturbance was recorded by the CCD camera. Representative intensity images of the channel end at the beginning of the capturing process ($t \leq 0$ s) and at $t = 0$ s after the capturing trigger are shown in Figure 5.2. Normalized intensity values and the mixing efficiencies of the images in Figure 5.2 are shown in Figure 5.3. Without acoustic disturbance, mixing in the channel solely relies on molecular diffu-

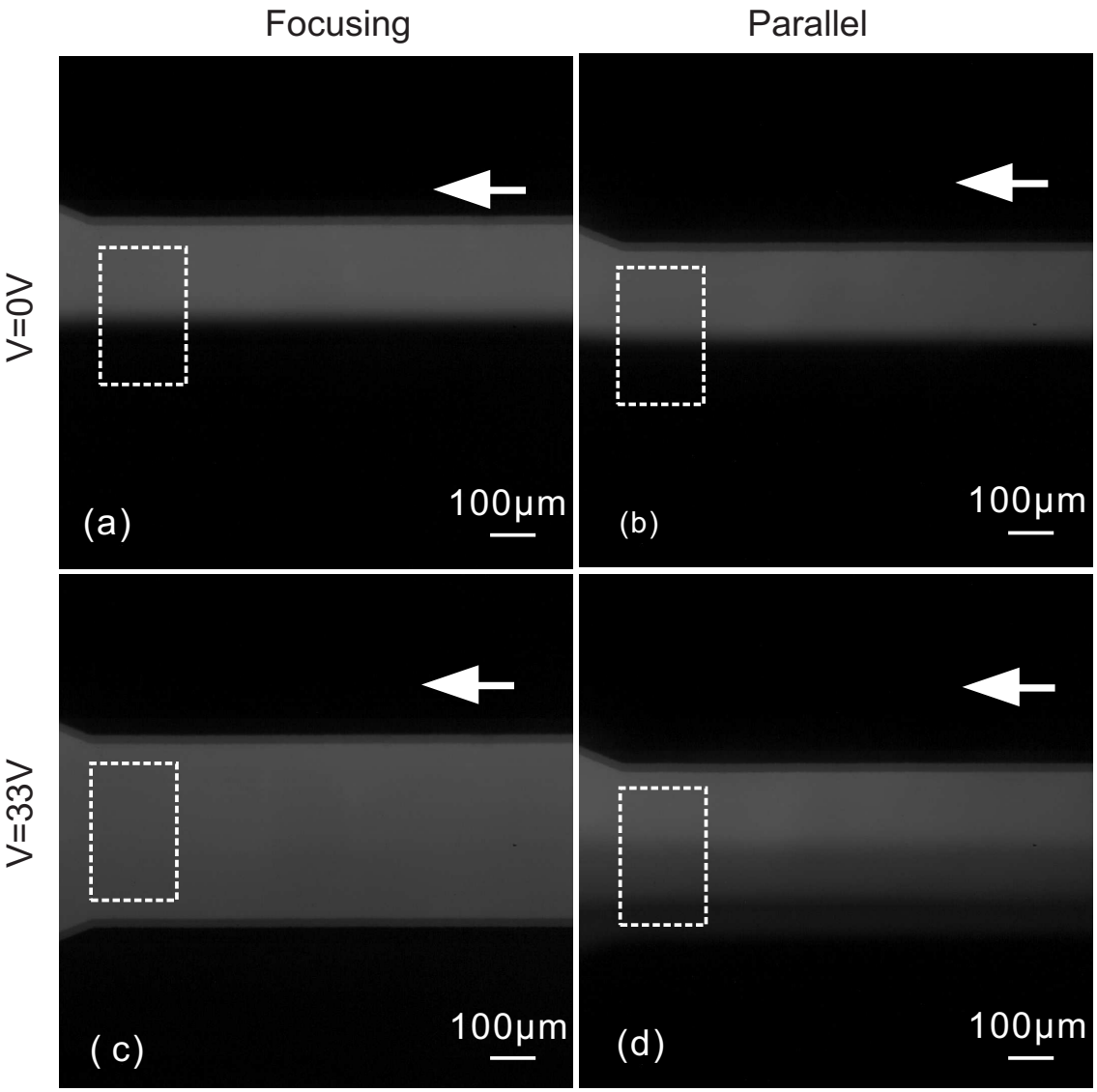

Figure 5.2: Mixing behavior at the end of the mixing channel of (a) focusing design and (b) parallel design when applied voltage is zero. Mixing state induced by SAW of (c) focused design and (d) parallel design when a RF signal of 33 V peak-to-peak is applied to the electrodes. Clear side-by-side interface of DI water and fluorescent solution is observed in (a) and (b). Better mixing quality is achieved by focusing SAW compared to parallel SAW ((c) compared to (d)). The flow directions are denoted by a white arrow. The Peclet number is 37.2×10^3. The boxes are the ROIs for the later evaluation of the mixing efficiency.

sion. The recorded images (Figure 5.2) and the evaluated data (Fig. 5.3) show that mixing at $t \leq 0$ s is poor and the efficiency is close to 0. When a driving voltage amplitude of 33 V peak-to-peak was applied to the electrodes, transversal acoustic streaming occurred and induced mixing can be observed immediately. The mixing process starts at $t > 0$ s and mixing efficiency increases with time as shown in Fig. 5.3.

A remarkable improvement in mixing efficiency was observed with the focusing design. The mixing efficiency was 0.78 while the mixing efficiency of the parallel design remained at about 0.5. At the same applied voltage, focusing design offers a much better mixing quality compared to the parallel design. It is understandable by that fact that focusing SAW delivers a much larger disturbance energy to a confined area in the mixing channel (Figure 5.1c) compared to a weaker energy spread over the entire channel in the case of parallel SAW (Figure 5.1b). The stronger the disturbance energy, the better is the mixing quality.

Mixing quantification could also be evaluated through the probability distribution function (PDF) or the histogram of the concentration of the images [65]. The probability values are obtained through the normalized intensity value of the images. These values are shown in Figure 5.4 under an applied peak-to-peak voltage of 80 V. The Peclet number in this case is 74.4×10^3, higher than that of Figures 5.2 and 5.3. For the parallel design, two peaks are observed near each side of the intensity spectrum indicating poor mixing, Figure 5.4(b). Good mixing achieved by focusing SAW is demonstrated as a sharp peak at the center of the PDF, Figure 5.4(a).

Figure 5.5 shows the mixing efficiency at different Peclet numbers driven by different voltages measured at the channel end. The results clearly show that under a lower applied

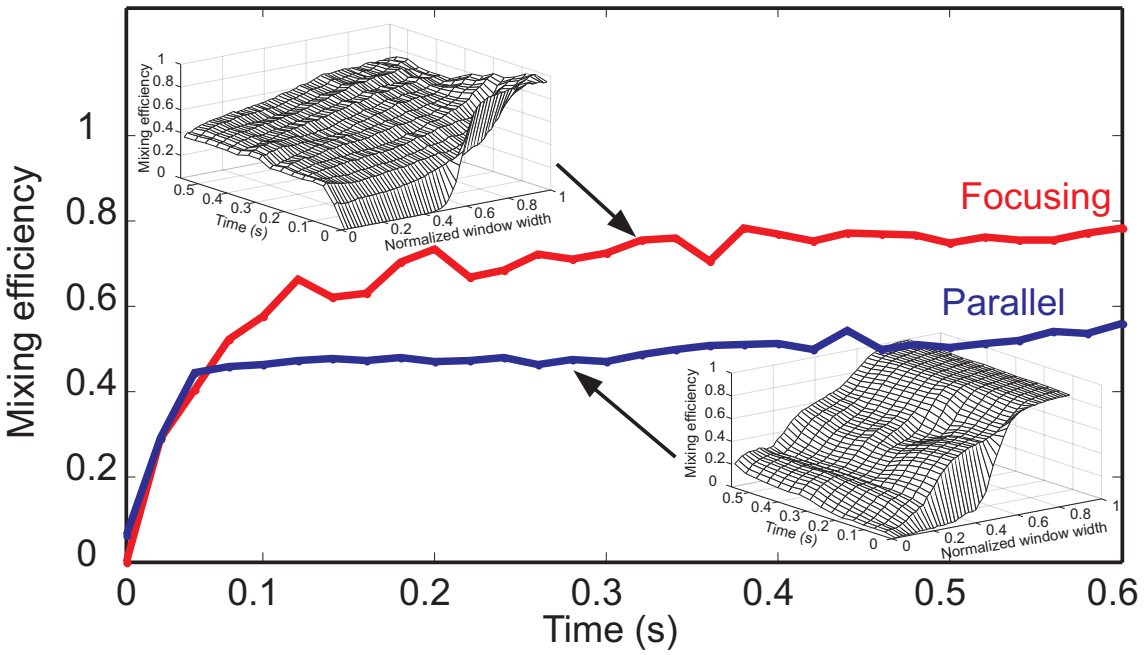

Figure 5.3: Mixing efficiency as function of time of the ROI indicated as the box in Figure 5.2 (applied voltage of 33V and Peclet number is 37.2×10^3) for the focusing design and the parallel design. The inserts are the corresponding normalized intensity values.

voltage and at the same flow rate, focusing SAW improves mixing efficiency significantly compared to parallel SAW . With a peak-to-peak applied voltage of 80 V, mixing efficiency of $\eta = 0.88$ for a Peclet number as high as $\mathrm{Pe} = 74.4 \times 10^3$ was achieved. Even with the applied peak-to-peak voltage of 100 V, the mixing efficiency of the parallel design at a lower Peclet of $\mathrm{Pe} = 14.8 \times 10^3$ was only about $\eta = 0.78$.

The mixing efficiency versus voltage curve has two distinct features. The first feature is its parabolic shape at lower voltages. This feature implies that mixing efficiency is a second-order function of the applied voltage. This feature is in agreement with the fact that mixing efficiency is proportional to the velocity of acoustic streaming. Acoustic streaming velocity in turn is a second-order function of the applied voltage as reported by Nguyen et al. [8]. The second feature is the limiting value for the mixing efficiency at different flow rates. Since the focusing design can achieve better mixing at lower applied voltage,

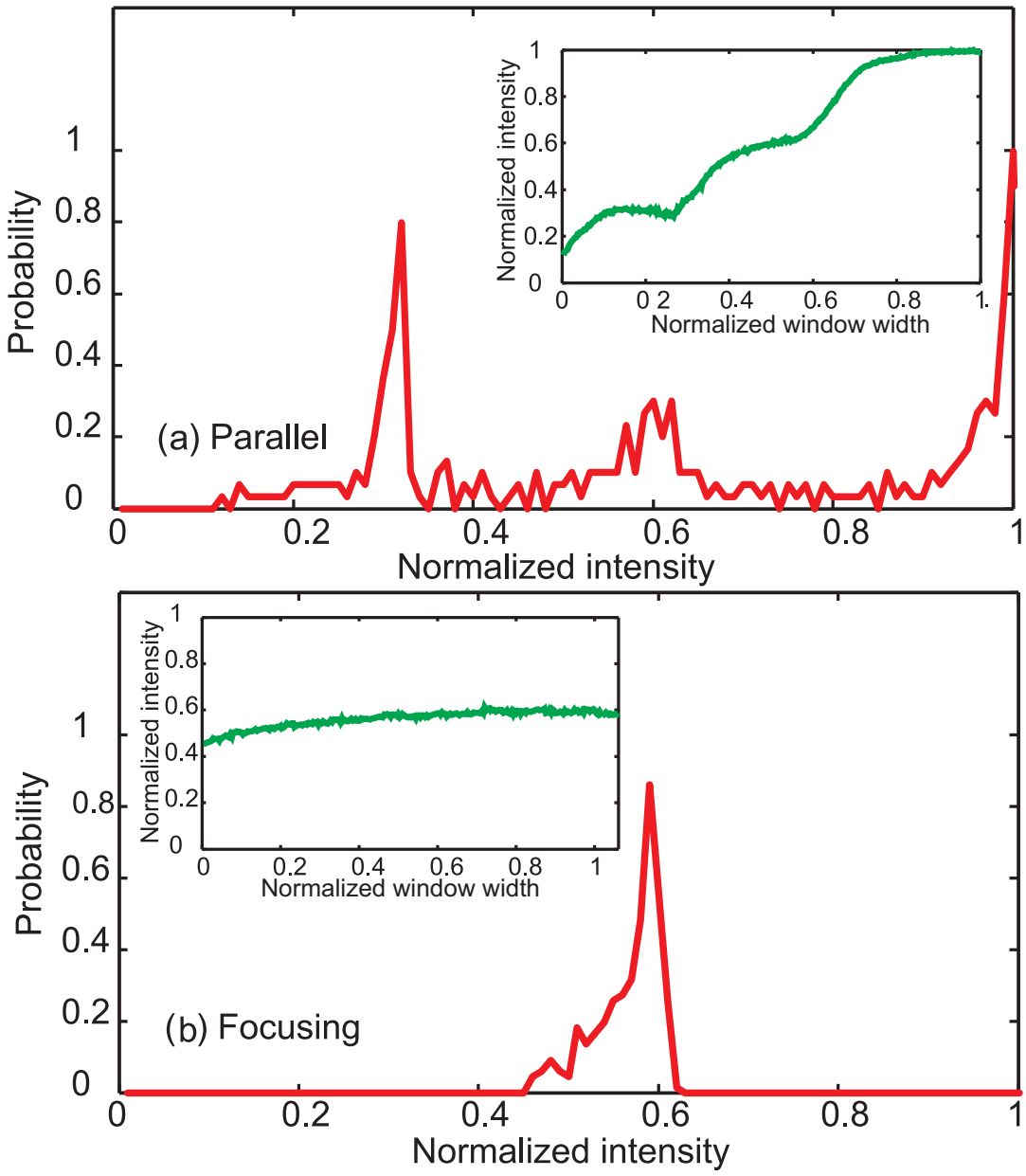

Figure 5.4: Probability distribution function of a ROI for (a) the parallel design and (b) the focused design. The data are evaluated at 0.6 s after turning on the SAW. The applied peak-to-peak voltage is about 80 V. The Peclet number is 74.4×10^3. The inserts show the corresponding normalized intensity values across the channel width.

the limiting value is observed to be 0.9 as shown in Figure 5.5(b). Further increase of the applied voltage will not improve the mixing efficiency. The efficiency tends to converge to this limiting value faster at lower Peclet numbers. Based on the trend shown in Figure 5.2(a), the parallel design could reach this limiting value at a higher voltage beyond 100 V. The effect of Peclet number on the efficiency curve is similar to that of a focused design.

Utilizing focusing SAW confines the wave to one area and improves mixing. However, a high applied voltage could also result in substrate heating and sample heating inside the microchannel which might be a hindrance for some temperature sensitive samples. An infrared (IR) camera (NEC Thermal Tracer TH9100MR) was used to investigate the thermal effect on the focusing SAW device. Figure 5.6(a) shows the captured state of a substrate under 75V applied voltage. The highest temperature (73 $^{\circ}$C) was observed at one area matched to the focual point of the IDT. The relationship between measured temperatures and load voltages were also plotted in Figure 5.6(b). The wide range temperature effect could be useful for various mixing applications.

One design factor that could affect mixing efficiency is the thickness of the side channel of the PDMS cover. The thicker the side channel is, the more acoustic energy is absorbed hence the lower the mixing efficiency will be. The PDMS side channel thickness in the above experiments was of 1.5mm thickness. One particular experiment for parallel design (at 100 V and Pe $= 74.4 \times 10^3$) was carried on with a PDMS channel of 6mm thickness. The mixing efficiency achieved in this case was 0.15, dropping by 50 % compared to 0.3 (achieved the case of 1.5mm thickness). To minimize wave damping, the side channel should be optimized to be as thin as possible but still maintains adequate bonding integrity.

In brief, mixing quality is significantly enhanced compared to the diffusive mixing,

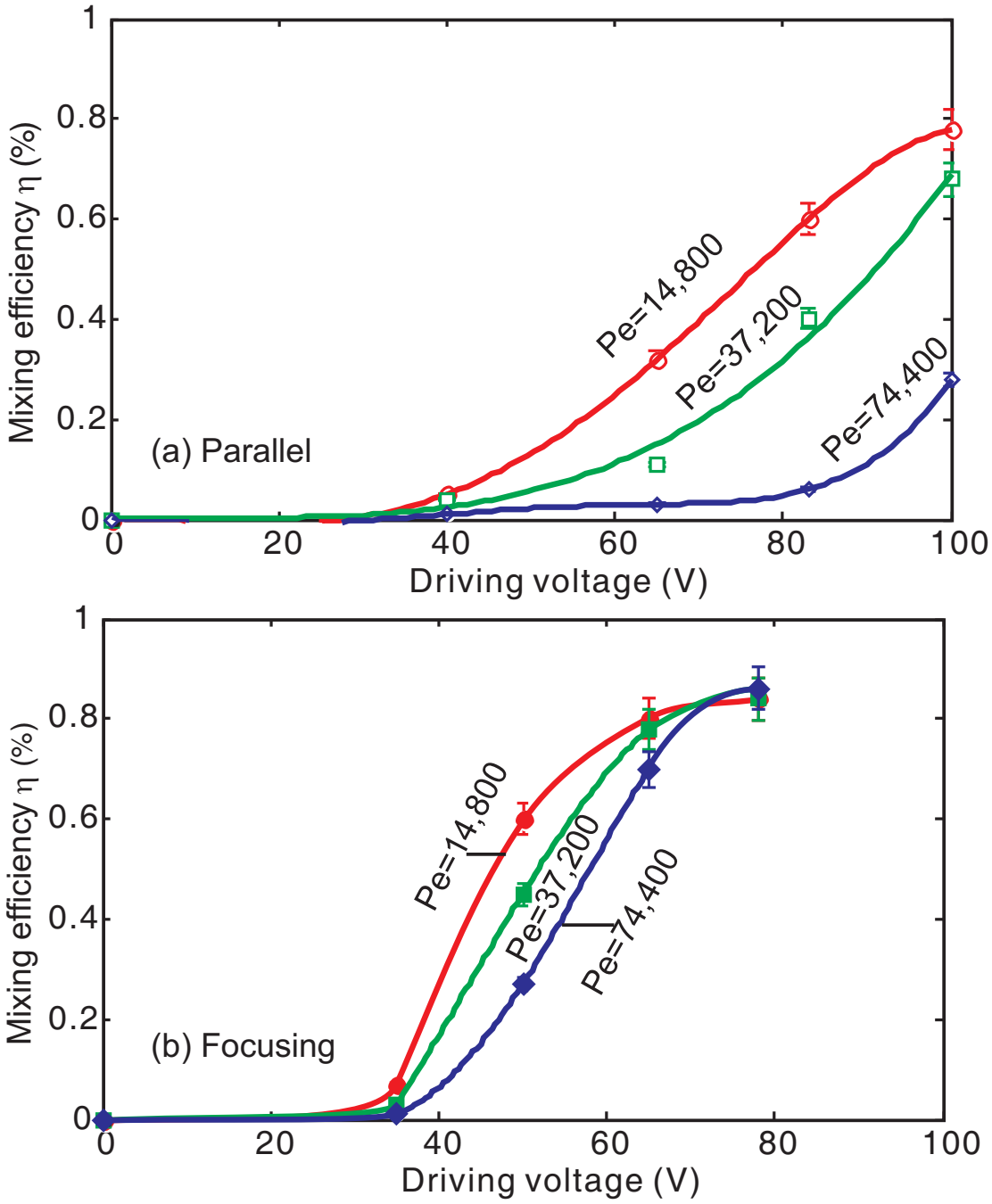

Figure 5.5: Mixing efficiency as function of the applied voltages at different Peclet numbers (solid lines are polynomial fits): (a) parallel design and (b) focusing design.

especially at the high-Peclet-number condition of the experiments. The focusing design shows a superior performance compared to the parallel design. The mixing speed is fast. Good mixing could be achieved within few tenths of a millisecond. The device provides a mixing efficiency close to 0.9 under an applied peak-to-peak voltage of 80 V and at a Peclet number as high as 74.4×10^3. The high Peclet number and the corresponding high flow rates make high-throughput applications with our micromixers possible. These ultrafast and high-performance micromixers could work as stand-alone devices or could be integrated into a more complex microfluidic platform.

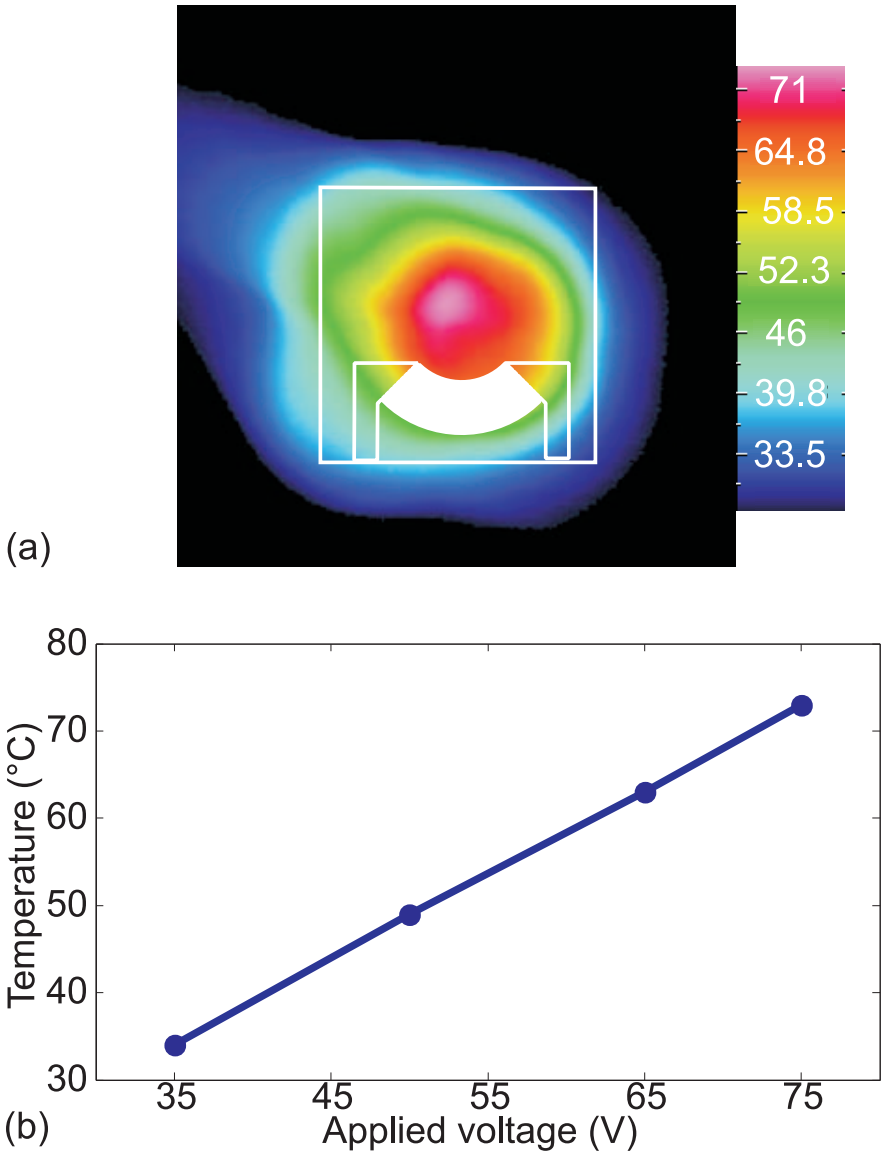

Figure 5.6: Temperature of SAW substrate induced by focusing design (a) temperature of substrate captured by IR camera with 75V input; (b) Temperature versus applied voltage.

Chapter 6

Behaviour of a Surface Acoustic Wave Driven Liquid Droplet on a Planar Surface

6.1 Motivation

Droplet-based microfluidics has been employed in many biomedical applications due to its feasible integration into a programmable platform. Moreover, droplet-based microfluidics offers distinct advantages over a continuous-flow system such as of low usage of reagents, faster processing time, fewer adhesion problems due to the reduction of contact to solid walls. Droplet-based labs on a chip usually involve actuation and manipulation of multiple droplets on a planar surface. In the past, different methods of droplet actuation have been reported. One of the popular mechanisms is electro wetting on dielectrics (EWOD) [86]. This platform usually requires an electrode network. Voltages applied on

the electrodes alter the contact angle and induce the motion of the droplet. Drawbacks of this method are the low driving force and the complicated design of the electrodes. Another mean to actuate droplets is achieved by exploiting thermo capillarity [87] or magnetic force [12]. However, the slow response and the need of magnetic liquids are the major disadvantages of these methods. Daniel et al. utilized the lateral vibration of the planar substrate to induce the droplet motion [88]. This method requires a network of fluidic tracks to guide the droplets along. Surface acoustic wave (SAW) actuation is another solution for droplet-based microfluidics. With advantages such as large driving force, ultra fast operation and trajectory independent of actuation electrodes, SAW promises to be an excellent platform for digital microfluidics.

Surface acoustic wave is generated by interdigitated electrodes deposited on a piezoelectric substrate. This surface wave induces internal streaming and causes a droplet to move [16]. SAW-driven trajectory control of small droplets down to nanoliter size has been demonstrated as nanopump [28, 29], sample dispenser [35, 89] and sample collector [21]. Besides, precise droplet positioning methods can be achieved by measuring the attenuation in transmission signal using pairs of IDT [37, 36] or by exploiting the echo signal [38]. The internal acoustic streaming was used for merging droplets and mixing for applications such as hybridization and polymerase chain reaction (PCR) of deoxyribonucleic acid (DNA) [19, 18, 32].

Through symmetry breaking of the acoustic wave propagation or with an addition of the reflector, a simple recirculatory flow can be generated using SAW [21]. Droplet atomizer is another example of diverse applications of SAW [90]. In the literature, droplet behavior such as walking, creeping has been studied qualitatively [91]. Du et al. investigated internal

streaming velocity in a droplet under the influence of SAW [29]. However, there still lack quantitative works on droplet kinematics. A good understanding of droplet kinematic is important for the application of SAW in a digital microfluidic platform. Brunet et al. [92] reported a quantitative work on the displacement and oscillation of droplets induced by SAW. In this work, relationship between droplet velocity, volume and viscosity were investigated in general. Droplet shape evolution, detailed velocity regimes and the stability of droplet is yet to be discussed.

In this part, we report the detailed investigation of droplet kinematics on a planar surface as a function of droplet size and the applied input SAW energy. The fluid droplets are first positioned on a $LiNbO_3$ substrate. Upon launching SAW, the evolution of droplet shape and droplet movement are captured and subsequently evaluated. Different droplet volumes and applied SAW energies were investigated in our experiments. The displacement and velocity of the droplet are studied as the function of droplet size and SAW energy. Different operating regimes of the droplet such as initial stationary state, acceleration and strong deformation, deceleration and steady motion with constant velocity were observed.

6.2 Device Concept

The SAW was generated by applying a continuous radio frequency signal to an inter-digitated electrodes (IDT) on a single-sided polished Y-cut 128° rotated $LiNbO_3$ substrate with a thickness of 500 μm. A 30 nm Ti/300 nm Au IDT was fabricated by a standard lift-off process. Due to the hydrophilic surface property, water droplet has a small contact angle on a clean and a polished $LiNbO_3$ substrate which could impede the droplet motion.

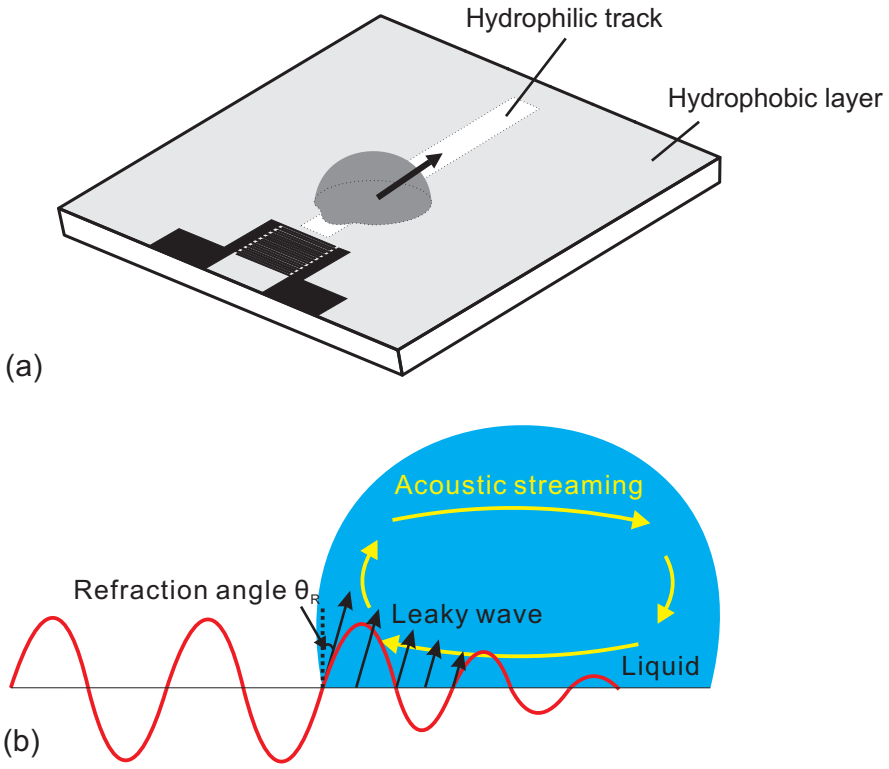

Figure 6.1: (a) Schematic representative of droplet sliding motion under influence of SAW in a patterned hydrophilic track on silanized piezoelectric substrate (b) The acoustic streaming driven motion of the droplet.

A surface modification process was required to coat a hydrophobic layer on the substrate and, hence induce better droplet actuation. We used octadecyltrichlorosilane (OTS, (CH_3)-$(CH_2)_{17}$-$SiCl_3$, Sigma Aldrich) to form a self-assembled mono-molecular layer on the substrate which results in an increase in the water droplet contact angle. To guide the droplet more accurately, we pattern a hydrophilic track on the above silanized surface as shown in Figure 6.1(a). A water droplet was pipetted by a micro pipette (Finnpipette, Thermo Scientific, United States) onto the path next to the IDT. When the transducer was turned on, leaky SAW was launched into the droplet and, in turn, induced acoustic streaming inside the droplet. When the acoustic energy was sufficiently large, the internal streaming became strong enough to deform the droplet shape and drove the droplet in the SAW propagation direction, Figure 6.1(b).

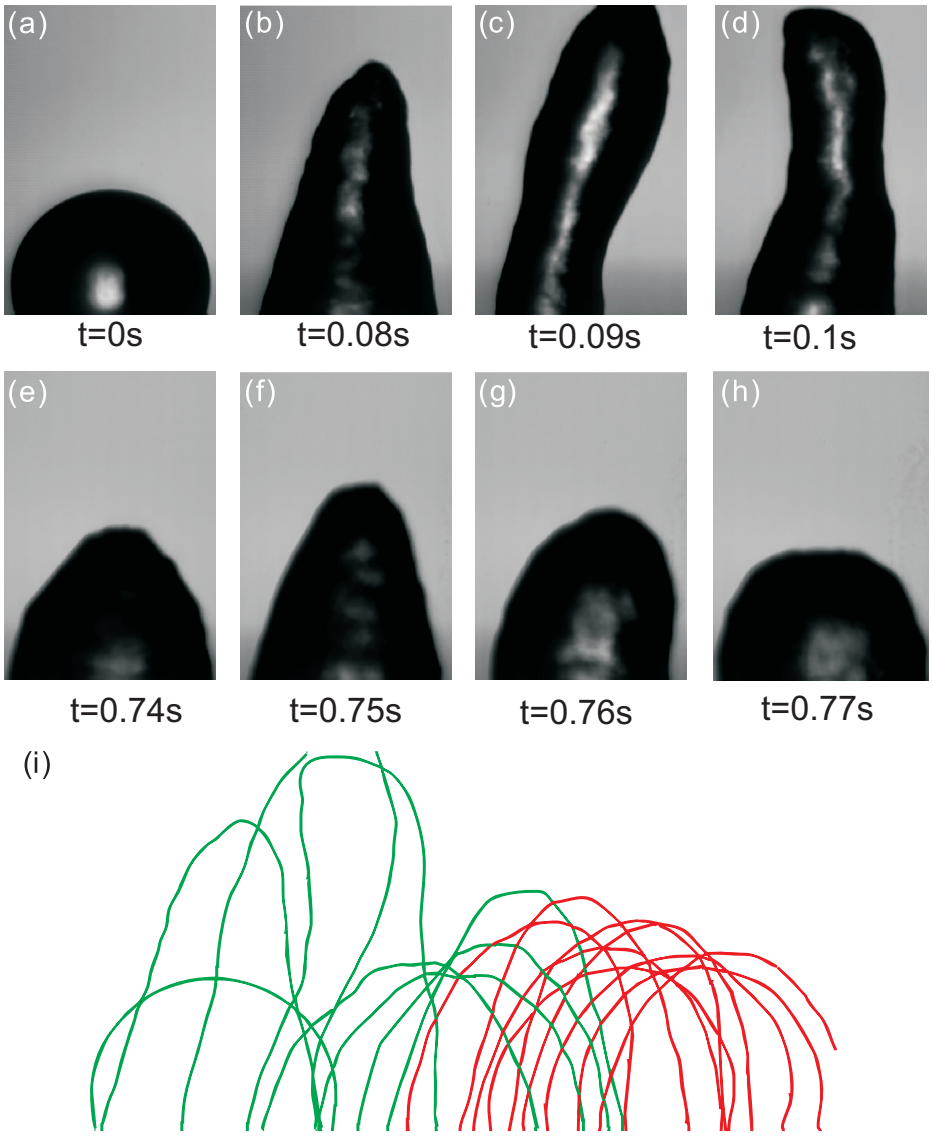

Figure 6.2: Snapshots of a water droplet under applied SAW. (a) Droplet in stationary state; (b-d) Distinct behaviors in the first few frames when SAW power is turned on; (e-h) Repeated behaviors in subsequent frames and (i) droplet evolution processed by MATLAB program captured per 2 frames (green) and per 4 frames (red).

6.3 Experimental Setup

Our SAW device was first characterized using a RF network analyzer (Agilent E5061A) employing the single electrode pair as both the emitter and receiver. The first resonance frequency was measured at 14 MHz. In the experiment, a three-degree-of-freedom (3DOF) micro stage (Melles Griort) was used to mount the SAW device. Different water volumes ranging from 2 μL to 6 μL were investigated in this experiment. A continuous RF signal with a working frequency of 14 MHz was supplied by a signal generator (Tektronix AFG3022). The signal was then amplified by a RF power amplifier system (EN440LA, 35 W) and fed to the interdigitated electrodes. Upon turning on the power, the droplet was driven from one electrode. Upon launching SAW, the evolution of the droplet shape and the droplet movement are captured and subsequently evaluated. These processes were recorded by the high-speed camera (Photron Fastcam) at a frame rate of 500 frames per second (fps). Different applied voltages were used to drive the droplets. A customized MATLAB program was written to capture the data. The program converts the recorded grey-scale images into binary images. These images were subsequently processed to extract the shape, the position and the velocity of the droplet. With the known recording frame rate, all the above data were plotted as functions of time.

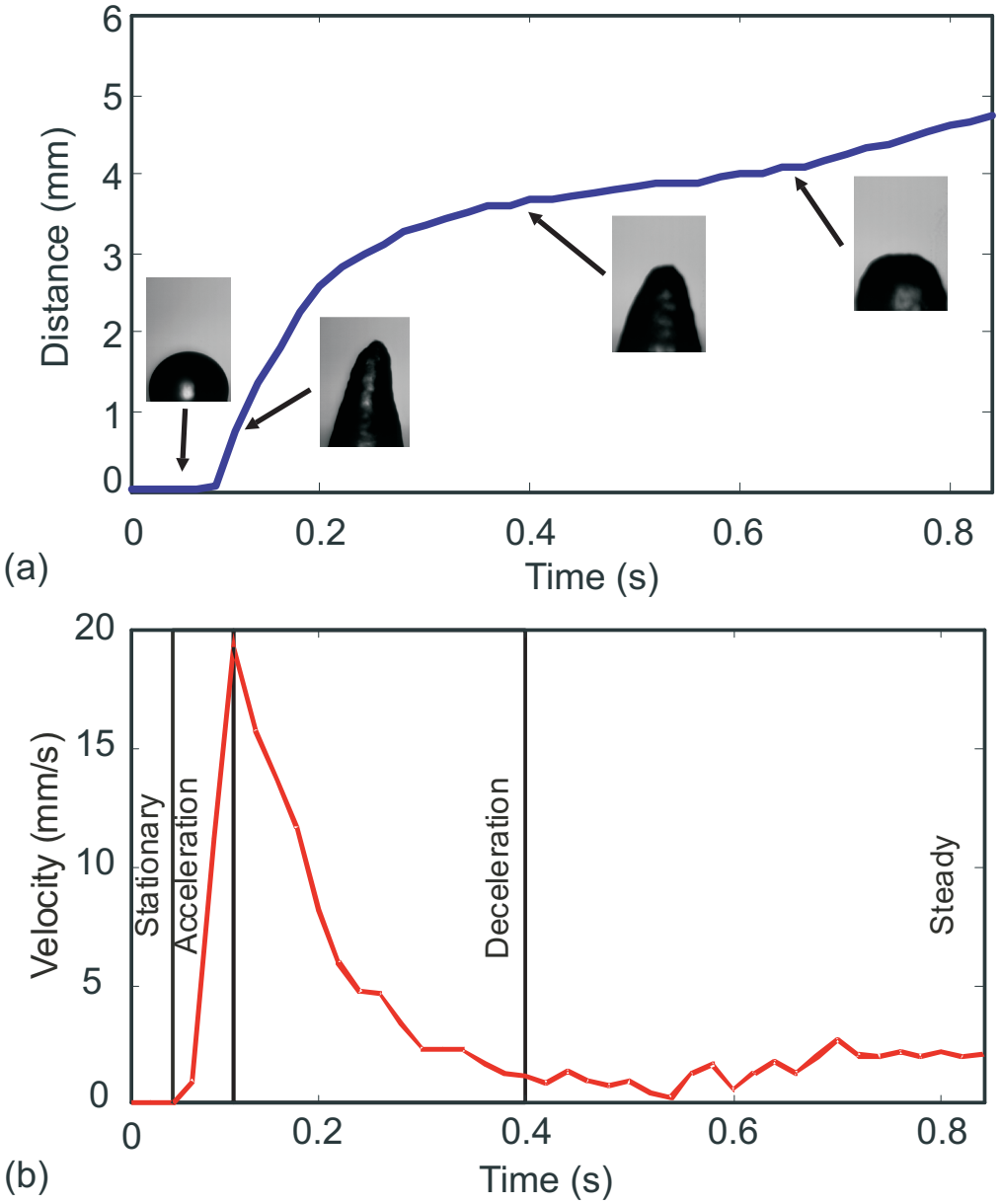

Figure 6.3: Droplet parameters of a 5 μL under 31 V peak-to-peak input during motion; (a) Distance versus time; (b) Velocity versus time; (c) Contact angles versus time; (d) Droplet base diameter versus time and (e) Droplet height versus time.

6.4 Results and Discussion

6.4.1 Drop Evolution under an applied SAW

Figure 6.2 shows the representative evolution of a 5 μL water droplet under 31 V peak-to-peak input voltage. The whole process was recorded in about 0.85 seconds. Droplet contour at different frames are recorded and stacked together to form the droplet evolution image. At the stationary state, the droplet retains its spherical shape. When the input signal was turned on (at time instance of 0.08s), instantaneous disturbance was observed in the droplet shape. Momentary asymmetry of drop angles appeared and droplet motion was induced, Figure 6.2(b). In the first few frames (indicated in green color), the acceleration to a maximum velocity was observed, where the droplet also achieves its maximum height, Figure 6.2(i). The droplet then slowed down and maintained a steady velocity until it stopped at the other IDT electrode. During this process, the droplet behaved in a periodic creeping-walking manner as reported in publication [91].

6.4.2 Distance and Velocity Characteristics of Droplet

Figure 6.3 shows the relationship of distance and velocity versus time of the above droplet. In figure 6.3(a), when RF signal is switched on, the droplet travels a distance of 3 mm in 0.15 s and then slowly completed the remaining distance in about 0.6 s. The droplet velocity is derived from the distance traveled to understand the droplet kinematics. As shown in Figure 6.3(b), the droplet velocity was characterized by four different regimes: stationary regime before the signal was turned on; acceleration regime where the droplet overcome friction and velocity ramped up to a maximum value of 20 mm/s; deceleration

regime in which droplet slowed down and finally reach a stable value of 2 mm/s in a steady manner. It was noticed that the acceleration happened in a very short period of time compared to a longer deceleration period of droplet. Droplet would take some time before a steady motion was achieved.

The contact angles of the droplet as shown in Figure 6.3(a) remains constant at stationary state then drop drastically to 70° once the SAW was applied. Repeated patterns of periodic creeping-walking were observed. It is noted that the advancing angle generally have larger value than receeding angle. The droplet also achieved the smallest base diameter and the highest height during the acceleration process, followed by cycles of rising up and down in values, Figure 6.3(b,c). It is very important for droplet actuation based SAW since many applications requiring precise control over distance and velocity. It is suggested that by slowly increasing the applied voltage, acceleration and deceleration behaviors could be minimized and promises a more controlled platform for droplet-based microfluidics.

6.4.3 Maximum Velocity Characteristics

The maximum velocity v_{max} of a droplet with volumes of 2 μL to 6 μL are plotted versus the applied voltage in Figure 6.5(a). Increasing input value results in a higher maximum velocity of the droplet. The maximum velocity v_{max} is characterized as a parabolic function of the input voltage. This relationship could be understood by the fact that, velocity is proportional to energy input which is the function of the square of the voltage. Figure 6.5(b) shows the effect of the volume on the value of maximum velocity. It appears that velocity v_{max} appears to have a constant value with different droplet volumes. SAW energy absorbed by a droplet is proportional to the wetting area of the droplet. However, larger

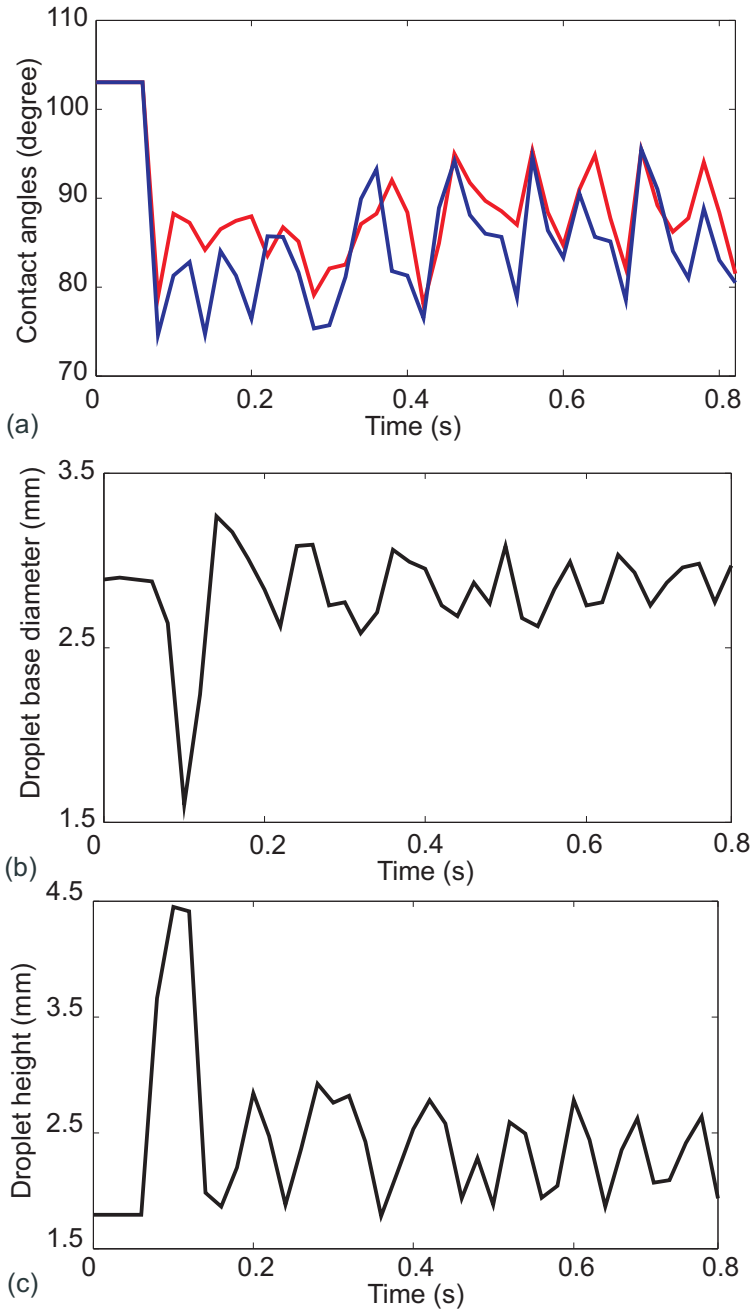

Figure 6.4: Droplet parameters of a 5 μL under 31 V peak-to-peak input voltage during motion; (a) Contact angles versus time; (b) Droplet base diameter versus time and (c) Droplet height versus time.

wetting area results in larger sliding friction force. It is believed that these two effects cancel each other and give rise to a constant value of v_{max} of droplet. If even higher voltage is applied to droplet, part of droplet will be jetted airborne.

6.4.4 Velocity Characteristic in Steady Regime

We are more interested in the velocity of droplet in steady regime as this steady velocity would be exploited in SAW droplet-based application. The behavior of velocity versus voltage and volume is plotted in Figure 6.6. Compared to v_{max} , the velocity value in this regime is much smaller and in the range from 0.5 mm/s to 5 mm/s. Figure 6.6(a) shows that the steady velocity increases with increasing applied voltage for droplet of volume less than 4 μL. Above this critical volume, the droplet velocity is inversely proportional to the applied voltage. As seen in Figure 6.6(b), when applied voltage is less than 35 V p-p, droplet velocity achieved is directly proportional to the volume. At 31 V, the steady velocity of the droplets with different volumes seems to arrive at a saturated value.

In conclusion, a study the kinematic behaviour of a sessile liquid droplet on a planar surface driven by SAW was carried out. The sample was fabricated using the standard lift-off process. A self-assembled monolayer was coated to enhance the droplet motion. Different droplet volumes under the applied SAW energy were investigated. Droplet evolution from stationary state to steady motion was evaluated and discussed. Different operating regimes of the droplet kinematics were observed. Corresponding maximum velocity of the droplet was achieved during the acceleration process is characterized as a function of the input voltage and the droplet volume. The maximum velocity value is proportional to the increasing applied voltage and volumes. The results obtained in this chaptor are important

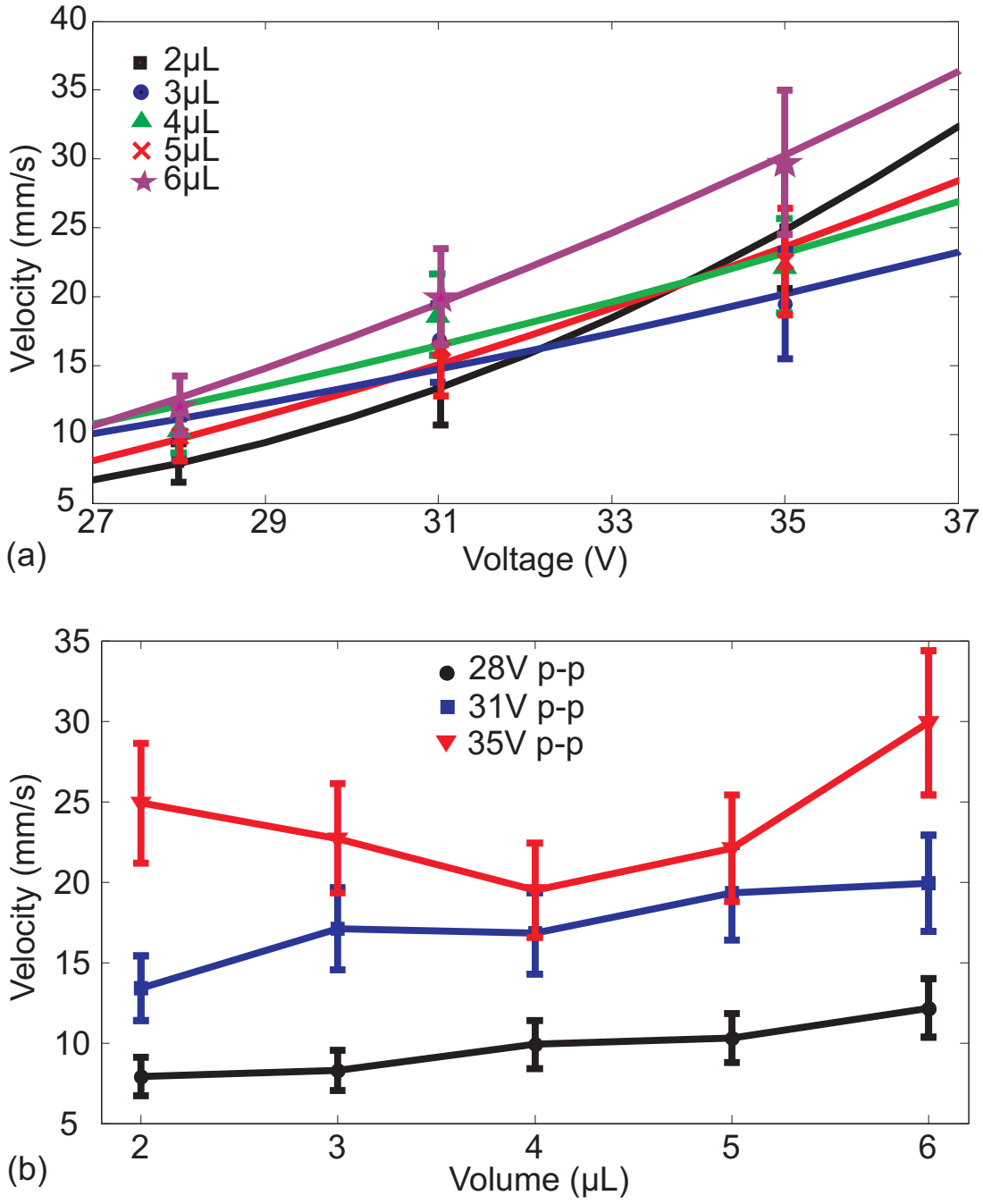

Figure 6.5: (a) Maximum velocities as a function of applied voltage b) Maximum velocity as a function of volume.

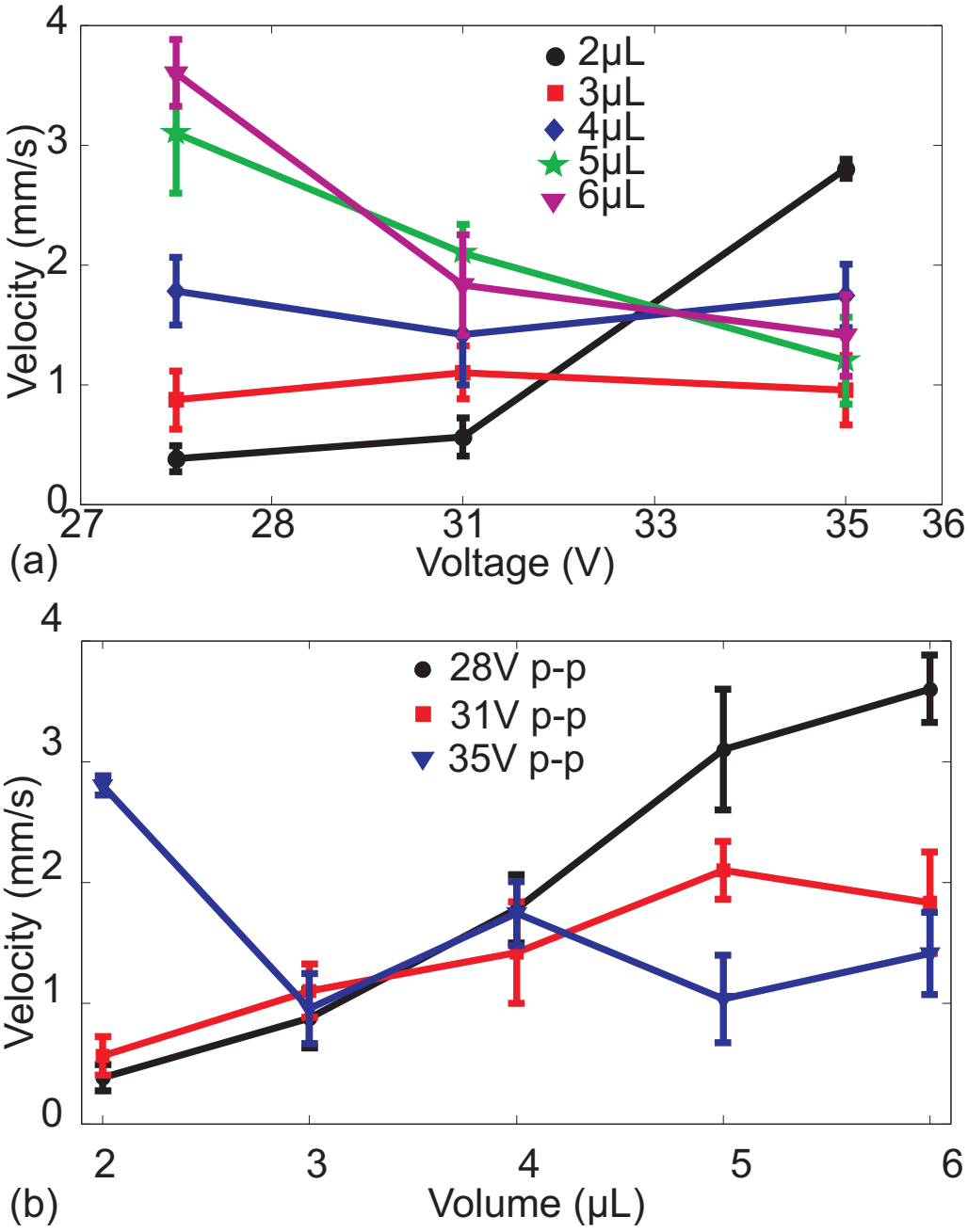

Figure 6.6: (a) Velocity as a function of applied voltage (b) velocity as a function of volume.

for SAW-driven droplet-based microfluidic applications where steady and well controlled motion is preferred.

Chapter 7

Investigation of surface acoustic wave in droplet formation

7.1 Motivation

In the recent years, microfluidics has become a major interest in lab on chip technology due to its miniaturization ability. In general, microfluidic applications could be categorized as continuous-flow microfluidics and droplet microfluidics. In contrast to the former, the latter utilizes fluids in the form of droplet for transportation and manipulation. Droplet microfluidics offers advantages as low reagent usage, fast reaction rate and low cross contamination compared to continuous-flow microfluidics [93]. Droplet microfluidics has been used in various applications such as polymerase chain reaction (PCR) of deoxyribonucleic acid (DNA)[32], protein crystallisation [94] and nanoparticles synthesis [95]. The key factor in droplet microfluidics technology is the formation of droplet. Droplet is formed in an immiscible carrier fluid by either passive or active method. Passive method comprises

of focusing [96] and T-junction configuration[97]. In these methods, two immiscible liquids are pumped into a junction where the dispersed phase liquid is pulled and pinched off by the continuous phase liquid. In active method, droplet can be manipulated by external forces such as acoustic [98], thermal [99], pressure [100] and magnetic [101] forces. Surface acoustic wave (SAW) is an alternative solution for active droplet generation. The so-called acoustic streaming has been exploited in various microfluidic applications such as pumping [44], mixing [49, 18, 102], sorting [58] and patterning [56, 57]. In this chapter, we report the investigation of SAW pumping effect in droplet generation.

7.2 Device concept

Two configurations of microchannel are studied: focusing and T-junction. Figure 7.1 (a) shows the schematic diagram of focusing sample. Channel inlets width of continuous phase and dispersed phase liquid both have a value of 100 μm, focusing neck was designed to have a smallest width of 45 μm. The inlet widths for the dispersed and continuous phase channels for T-junction are 50 μm and 300 μm respectively, Figure 7.1(b). SAW was launched into the dispersed phase fluid by applying a continuous radio frequency (RF) signal to an interdigitated electrode (IDT). This IDT (Cr/Au) was patterned on a single crystal 128° Y-cut $LiNbO_3$ substrate through a lift-off process. The IDT was designed to have fingers of arc shape in order to focus the SAW energy into a focal point. This focal point is positioned at the centre of the disperse phase inlet. The width a the IDT finger has a value of 125 μm which resulted in a SAW resonance frequency of 14 MHz. Microchannel was machined in polydimethylsiloxane material (PDMS, Sylgard 184, Dow

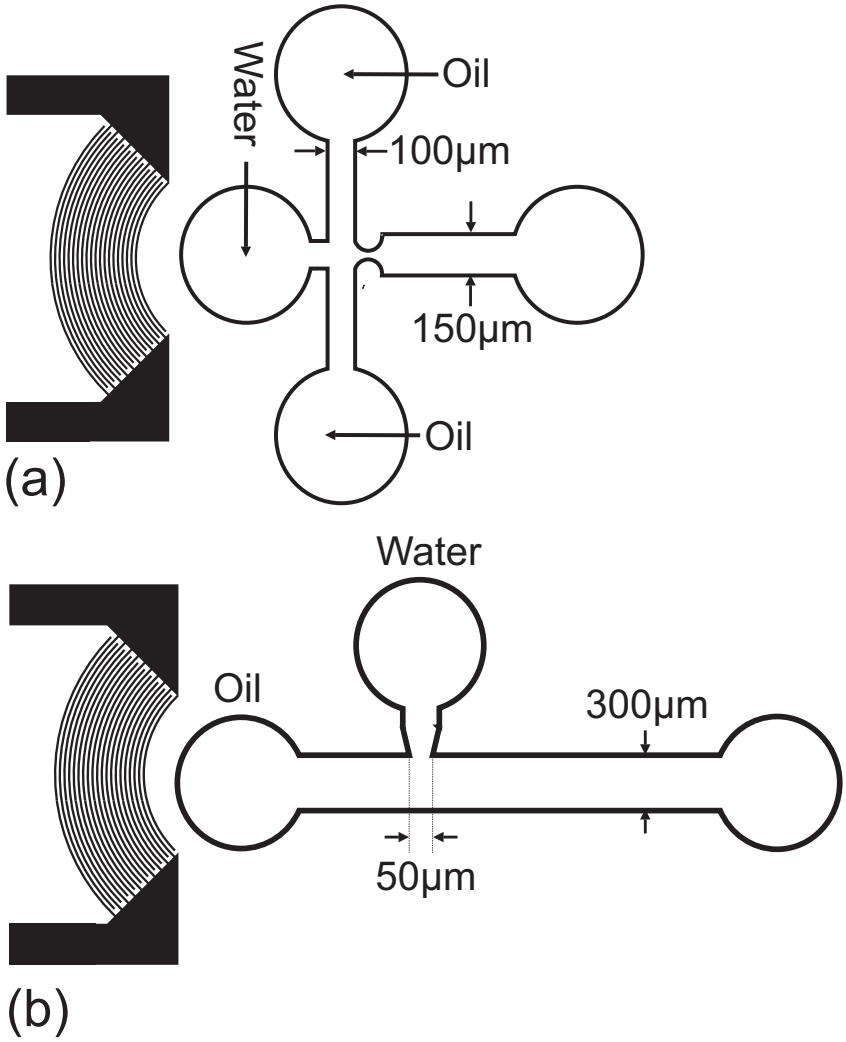

Figure 7.1: Schematic representative of SAW-based microfluidics device for droplet formation (a) SAW is launched into a dispersed phase of flow focusing configuration (b) SAW is launched into a continuous phase of the T-junction configuration.

Corning, USA) by soft lithography technique. The channels have a height of 50 μm. The microchannel and the piezoelectric substrate were firstly treated with oxygen plasma. They were carefully aligned under the microscope and bonded together to form our device.

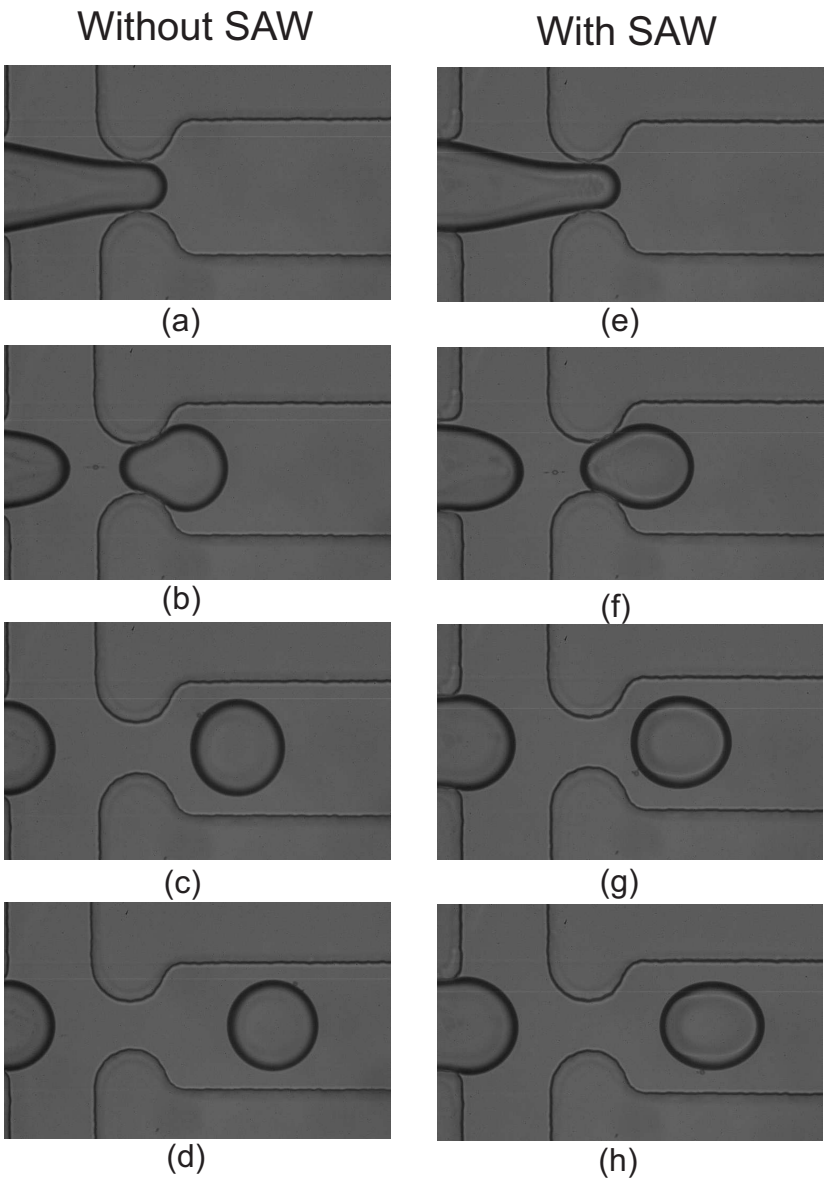

Figure 7.2: Formation of droplet under flow focusing configuration (a-d) Applied voltage is 0 V (e-h) Applied voltage is 70 Vp-p.

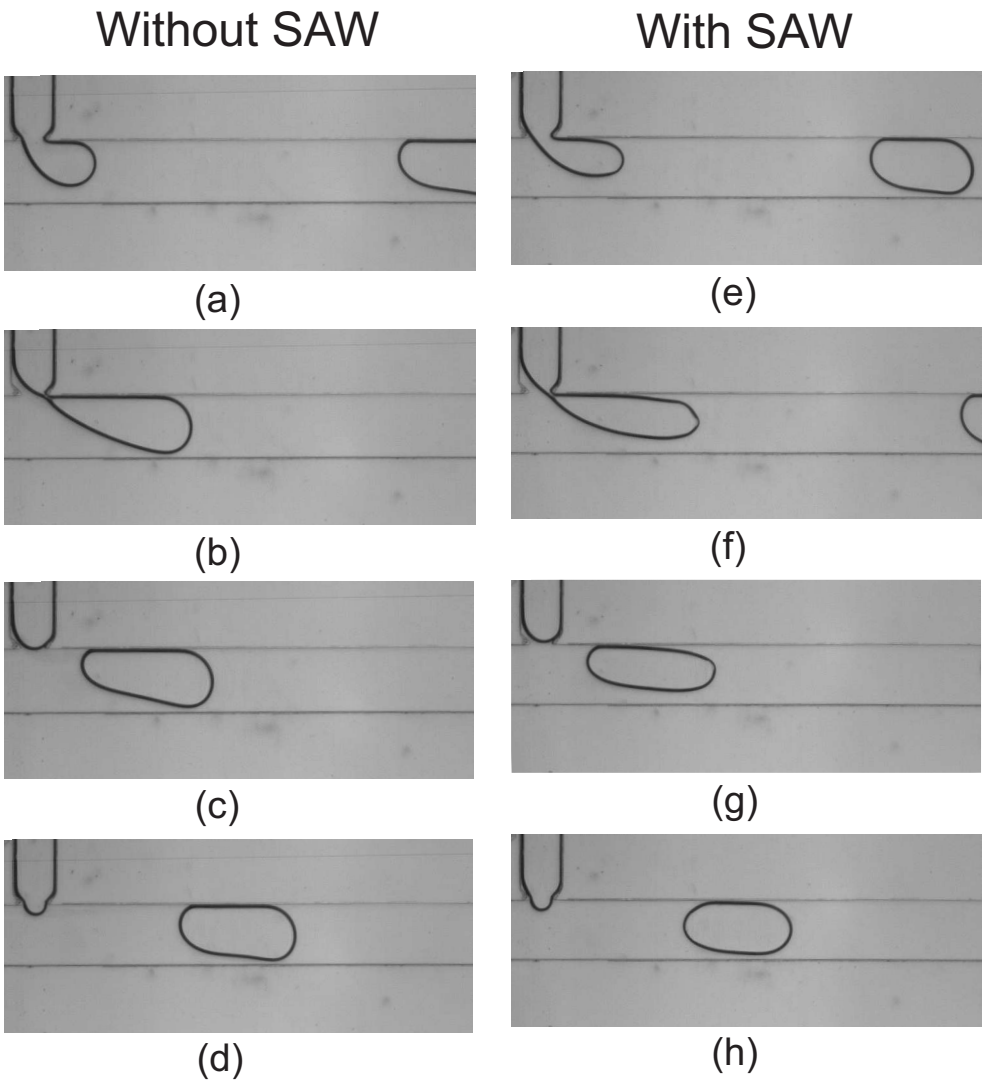

Figure 7.3: Formation of droplet under T-junction configuration (a-d) Applied voltage is 0 V (e-h) Applied voltage is 70 Vp-p.

7.3 Experimental setup

In our experiment, deionized (DI) water was used as dispersed phase fluid and mineral oil (Sigma M5904, St. Louis, USA) was used as continuous phase fluid. Surfactant Span 80 was added into the oil (2% by weight) to stabilize the formation of droplets. These liquids were pumped into the inlets by two precision syringe pumps (KD scientific, USA). An epi-fluorescent inverted microscope (Nikon Eclipse TE2000-E) was used to observe the droplet formation. Because $LiNbO_3$ has uniaxial birefringence, a linear filter (Hoya PL)was inserted into the microscope to get clear images of droplets. The droplet evolution from stretching to pinch-off was recorded by a high speed camera (Photron FASTCAM APX RS, USA) at a frame rate of 500 frames-per-second (fps). The recorded image was then processed by a customized MATLAB program. The program converted the recorded grey-scale images into binary images and measured the area of generated droplet. Average droplet radius is calculated based on the processed area. With the known frame rate, the droplet generation frequency was calculated.

7.4 Results and Discussions

7.4.1 Effect of SAW on droplet formation in focusing configuration

In the focusing device, channel inlets width of continuous phase and dispersed phase liquid both have a value of 100 μm, focusing neck was designed to have a smallest width of 45 μm. The flow rates of oil and water are fixed at 5 μL/h and 20 μL/h. Compared to the left column (under 0V applied), the droplet tends to be suppressed along the channel

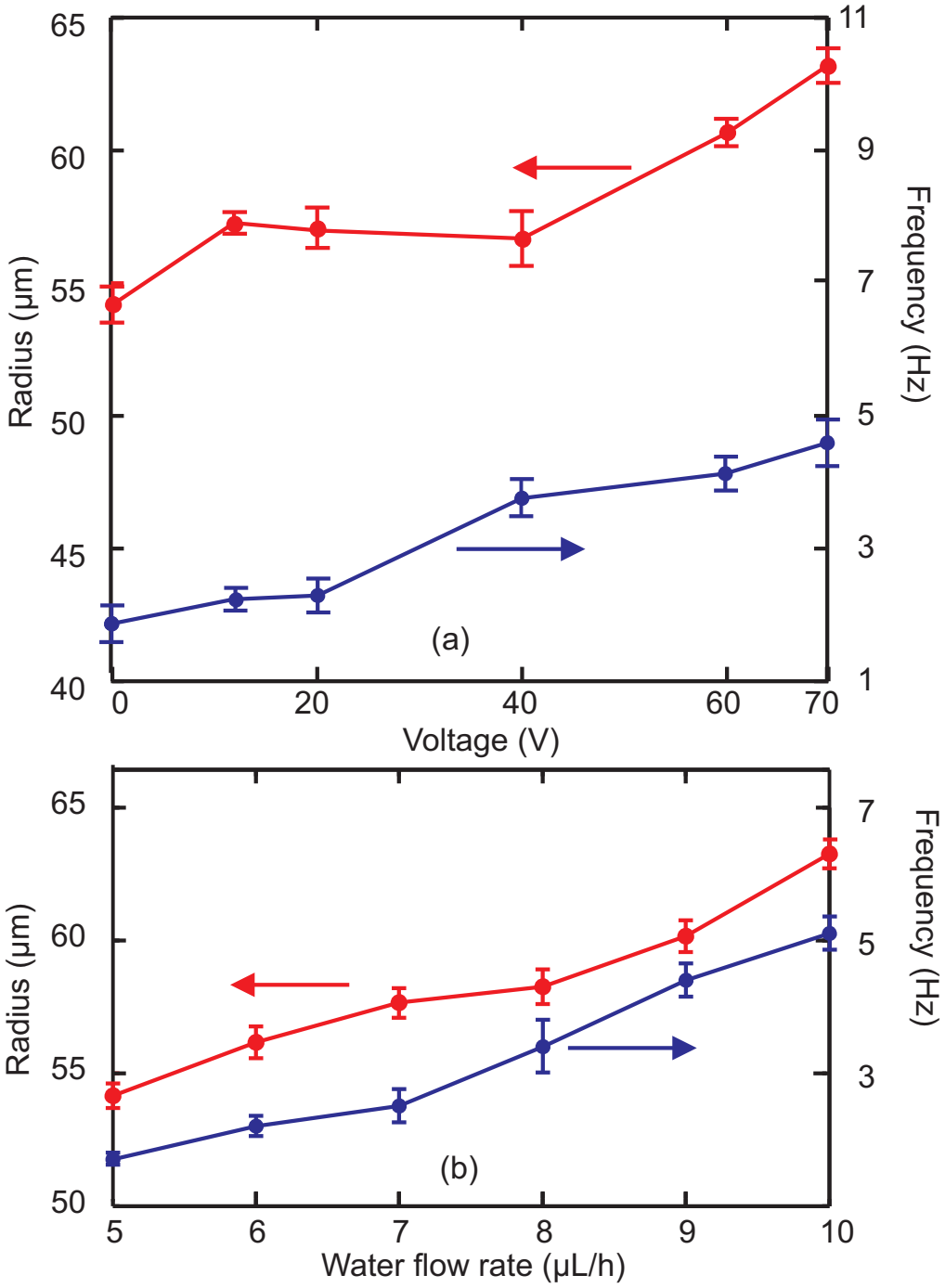

Figure 7.4: Average droplet radius and formation frequency in the flow focusing configuration: (a) as a function of applied voltage for SAW; (b) as a function of water flow rate without SAW.

after it pinched off from the neck (SAW has an input voltage of 70 V p-p),Figure 7.2. As a result, the droplet changed to the form of an ellipsoid from the orginal circular shape.

Figure 7.4 plots the average droplet radius and frequency of the droplet formed versus the applied voltage for focusing device. With SAW, the average droplet radius and the formation frequency increase with the applied voltage, Figure 7.4(a). To verify the pumping effect of SAW for the water inlet, the same experiment was carried out without SAW but with increasing water flow rate. The results show the same trend for the droplet radius and the formation frequency, Figure 7.4(b).

7.4.2 Effect of SAW on droplet formation in T-junction configuration

The inlet widths for the dispersed and continuous phase channels are 50 μm and 300 μm respectively for the T-junction, Figure 7.1(b). The flow rate of oil and water were fixed at 10 μL/h and 50 μL/h. Figures 7.3(a-d) show the droplet formation when there is no applied voltage. Figures 7.3(e-h) are the droplets under applied voltage of 70 V p-p. Compared to a droplet formed under a pure hydrodynamics formation, the droplet formed under SAW is dragged along the channel from the junction until break up. The higher the voltage is, the longer droplet is stretched. This distortion shape could be explained by the reflected wave along the microchannel induced by SAW. When SAW propagate into the microchannel, a portion of SAW will be reflected from the channel walls as discussed by Tan et.al [46]. These waves would continue to propagate in the channel and change the shape of the droplet. The result observed is the stretching of droplet along the microchannel.

In the case of the T-junction configuration, Figure 7.5(a) shows that droplet radius and frequency only slightly decrease with the applied voltage. The verifying experiment with-

out SAW and with increasing oil flow rate shows the same trend for the droplet radius, Figure 7.5(b). However, the formation frequency increases with increasing flow rate. Without SAW, decreasing droplet size forces the formation frequency to increase because the flow rate of water remains constant. With SAW, the droplet size and the formation frequency remains almost constant a at higher applied voltage or a higher SAW energy. This phenomena could be explained by the competing effect between stretching by SAW and hydrodynamic squeezing by the oil flow. As shown in Figure 7.3(b) and (f), SAW stretches the forming droplet leading to a larger gap between the droplet and the opposite channel wall. This gap makes squeezing by the oil flow ineffective.

In conclusion, this chapter investigates the effect of SAW on droplet formation. SAW generated from focusing electrode was launched into the dispersed fluid of the flow-focusing configuration and continuous fluid of T-junction configuration, respectively. In both configurations, the droplet shape is distorted along the channel due to the propagation of the wave. The results show that only in the flowfocusing configuration the droplet size and the formation frequency can be effectively controlled by the SAW.

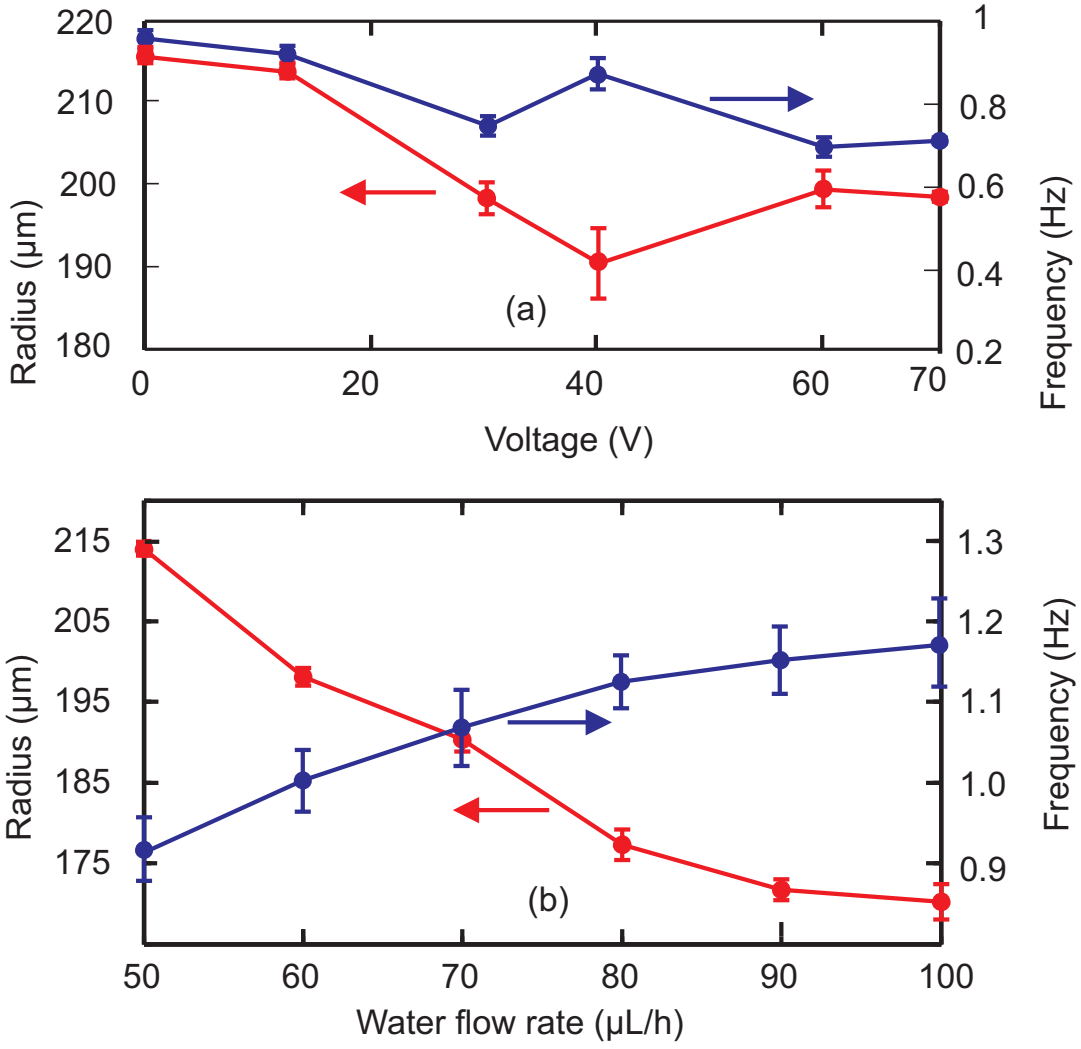

Figure 7.5: Average droplet radius and formation frequency in the T-junction configuration: (a) as a function of applied voltage for SAW; (b) as a function of water flow rate without SAW.

Chapter 8

Particles sorting based on SSAW

8.1 Motivation

Microfluidics has been widely used in the field of chemical, biological processes and lab-on-a-chip applications [103, 104]. Fundamental operations in microfluidics such as pumping, mixing, sorting are proven to be challenging at micro scale [105]. Particles sorting and manipulation is the key factor in biological and chemical analyses such as cancer research, drug screening, transplantation immunology and tissue engineering [106, 107]. Simple and efficient particle manipulation and sorting method is of great interest in the research community. Up to date, passive and active particle sorting have been reported. Passive methods utilize the hydrodynamic behaviors of the flow in special geometry microchannel to achieve the purpose [108]. The operation of this method is simple since no external force is involved. However, due to additional features in the device, fabrication process tended to be more complicated and the device generally occupies large footprint. Particles could be sorted based on external mean as well. External actuation induced sort-

ing such as magnetic, dielectrophoretic, optical and acoustic have been investigated in the literature. In magnetic actuation, cells or particles of interest are firstly labeled by attaching with magnetic particles [109]. These labeled particles could be manipulated by an external magnetic field source. Kong et al.[110] has demonstrated magnetic switching locally of particles by integrating microcoils into a microfluidics device. Dielectrophoretic actuation mainly relies on an electric field to manipulate particles to move to a specific direction. Particle of different charge and polarization properties could be sorted effectively in this method [111]. Acoustophoresis is another method in particle trapping and manipulation [112]. In general, an bulk transducer is attached to the microfluidics sample. The wave generated by this transducer is coupled into the channel with a width designed as half of the bulk acoustic wavelength (BAW). The result is the formation of a standing wave along the channel length. Dispensed particles would experience an acoustic radiance force which attracts them to the pressure nodes. This method is promising since particles could be manipulated in a non contact condition. However, in order to achieve the standing wave, the sample material required to process a good acoustic reflection which may be a hindrance to PDMS based device. The larger size and the opaque of the transducer material could restrict device application. A new approach in acoustophoresis is to use standing surface acoustic wave (SSAW). SSAW has been reported in particles focusing and particles patterning[54, 57]. In this chapter, a SSAW particles manipulation method in a microchannel is proposed. SAW is generated by an interdigitated electrode deposited directly on a piezoelectric substrate which enable miniaturization. The substrate is transparent and is able to bond with PDMS which is advantageous than the traditional BAW method. This method is fast, effective and is able to controlled by external device.

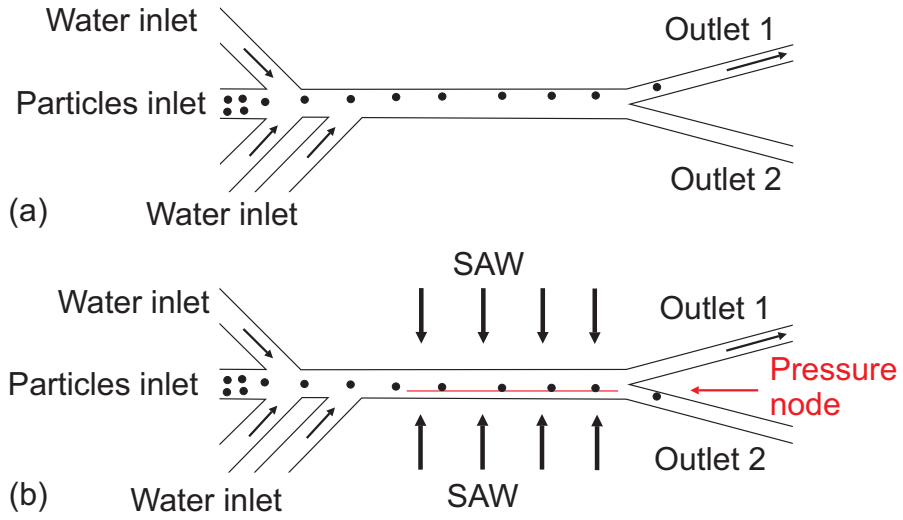

Figure 8.1: Representative of SSAW sample (a) Particles are hydrodynamically focused by 3 water sheaths flow and go to outlet 1 (b) Particles are attracted to the pressure node and directed to outlet 2 when SSAW is generated.

8.2 Device concept

SAW is a propagating surface wave generated by an interdigitated electrode. Employing one pair of identical electrodes which are positioned opposite each other, constructive interference of these two SAWs resulted in a standing SAW along the propagatin area. When a microchannel is placed on top of the surface, pressure nodes and anti nodes are induced in the liquid. The number of nodes formed inside the microchannel is dependent on the SAW wavelength and its width. Dispensed particles will be attracted towards this node (antinode) due to the acoustic radiance force. The force acting on particles is the function of particle size, material properties and density of particles inside the liquid. Utilizing this acoustic radiance force, particle manipulation and sorting (based on particle size) could be achieved.

Figure 8.1 shows the representative pictures of the SAW sorting device. It includes 4 inlets channel: 3 water inlets of the same flow rate and 1 particles inlet and two out-

lets. Particles were hydrodynamically focused into a line and transported into outlet 1 by controlling the flow rates of water and particles inlet as shown in Figure 8.1(a). The microchannel width (200 μm) was designed to be exactly half of the wavelength of the SAW so that only one node (anti-node) appear inside the channel. The channel was placed on top of the sample in a configuration such that this node (anti-node) line along the entrance of outlet 2, Figure 8.1(b). When standing SAW were presented along the propagating area. Acoustic radiance force was induced in the channel. The formula for this radiance force acting on a spherical particle has been mentioned (equation 2.1) :

$$F_{\mathrm{r}} = -\left(\frac{\pi {p_0}^2 V_{\mathrm{p}} \beta_{\mathrm{m}}}{2\lambda}\right) \phi(\beta, 0)\, sin(2kx) \tag{8.1}$$

This radiance force is proportional to the input signal. When the input signal is larger enough, particles would be attracted into the node and hence exit into outlet 2.

8.3 Experiment and discussion

The intedigitated electrodes were fabricated onto a $LiNbO_3$ through a lift-off process. Photoresist (AZ9260) was patterned on the substrate. Metal (Ti 30 nm and Au 300nm) were then deposited by a sputterting process. Sample was subsequently released in Acetone to form the electrode. Channel structure were patterned in thick negative photoresist SU-8. The thickness of the SU-8 is 150 μm and define the channel depth. PDMS was mixed, casted and peeled off from the mold. The PDMS channel and substrate were treated in oxygen plasma and brought into contact to form the boding. Due to the alignment of the pressure node, alignment marks were needed during the bonding process. Figure 8.2 shows

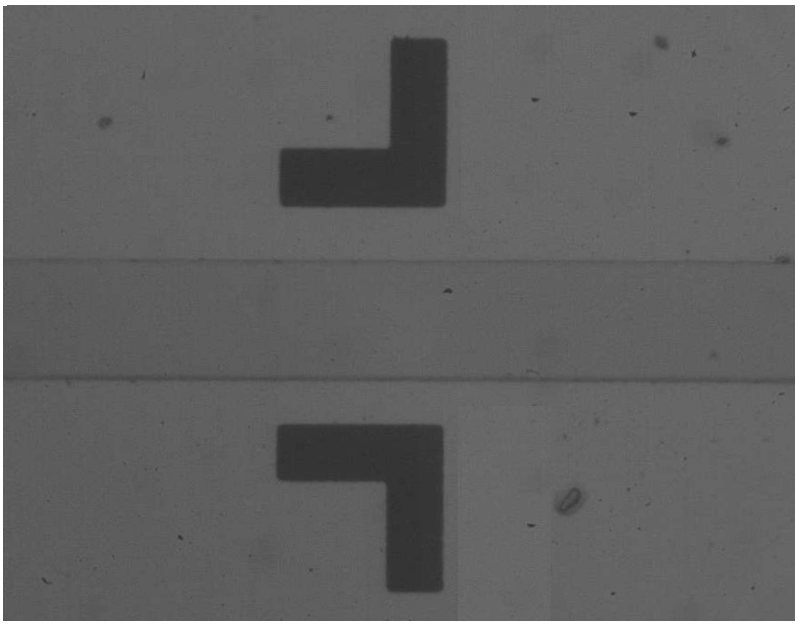

Figure 8.2: The SSAW sorting sample after bonding process. The sample is well aligned in between the alignment marks.

a well aligned sample with the help of the alignment marks on the substrate.

The resonance frequency of the SAW was measured at 10 MHz by a network analyzer (Agilent E5061A Network Analyzer). An RF signal of resonance frequency was generated by a signal generator (Tektronix AFG3022). It was then amplified to a value of 50 V peak-to-peak by an RF power amplifier (Amplifier Research 25A250A-25W) and was applied to the electrodes. Dispensed polymer particles (NIST traceable, Duke Scientific) (concentration 1.9×10^5 per ml; standard deviation of 0.09 μm) of size 10 μm were used in the experiment. The particles were diluted in DI water by volume (1 particles : 2 water). DI water and the diluted particles were pumped into the inlets by two precision syringe pumps (KD scientific, USA). A high speed camera (Photron FASTCAM APX RS, USA) attached to an inverted microscope (Nikon Eclipse TE2000-E) was used to capture the sorting process of particles. In the experiment, optimized flow rate of diluted particles (5 μL/h) and water (35 μL/h) in each water inlet) were used to focus the particles. When SAW was turned on,

the acoustic radiance force deflects the particles to the pressure node (anti-node). Figure 8.3(a) shows the instant SAW is turned on. The particles continue to follow the node and are sorted into outlet 2, 8.3(b). By turning the SAW on and off, particles are demonstrated to be sorted into the corresponding outlet channel.

Standing surface acoustic wave (SSAW) is a promising approach for particles manipulating and sorting. The induced acoustic radiance force acting on dispersed particles is able to direct microparticles to the outlet of interest. The actuation method is fast, effective and operates in a non contact manner. The fabrication process is based on standard lithography and is suitable for mass production. The device could be integrated into a more complex device for cells detection and high speed sorting applications.

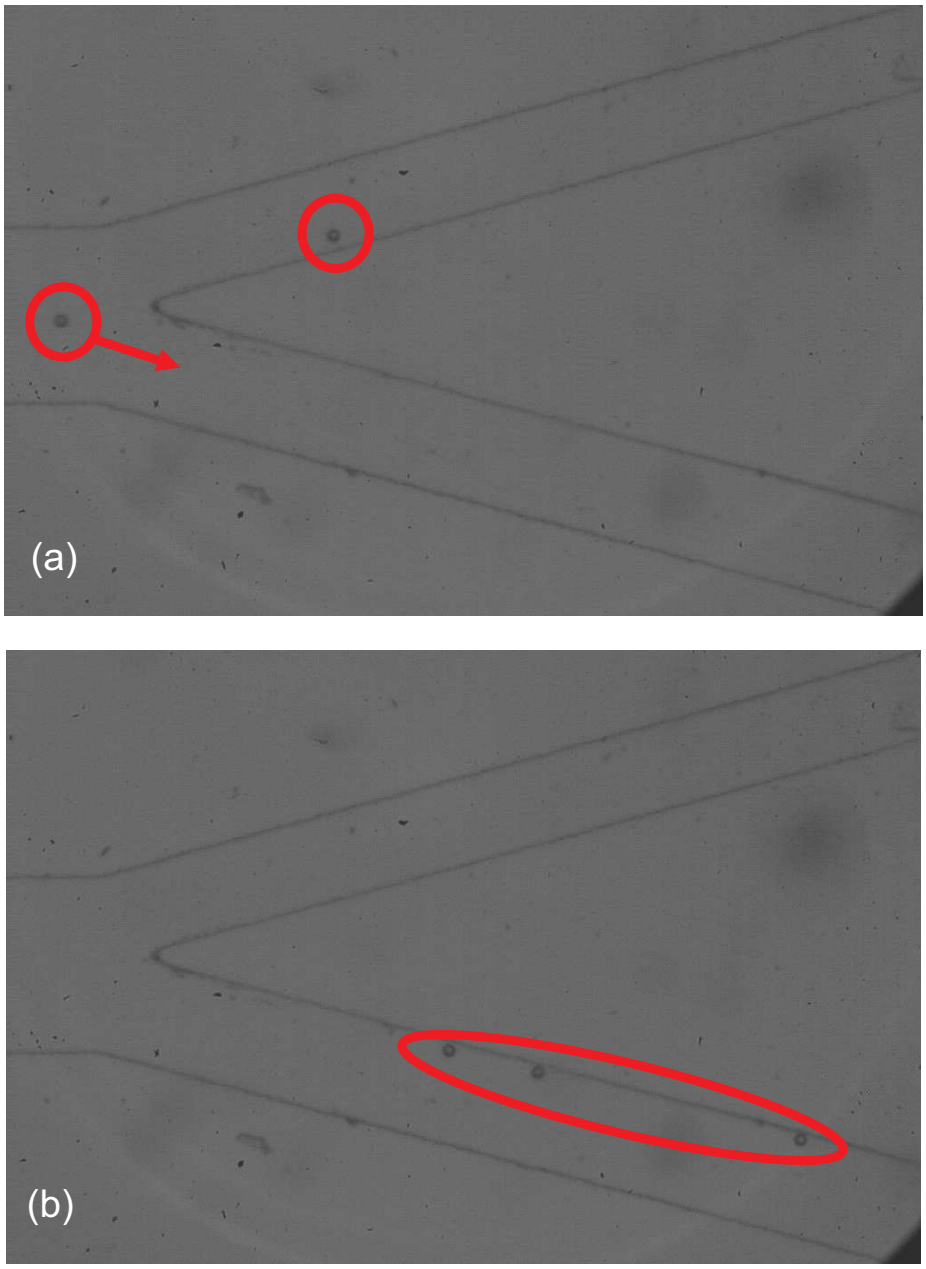

Figure 8.3: Experimental results of the sorting process (a) At the moment SAW is turned on, particles starts to stream into outlet 2 (b) After t=0.5 s, all the particles are sorted into outlet 2.

Chapter 9

Future Work

In the frame work of the present project, we have investigated the concept of surface acoustic wave in microlfuidics application. The fabrication and integration of a SAW device with a microchannel network has been demonstrated to form an active SAW mixer. This active mixer exploits the acoustic streaming effect to significantly improve the mixing efficiency at microscale. Behaviour of droplet motion guided by a hydrophilic track has been studied. Different working regime of a moving droplet was observed. Understanding droplet behavior is crucial for the use of SAW induced droplet motion in various microfluidic application. Multiphase SAW platform has been proposed. Droplet formation (focusing and T-junction configuration) under the influence of SAW has been investigated. The droplet shape is distorted along the channel due to the effect of propagating wave.

There are still room to achieve deeper understanding mechanisms that govern the SAW-driven fluid. Following future works in SAW can be carried out:

1 - Acoustic streaming flow pattern induced by SAW .

2 - The mechanism of droplet destabilize under strong SAW is not well understood al-

though some progress has been made to explain the vibration at the droplet surface.

3 - There are stil a lack of numerical and modelling work on acoustic streaming by SAW which would help to understand the complicated 3-D acoustic streaming in many applications.

4 - The reflected wave at liquid medium and channel wall (continuous phase application) could be coupled with the propagating wave for particles manipulating purpose. By chaging the reflected wave, various applications could be realized.

5 - Particles could be selectively sorted based on the configuration proposed in Chapter 8. By integrating optical detection, the size of a particle is realized. Utilizing an control circuit, SSAW is able to form along the channel in a desired amount of time and sort the particle of interest size.

Publications

1. T.D. Luong and N.T. Nguyen. Surface Acoustic Wave Driven Microfluidics - a Review. *Micro and Nanosystems*, 217-225, 2010.

2. T.D. Luong, V.N. Phan and N.T. Nguyen. High-throughput micromixers based on acoustic streaming induced by surface acoustic wave. *Microfluidics and Nanofluidics*, Vol. 10, No.3, pp. 619-625, 2011.

Bibliography

[1] http://en.wikipedia.org/wiki/Surface_acoustic_wave.

[2] R. M. White. Surface elastic waves. *Proceedings of the IEEE*, 58(8):1238–1276, 1970.

[3] Colins K Campbell. *Surface Acoustic Wave Devices for Mobile and Wireless Communications*. Academic Press, Inc., Orlando, FL, USA, 1998.

[4] M. G. Schweyer, J. C. Andle, D. J. McAllister, and J. F. Vetelino. An acoustic plate mode sensor for aqueous mercury. *Sensors and Actuators, B: Chemical*, 35(1-3):170–175, 1996.

[5] Amnon Yariv and Pochi Yeh. *Optical Waves In Crystals: Propagation And Control Of Laser Radiation*. John Wiley and Sons, New York, 1984.

[6] http://en.wikipedia.org/wiki/Acousto-optics.

[7] A. Wixforth. Acoustically driven programmable microfluidics for biological and chemical applications. *JALA - Journal of the Association for Laboratory Automation*, 11(6):399–405, 2006.

[8] Nam-Trung Nguyen and Richard M. White. Acoustic streaming in micromachined flexural plate wave devices: numerical simulation and experimental verification. *IEEE Transactions on Ultrasonics, Ferroelectrics, and Frequency Control*, 47(6):1463–1471, 2000.

[9] M. K. Chaudhury and G. M. Whitesides. How to make water run uphill. *Science*, 256(5063):1539–1544, 1992.

[10] Z. Jiao, N. T. Nguyen, and X. Huang. Thermocapillary actuation of liquid plugs using a heater array. *Sensors and Actuators, A: Physical*, 140(2):145–155, 2007.

[11] M. G. Pollack, R. B. Fair, and A. D. Shenderov. Electrowetting-based actuation of liquid droplets for microfluidic applications. *Applied Physics Letters*, 77(11):1725–1726, 2000.

[12] N. T. Nguyen, K. M. Ng, and X. Huang. Manipulation of ferrofluid droplets using planar coils. *Applied Physics Letters*, 89(5), 2006.

[13] Jinjie Shi. *Biofunctionalized Nano-Electro-Mechanical-Systems (Bio-NEMS): Acoustic twezzersapplying acoustics in microfluidics and active plasmonics*. PhD thesis, 2009.

[14] L. Y. Yeo and J. R. Friend. Ultrafast microfluidics using surface acoustic waves. *Biomicrofluidics*, 3(1), 2009.

[15] Y. Q. Fu, J. K. Luo, X. Y. Du, A. J. Flewitt, Y. Li, G. H. Markx, A. J. Walton, and W. I. Milne. Recent developments on zno films for acoustic wave based bio-

sensing and microfluidic applications: a review. *Sensors and Actuators, B: Chemical*, 143(2):606–619, 2010.

[16] A. Wixforth, C. Strobl, Ch Gauer, A. Toegl, J. Scriba, and Z. V. Guttenberg. Acoustic manipulation of small droplets. *Analytical and Bioanalytical Chemistry*, 379(7-8):982–991, 2004.

[17] P. Paik, V. K. Pamula, and R. B. Fair. Rapid droplet mixers for digital microfluidic systems. *Lab on a Chip - Miniaturisation for Chemistry and Biology*, 3(4):253–259, 2003.

[18] T. Frommelt, M. Kostur, M. Wenzel-Schfer, P. Talkner, P. Hnggi, and A. Wixforth. Microfluidic mixing via acoustically driven chaotic advection. *Physical Review Letters*, 100(3), 2008.

[19] A. Wixforth. Acoustically driven planar microfluidics. *Superlattices and Microstructures*, 33(5-6):389–396, 2003.

[20] H. Li, J. R. Friend, and L. Y. Yeo. Microfluidic colloidal island formation and erasure induced by surface acoustic wave radiation. *Physical Review Letters*, 101(8), 2008.

[21] H. Li, J. R. Friend, and L. Y. Yeo. Surface acoustic wave concentration of particle and bioparticle suspensions. *Biomedical Microdevices*, 9(5):647–656, 2007.

[22] R. Shilton, M. K. Tan, L. Y. Yeo, and J. R. Friend. Particle concentration and mixing in microdrops driven by focused surface acoustic waves. *Journal of Applied Physics*, 104(1), 2008.

[23] D. Beyssen, L. Le Brizoual, P. Alnot, and I. Perry. Droplet heating system based on saw/liquid interaction. *Syst me de chauffage de goutte bas sur l'interaction SAW-liquide*, (6):64–69, 2007.

[24] D. Beyssen, L. Le Brizoual, O. Elmazria, and P. Alnot. Microfluidic device based on surface acoustic wave. *Sensors and Actuators, B: Chemical*, 118(1-2):380–385, 2006.

[25] J. K. Luo, Y. Q. Fu, Y. Li, X. Y. Du, A. J. Flewitt, A. J. Walton, and W. I. Milne. Moving-part-free microfluidic systems for lab-on-a-chip. *Journal of Micromechanics and Microengineering*, 19(5), 2009.

[26] A. Wixforth, C. Gauer, J. Scriba, M. Wassermeier, and R. Kirchner. Flat fluidics: A new route toward programmable biochips. volume 4982 of *Microfluidics, BioMEMS, and Medical Microsystems*, pages 235–242, San Jose, CA, 2003.

[27] J. B. Brzoska, I. Ben Azouz, and F. Rondelez. Silanization of solid substrates: A step toward reproducibility. *Langmuir*, 10(11):4367–4373, 1994.

[28] Y. Q. Fu, X. Y. Du, J. K. Luo, A. J. Flewitt, W. I. Milne, D. S. Lee, N. M. Park, S. Maeng, S. H. Kim, Y. J. Choi, and J. Park. Saw streaming in zno surface acoustic wave micromixer and micropump. 6th IEEE Conference on SENSORS, IEEE SENSORS 2007, pages 478–483, Atlanta, GA, 2007.

[29] X. Y. Du, Y. Q. Fu, J. K. Luo, A. J. Flewitt, and W. I. Milne. Microfluidic pumps employing surface acoustic waves generated in zno thin films. *Journal of Applied Physics*, 105(2), 2009.

[30] A. Renaudin, P. Tabourier, V. Zhang, J. C. Camart, and C. Druon. Saw nanopump for handling droplets in view of biological applications. *Sensors and Actuators, B: Chemical*, 113(1):389–397, 2006.

[31] S. Thalhammer. Programmable lab-on-a-chip system for single cell analysis. volume 7364 of *Nanotechnology IV*, Dresden, 2009.

[32] Z. Guttenberg, H. Mller, H. Habermller, A. Geisbauer, J. Pipper, J. Felbel, M. Kielpinski, J. Scriba, and A. Wixforth. Planar chip device for pcr and hybridization with surface acoustic wave pump. *Lab on a Chip - Miniaturisation for Chemistry and Biology*, 5(3):308–317, 2005.

[33] Y. Bourquin, J. Reboud, R. Wilson, and J. M. Cooper. Tuneable surface acoustic waves for fluid and particle manipulations on disposable chips. *Lab on a Chip - Miniaturisation for Chemistry and Biology*, 10(15):1898–1901, 2010.

[34] M. K. Tan, J. R. Friend, and L. Y. Yeo. Microparticle collection and concentration via a miniature surface acoustic wave device. *Lab on a Chip - Miniaturisation for Chemistry and Biology*, 7(5):618–625, 2007.

[35] C. J. Strobl, Z. Von Guttenberg, and A. Wixforth. Nano- and pico-dispensing of fluids on planar substrates using saw. *IEEE Transactions on Ultrasonics, Ferroelectrics, and Frequency Control*, 51(11):1432–1436, 2004.

[36] J. Benns, S. Alzuaga, F. Chrioux, S. Ballandras, P. Vairac, J. E. Manceau, and F. Bastien. Detection and high-precision positioning of liquid droplets using saw

systems. *IEEE Transactions on Ultrasonics, Ferroelectrics, and Frequency Control*, 54(10):2146–2151, 2007.

[37] T. T. Wu and I. H. Chang. Actuating and detecting of microdroplet using slanted finger interdigital transducers. *Journal of Applied Physics*, 98(2):1–7, 2005.

[38] A. Renaudin, P. Tabourier, J. C. Camart, and C. Druon. Surface acoustic wave two-dimensional transport and location of microdroplets using echo signal. *Journal of Applied Physics*, 100(11), 2006.

[39] J. Benns, S. Alzuaga, S. Ballandras, F. Chrioux, F. Bastien, and J. F. Manceau. Droplet ejector using surface acoustic waves. volume 2 of *2005 IEEE Ultrasonics Symposium*, pages 823–826, Rotterdam, 2005.

[40] M. K. Tan, J. R. Friend, and L. Y. Yeo. Interfacial jetting phenomena induced by focused surface vibrations. *Physical Review Letters*, 103(2), 2009.

[41] J. R. Friend, L. Y. Yeo, D. R. Arifin, and A. Mechler. Evaporative self-assembly assisted synthesis of polymeric nanoparticles by surface acoustic wave atomization. *Nanotechnology*, 19(14), 2008.

[42] M. Alvarez, J. R. Friend, and L. Y. Yeo. Surface vibration induced spatial ordering of periodic polymer patterns on a substrate. *Langmuir*, 24(19):10629–10632, 2008.

[43] T. Saiki, K. Okada, and Y. Utsumi. Proposal of a novel liquid flow actuator for lab-on-chips operated by surface acoustic wave. s20th International Microprocesses and Nanotechnology Conference, MNC 2007, pages 332–333, Kyoto, 2007.

[44] D. Fukuoka and Y. Utsumi. Fabrication of the cyclical fluid channel using the surface acoustic wave actuator and continuous fluid pumping in the cyclical fluid channel. *Microsystem Technologies*, 14(9-11):1395–1398, 2008.

[45] G. Lindner, H. Faustmann, T. Fischer, S. Krempel, M. Munch, S. Rothballer, and M. Schmitt. Acoustic surface wave induced propagation of liquids in open channels. 2007 IEEE Ultrasonics Symposium, IUS, pages 2331–2334, New York, NY, 2007.

[46] M. K. Tan, L. Y. Yeo, and J. R. Friend. Rapid fluid flow and mixing induced in microchannels using surface acoustic waves. *Europhysics Letters*, 87(4), 2009.

[47] S. Girardo, M. Cecchini, F. Beltram, R. Cingolani, and D. Pisignano. Polydimethylsiloxane-**L***i***N***b***O**$_3$ surface acoustic wave micropump devices for fluid control into microchannels. *Lab on a Chip - Miniaturisation for Chemistry and Biology*, 8(9):1557–1563, 2008.

[48] L. Masini, M. Cecchini, S. Girardo, R. Cingolani, D. Pisignano, and F. Beltram. Surface-acoustic-wave counterflow micropumps for on-chip liquid motion control in two-dimensional microchannel arrays. *Lab on a Chip - Miniaturisation for Chemistry and Biology*, 10(15):1997–2000, 2010.

[49] K. Sritharan, C. J. Strobl, M. F. Schneider, A. Wixforth, and Z. Guttenberg. Acoustic mixing at low reynold's numbers. *Applied Physics Letters*, 88(5):1–3, 2006.

[50] W. K. Tseng, J. L. Lin, W. C. Sung, S. H. Chen, and G. B. Lee. Active micromixers using surface acoustic waves on y-cut 128 linbo¡sub¿3¡/sub¿. *Journal of Micromechanics and Microengineering*, 16(3):539–548, 2006.

[51] T. Franke, A. R. Abate, D. A. Weitz, and A. Wixforth. Surface acoustic wave (saw) directed droplet flow in microfluidics for pdms devices. *Lab on a Chip - Miniaturisation for Chemistry and Biology*, 9(18):2625–2627, 2009.

[52] T. Franke, S. Braunmller, L. Schmid, A. Wixforth, and D. A. Weitz. Surface acoustic wave actuated cell sorting (sawacs). *Lab on a Chip - Miniaturisation for Chemistry and Biology*, 10(6):789–794, 2010.

[53] T. Franke, S. Braunmller, T. Frommelt, and A. Wixforth. Sorting of solid and soft objects in vortices driven by surface acoustic waves. volume 7365, 2009.

[54] J. Shi, X. Mao, D. Ahmed, A. Colletti, and T. J. Huang. Focusing microparticles in a microfluidic channel with standing surface acoustic waves (ssaw). *Lab on a Chip - Miniaturisation for Chemistry and Biology*, 8(2):221–223, 2008.

[55] C. D. Wood, S. D. Evans, J. E. Cunningham, R. O'Rorke, C. Wlti, and A. G. Davies. Alignment of particles in microfluidic systems using standing surface acoustic waves. *Applied Physics Letters*, 92(4), 2008.

[56] C. D. Wood, J. E. Cunningham, R. O'Rorke, C. Wlti, E. H. Linfield, A. G. Davies, and S. D. Evans. Formation and manipulation of two-dimensional arrays of micron-scale particles in microfluidic systems by surface acoustic waves. *Applied Physics Letters*, 94(5), 2009.

[57] J. Shi, D. Ahmed, X. Mao, S. C. S. Lin, A. Lawit, and T. J. Huang. Acoustic tweezers: Patterning cells and microparticles using standing surface acoustic waves

(ssaw). *Lab on a Chip - Miniaturisation for Chemistry and Biology*, 9(20):2890–2895, 2009.

[58] J. Shi, H. Huang, Z. Stratton, Y. Huang, and T. J. Huang. Continuous particle separation in a microfluidic channel via standing surface acoustic waves (ssaw). *Lab on a Chip - Miniaturisation for Chemistry and Biology*, 9(23):3354–3359, 2009.

[59] C. Eckart. Vortices and streams caused by sound waves. *Physical Review*, 73(1):68–76, 1948.

[60] J. J. Markham. Second-order acoustic fields: Streaming with viscosity and relaxation. *Physical Review*, 86(4):497–502, 1952.

[61] W. L. Nyborg. Acoustic streaming. *Physicals Acoustics*, 75(9):1415–1422, 1949.

[62] Richard Morgan Moroney. *Ultrasonic Microtransport*. PhD thesis, 1995.

[63] D. S Ballantine, R. M White, S. J Martin, A. J Ricco, G. C Frye, E. T Zellars, and H. Wohltjen. *Acoustic Wave Sensors - Theory, Design, and Physico-Chemical Applications*. Elsevier, 1997.

[64] G. M. Whitesides, E. Ostuni, S. Takayama, X. Jiang, and D. E. Ingber. Soft lithography in biology and biochemistry. *Annual Review of Biomedical Engineering*, 3:335–373, 2001.

[65] N. T. Nguyen. *Micromixers: Fundamentals, Design and Fabrication*. William Andrew, 2009.

[66] V. Hessel, H. Lowe, and F. Schonfeld. Micromixers - a review on passive and active

mixing principles. *Chemical Engineering Science*, 60(8-9 SPEC. ISS.):2479–2501, 2005.

[67] N. T. Nguyen and Z. Wu. Micromixers - a review. *Journal of Micromechanics and Microengineering*, 15(2), 2005.

[68] M. Koch, H. Witt, A. G. R. Evans, and A. Brunnschweiler. Improved characterization technique for micromixers. *Journal of Micromechanics and Microengineering*, 9(2):156–158, 1999.

[69] P. Hinsmann, J. Frank, P. Svasek, M. Harasek, and B. Lendl. Design, simulation and application of a new micromixing device for time resolved infrared spectroscopy of chemical reactions in solution. *Lab on a Chip - Minituarization for Chemistry and Biology*, 1(1):16–21, 2001.

[70] V. Hessel, S. Hardt, H. Lowe, and F. Schonfeld. Laminar mixing in different interdigital micromixers: I. experimental characterization. *AIChE Journal*, 49(3):566–577, 2003.

[71] B. He, B. J. Burke, X. Zhang, R. Zhang, and F. E. Regnier. A picoliter-volume mixer for microfluidic analytical systems. *Analytical Chemistry*, 73(9):1942–1947, 2001.

[72] M. S. Munson and P. Yager. Simple quantitative optical method for monitoring the extent of mixing applied to a novel microfluidic mixer. *Analytica Chimica Acta*, 507(1):63–71, 2004.

[73] M. Yi and H. H. Bau. The kinematics of bend-induced mixing in micro-conduits. *International Journal of Heat and Fluid Flow*, 24(5):645–656, 2003.

[74] C. C. Hong, J. W. Choi, and C. H. Ahn. A novel in-plane passive microfluidic mixer with modified tesla structures. *Lab on a Chip - Miniaturisation for Chemistry and Biology*, 4(2):109–113, 2004.

[75] S. J. Park, J. K. Kim, J. Park, S. Chung, C. Chung, and J. K. Chang. Rapid three-dimensional passive rotation micromixer using the breakup process. *Journal of Micromechanics and Microengineering*, 14(1):6–14, 2004.

[76] R. H. Liu, M. A. Stremler, K. V. Sharp, M. G. Olsen, J. G. Santiago, R. J. Adrian, H. Aref, and D. J. Beebe. Passive mixing in a three-dimensional serpentine microchannel. *Journal of Microelectromechanical Systems*, 9(2):190–197, 2000.

[77] A Deshmukh, D Liepmann, and AP Pisano. Continuous micromixer with pulsatile micropumps, 2000.

[78] A. Ould El Moctar, N. Aubry, and J. Batton. Electro-hydrodynamic micro-fluidic mixer. *Lab on a Chip - Miniaturisation for Chemistry and Biology*, 3(4):273–280, 2003.

[79] M. H. Oddy, J. G. Santiago, and J. C. Mikkelsen. Electrokinetic instability micromixing. *Analytical Chemistry*, 73(24):5822–5832, 2001.

[80] H. H. Bau, J. Zhong, and M. Yi. A minute magneto hydro dynamic (mhd) mixer. *Sensors and Actuators, B: Chemical*, 79(2-3):207–215, 2001.

[81] H. Mao, T. Yang, and P. S. Cremer. A microfluidic device with a linear temperature gradient for parallel and combinatorial measurements. *Journal of the American Chemical Society*, 124(16):4432–4435, 2002.

[82] Z. Yang, S. Matsumoto, H. Goto, M. Matsumoto, and R. Maeda. Ultrasonic micromixer for microfluidic systems. *Sensors and Actuators, A: Physical*, 93(3):266–272, 2001.

[83] R. H. Liu, J. Yang, M. Z. Pindera, M. Athavale, and P. Grodzinski. Bubble-induced acoustic micromixing. *Lab on a Chip - Miniaturisation for Chemistry and Biology*, 2(3):151–157, 2002.

[84] D. Ahmed, X. Mao, J. Shi, B. K. Juluri, and T. J. Huang. A millisecond micromixer via single-bubble-based acoustic streaming. *Lab on a Chip - Miniaturisation for Chemistry and Biology*, 9(18):2738–2741, 2009.

[85] A. H. Meng, N. T. Nguyen, and R. M. White. Focused flow micropump using ultrasonic flexural plate waves. *Biomedical Microdevices*, 2(3):169–174, 2000.

[86] S. K. Cho, H. Moon, and C. J. Kim. Creating, transporting, cutting, and merging liquid droplets by electrowetting-based actuation for digital microfluidic circuits. *Journal of Microelectromechanical Systems*, 12(1):70–80, 2003.

[87] N.T Nguyen and XY. Huang. Thermocapillary effect of a liquid plug in transient temperature fields. *Japanese Journal of Applied Physics, Part 1: Regular Papers and Short Notes and Review Papers*, 44:1139–1142, 2005.

[88] S. Daniel, M. K. Chaudhury, and P. G. De Gennes. Vibration-actuated drop motion on surfaces for batch microfluidic processes. *Langmuir*, 21(9):4240–4248, 2005.

[89] L. Y. Yeo and J. R. Friend. Ultrafast microfluidics using surface acoustic waves. *Biomicrofluidics*, 3(1), 2009.

[90] A. Qi, L. Y. Yeo, and J. R. Friend. Interfacial destabilization and atomization driven by surface acoustic waves. *Physics of Fluids*, 20(7), 2008.

[91] A. Renaudin, E. Galopin, V. Thomy, C. Druon, and F. Zoueshtiagh. Creeping, walking and jumping drop. *Physics of Fluids*, 19(091111), 2007.

[92] P. Brunet, M. Baudoin, O. B. Matar, and F. Zoueshtiagh. Droplet displacements and oscillations induced by ultrasonic surface acoustic waves: A quantitative study. *Physical Review E - Statistical, Nonlinear, and Soft Matter Physics*, 81(3), 2010.

[93] S. Y. Teh, R. Lin, L. H. Hung, and A. P. Lee. Droplet microfluidics. *Lab on a Chip - Miniaturisation for Chemistry and Biology*, 8(2):198–220, 2008.

[94] B. Zheng, L. S. Roach, and R. F. Ismagilov. Screening of protein crystallization conditions on a microfluidic chip using nanoliter-size droplets. *Journal of the American Chemical Society*, 125(37):11170–11171, 2003.

[95] E. M. Chan, A. P. Alivisatos, and R. A. Mathies. High-temperature microfluidic synthesis of cdse nanocrystals in nanoliter droplets. *Journal of the American Chemical Society*, 127(40):13854–13861, 2005.

[96] S. L. Anna, N. Bontoux, and H. A. Stone. Formation of dispersions using ”flow focusing” in microchannels. *Applied Physics Letters*, 82(3):364–366, 2003.

[97] T. Thorsen, R. W. Roberts, F. H. Arnold, and S. R. Quake. Dynamic pattern formation in a vesicle-generating microfluidic device. *Physical Review Letters*, 86(18):4163–4166, 2001.

[98] A. Bransky, N. Korin, M. Khoury, and S. Levenberg. A microfluidic droplet generator based on a piezoelectric actuator. *Lab on a Chip - Miniaturisation for Chemistry and Biology*, 9(4):516–520, 2009.

[99] N. T. Nguyen, T. H. Ting, Y. F. Yap, T. N. Wong, J. C. K. Chai, W. L. Ong, J. Zhou, S. H. Tan, and L. Yobas. Thermally mediated droplet formation in microchannels. *Applied Physics Letters*, 91(8), 2007.

[100] C. Y. Lee, Y. H. Lin, and G. B. Lee. A droplet-based microfluidic system capable of droplet formation and manipulation. *Microfluidics and Nanofluidics*, 6(5):599–610, 2009.

[101] S. H. Tan, N. T. Nguyen, L. Yobas, and T. G. Kang. Formation and manipulation of ferrofluid droplets at a microfluidic t-junction. *Journal of Micromechanics and Microengineering*, 20(4), 2010.

[102] T. D. Luong, V. N. Phan, and N. T. Nguyen. High-throughput micromixers based on acoustic streaming induced by surface acoustic wave. *Microfluidics and Nanofluidics*, pages 1–7, 2010.

[103] S. Lutz, P. Weber, M. Focke, B. Faltin, J. Hoffmann, C. Mller, D. Mark, G. Roth, P. Munday, N. Armes, O. Piepenburg, R. Zengerle, and F. Von Stetten. Microfluidic lab-on-a-foil for nucleic acid analysis based on isothermal recombinase polymerase amplification (rpa). *Lab on a Chip - Miniaturisation for Chemistry and Biology*, 10(7):887–893, 2010.

[104] C. K. Fredrickson and Z. H. Fan. Macro-to-micro interfaces for microfluidic devices. *Lab on a Chip - Miniaturisation for Chemistry and Biology*, 4(6):526–533, 2004.

[105] A. J. Tudos, G. A. J. Besselink, and R. B. M. Schasfoort. Trends in miniaturized total analysis systems for point-of-care testing in clinical chemistry. *Lab on a Chip - Minituarization for Chemistry and Biology*, 1(2):83–95, 2001.

[106] M. Eisenstein. Cell sorting: divide and conquer. *Nature.*, 441(7097):1179–1185, 2006.

[107] J. C. Baret, O. J. Miller, V. Taly, M. Ryckelynck, A. El-Harrak, L. Frenz, C. Rick, M. L. Samuels, J. B. Hutchison, J. J. Agresti, D. R. Link, D. A. Weitz, and A. D. Griffiths. Fluorescence-activated droplet sorting (fads): Efficient microfluidic cell sorting based on enzymatic activity. *Lab on a Chip - Miniaturisation for Chemistry and Biology*, 9(13):1850–1858, 2009.

[108] L. R. Huang, E. C. Cox, R. H. Austin, and J. C. Sturm. Continuous particle separation through deterministic lateral displacement. *Science*, 304(5673):987–990, 2004.

[109] K. E. McCloskey, L. R. Moore, M. Hoyos, A. Rodriguez, J. J. Chalmers, and M. Zborowski. Magnetophoretic cell sorting is a function of antibody binding capacity. *Biotechnology Progress*, 19(3):899–907, 2003.

[110] T. F. Kong, E. H. S. Huan Shin, H. S. Sugiarto, H. F. Liew, X. Wang, W. S. Lew, N. T. Nguyen, and Y. Chen. An efficient microfluidic sorter: Implementation of double meandering micro striplines for magnetic particles switching. *Microfluidics and Nanofluidics*, 10(5):1069–1078, 2011.

[111] K. P. Chen, J. R. Pacheco, M. A. Hayes, and S. J. R. Staton. Insulator-based dielectrophoretic separation of small particles in a sawtooth channel. *Electrophoresis*, 30(9):1441–1448, 2009.

[112] A. Nilsson, F. Petersson, H. Jnsson, and T. Laurell. Acoustic control of suspended particles in micro fluidic chips. *Lab on a Chip - Miniaturisation for Chemistry and Biology*, 4(2):131–135, 2004.